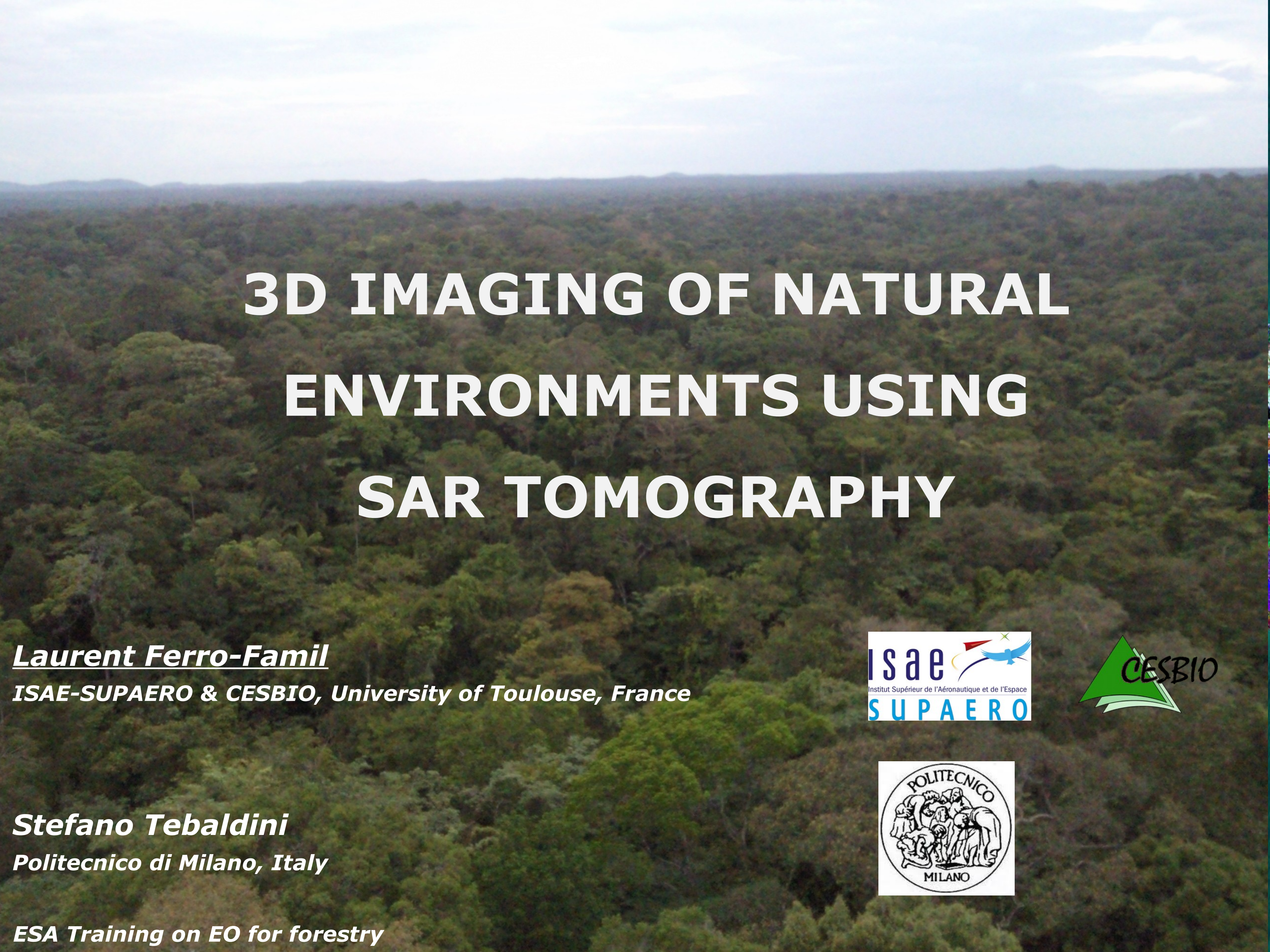

3D IMAGING OF NATURAL ENVIRONMENTS USING SAR TOMOGRAPHY

Laurent Ferro-Famil
ISAE-SUPAERO & CESBIO, University of Toulouse, France

Stefano Tebaldini
Politecnico di Milano, Italy

ESA Training on EO for forestry

From InSAR to PolinSAR and PolTomoSAR

Basic concept of tomographic imaging

> ***“Fundamentally, tomographic imaging deals with reconstructing an image from its projections”***
>
> **A.C. Kak, M. Slaney, PCT, 1987**

Projections of 2 cylinders

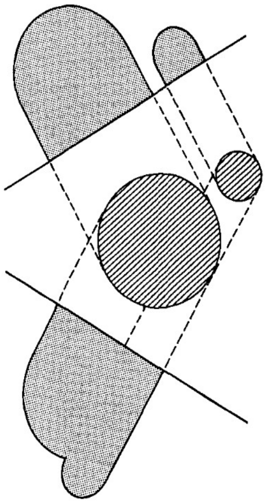

Fourier slice theorem in the non diffracting case

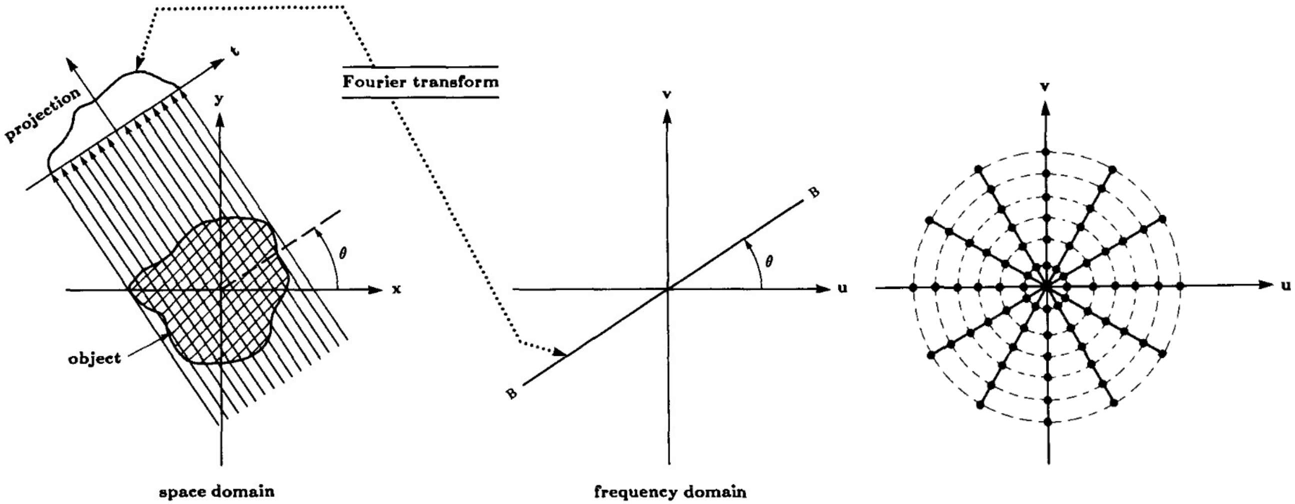

Synthetic Aperture Radar tomographic imaging

- Diffraction tomography
- Coherent processing
- Generalization of interferometric SAR processing using **a synthetic array**

Polarimetric SAR tomography

BIOMASS
PolTomoSAR mode

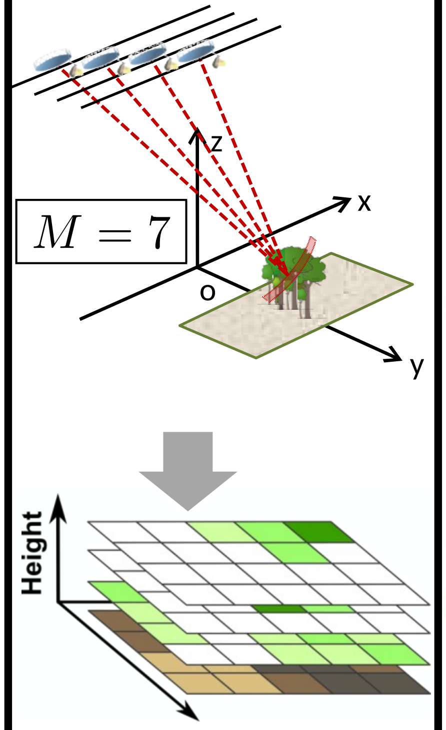

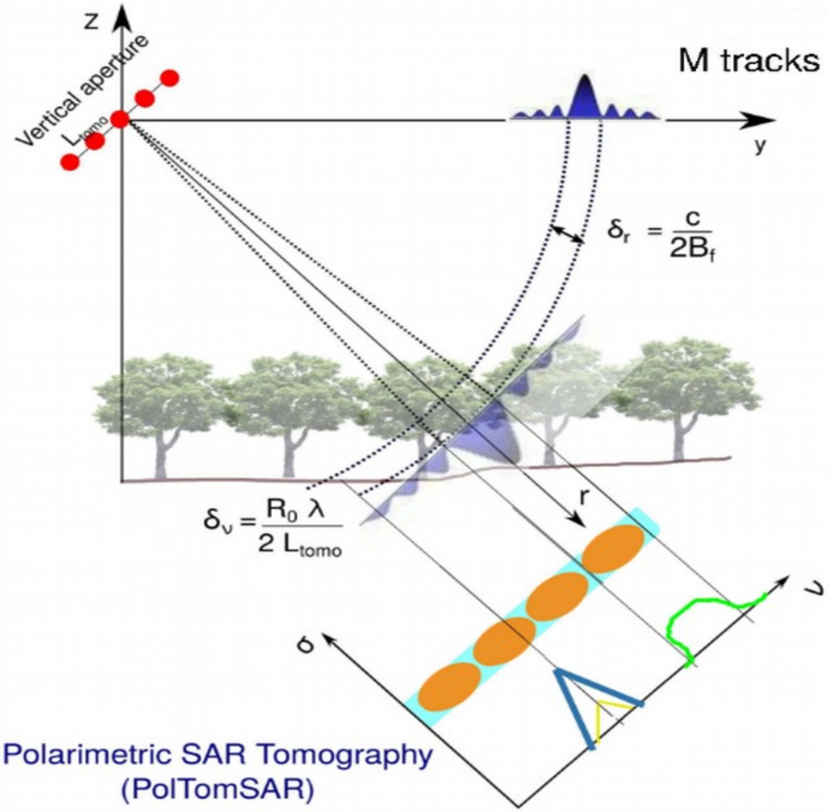

Polarimetric SAR Tomography
(PolTomSAR)

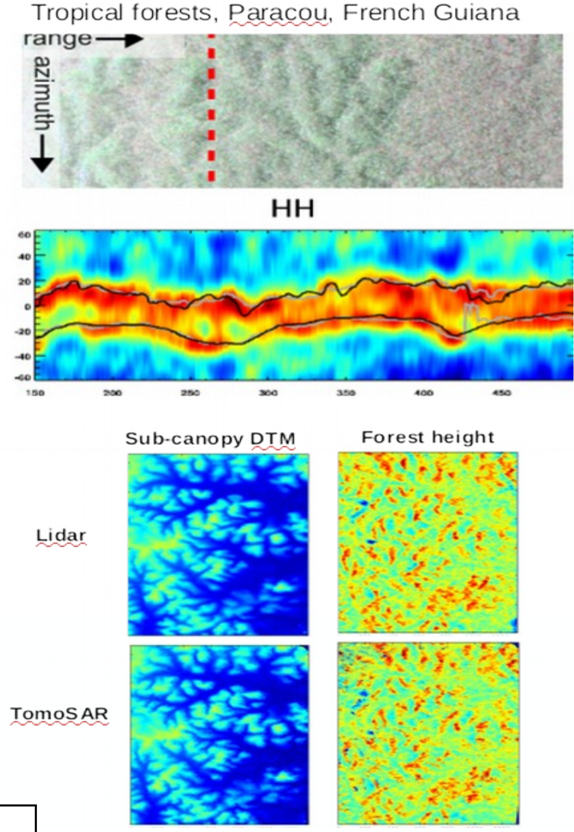

$$\delta z \propto \frac{1}{L_{tomo}} \approx \frac{z_{amb}}{M}$$

InSAR vertical decorrelation over volumes

Volumetric media inSAR response modeling

- Vertical reflectivity structure $\sigma_{v_e}(\vec{r}) = \sigma_{v_e}(z) = A_{v_e} f(z)$

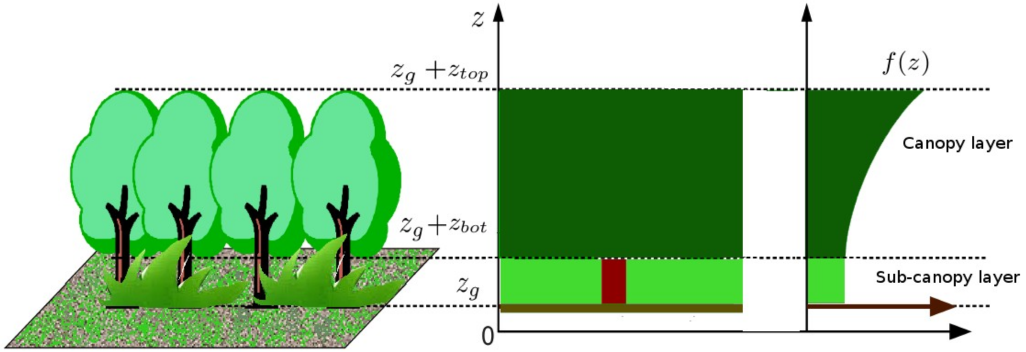

- InSAR coherence $\gamma = \gamma_{th} \quad \gamma_{proc} \quad \gamma_{temp} \quad \gamma_{surf} \quad \gamma_z$

- Decorrelation due to vertical structure :

$$\boxed{\gamma_z = \frac{\int \sigma_{v_e}(z)\, \mathrm{e}^{jk_z z}\, \mathrm{d}z}{\int \sigma_{v_e}(z)\mathrm{d}z}}$$

$$k_z = \frac{k_c B_\perp}{r \sin\theta}$$

- Fourier transform-like **coherence-structure relationship**

$$\boxed{\gamma_z \overset{FT}{\longleftrightarrow} \sigma_{v_e}(z)}$$

L. Ferro-Famil & S.Tebaldini

InSAR RVOG model

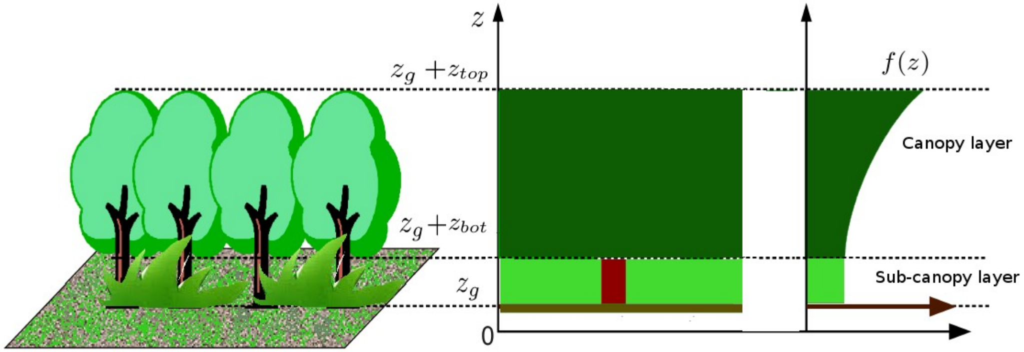

Modeling at order 1

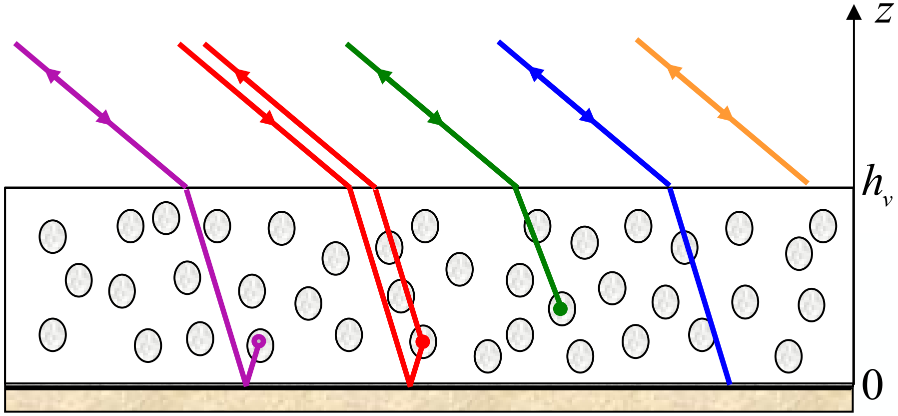

Parameter Estimation

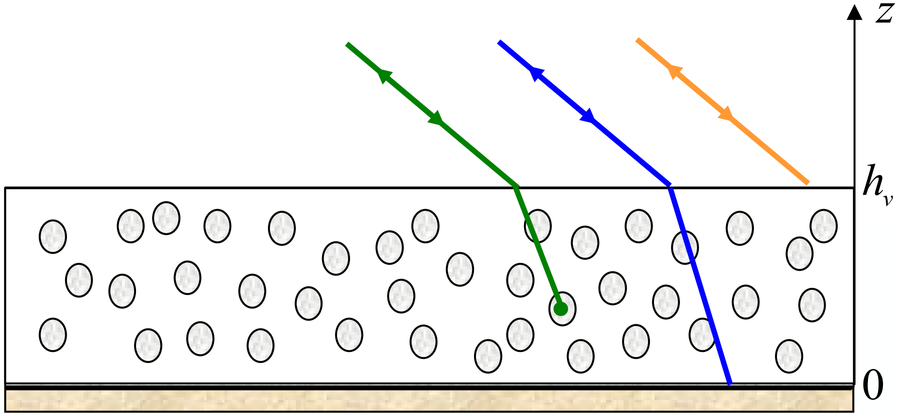

Parameter estimation often requires to simplify models

- omitting negligible terms
- merging contributions that cannot be discriminated (e.g. ground and double-bounce)

InSAR RVOG model

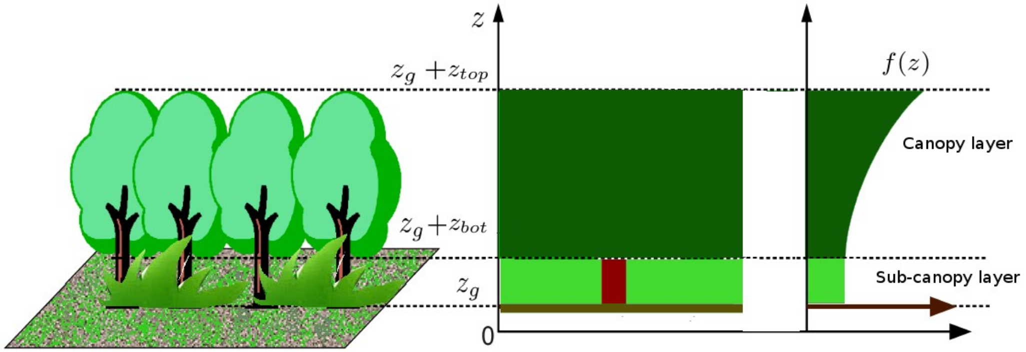

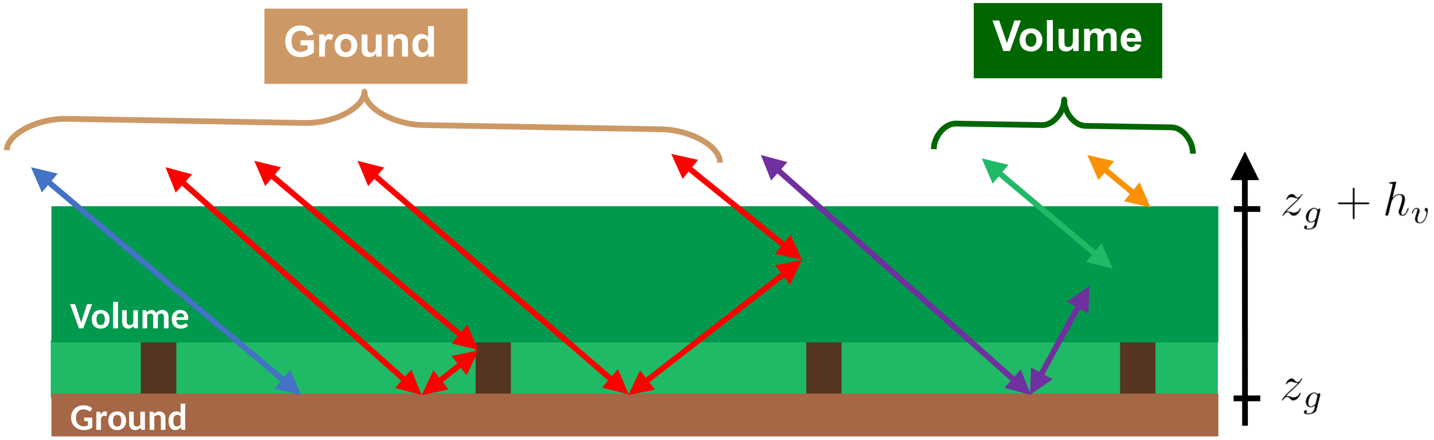

- 2 significant and uncorrelated mechanisms :

  ⇨ volume + underlying ground
- low density medium

  ⇨ no refraction

InSAR RVOG analysis

Ground only

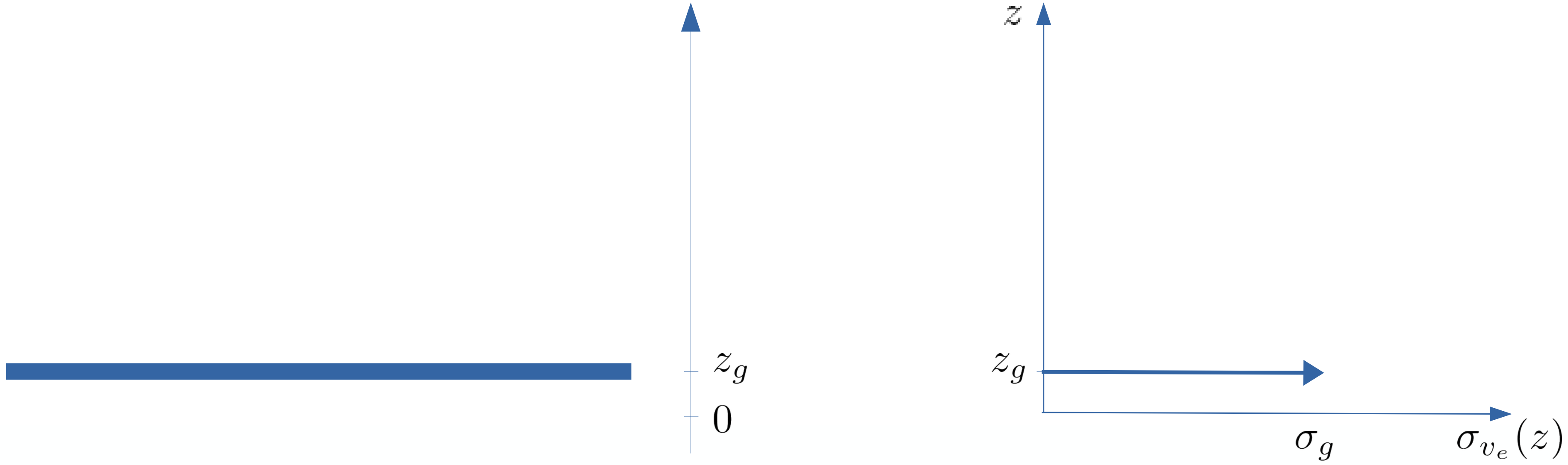

$$\gamma_z = \frac{\int \sigma_{v_e}(z)\, \mathrm{e}^{jk_z z}\, \mathrm{d}z}{\int \sigma_{v_e}(z) \mathrm{d}z}$$

$$\sigma_{v_e}(z) = \sigma_g \delta(z - z_g) \quad \Rightarrow \quad \gamma_z = \mathrm{e}^{jk_z z_g}$$

InSAR well adapted to topography estimation

InSAR RVOG analysis

Non attenuating random volume only

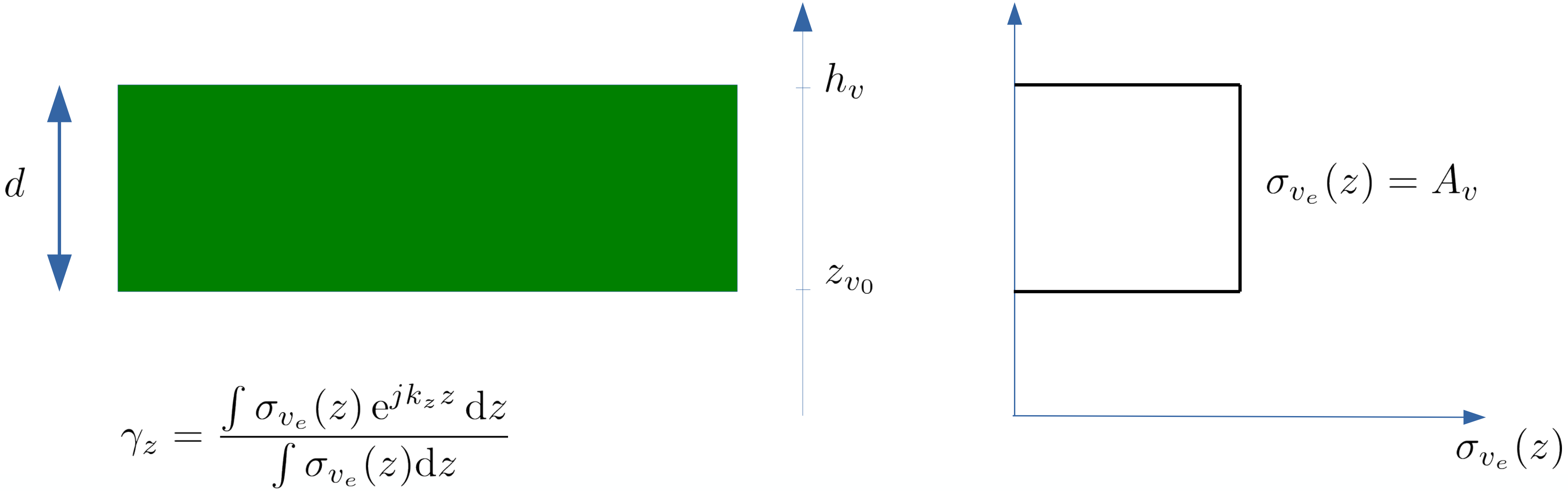

$$\gamma_z = \frac{\int \sigma_{v_e}(z)\, \mathrm{e}^{jk_z z}\, \mathrm{d}z}{\int \sigma_{v_e}(z) \mathrm{d}z}$$

No underlying ground

Null extinction: $\sigma_{v_e}(z) = A_v$

$$\gamma_z = \frac{1}{d} \int_{z_{v0}}^{h_v} \mathrm{e}^{jk_z z}\, \mathrm{d}z$$

$$\gamma_z = \mathrm{e}^{jk_z \frac{h_v + z_{v0}}{2}} \operatorname{sinc}\left(\frac{k_z d}{2}\right)$$

InSAR RVOG analysis

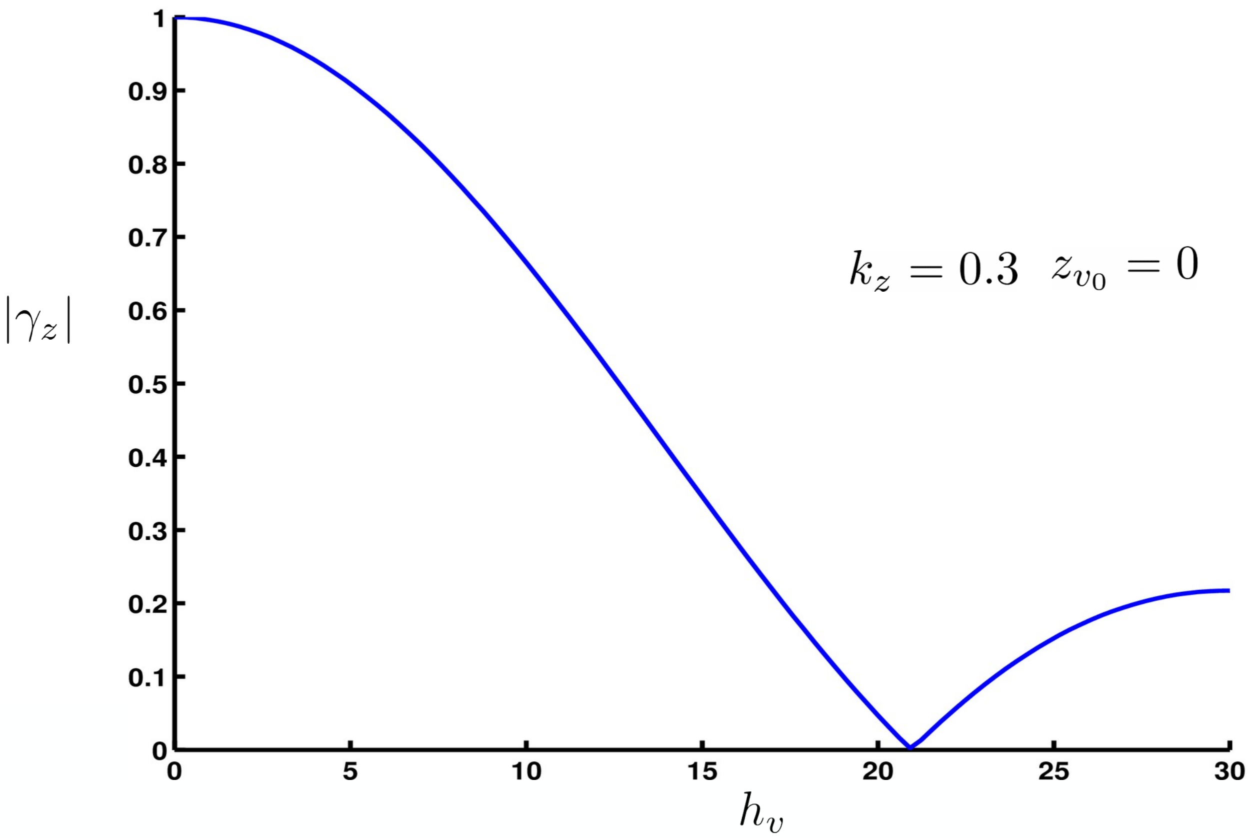

Volume center height

Volume width

$$\gamma_z = \mathrm{e}^{jk_z \frac{h_v + z_{v0}}{2}} \mathrm{sinc}\left(\frac{k_z d}{2}\right)$$

InSAR well adapted to volume analysis under specific conditions

InSAR RVOG analysis

Attenuating random volume only

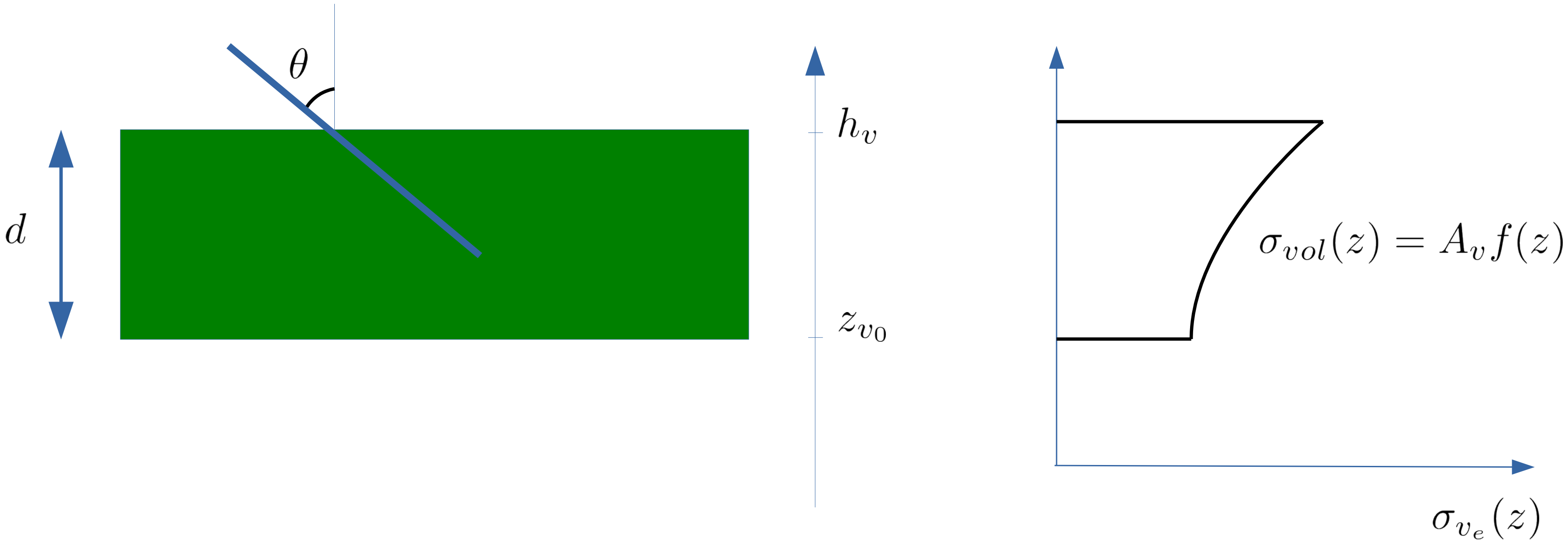

Linear differential extinction $$\mathrm{d}I = -\kappa_e I \mathrm{d}s = -\frac{\kappa_e}{\cos\theta} I \mathrm{d}z$$

Effective reflectivity density
constant extinction $$\sigma_{vol}(z) = A_v \, \mathrm{e}^{-2\frac{\kappa_e}{\cos\theta}(h_v - z)} = A_v f(z)$$

Backscattered volume intensity $$I_v = \int_{z_{v0}}^{h_v} \sigma_{vol}(z)\mathrm{d}z = \int_{z_{v0}}^{h_v} A_v f(z)\mathrm{d}z$$

InSAR RVOG analysis

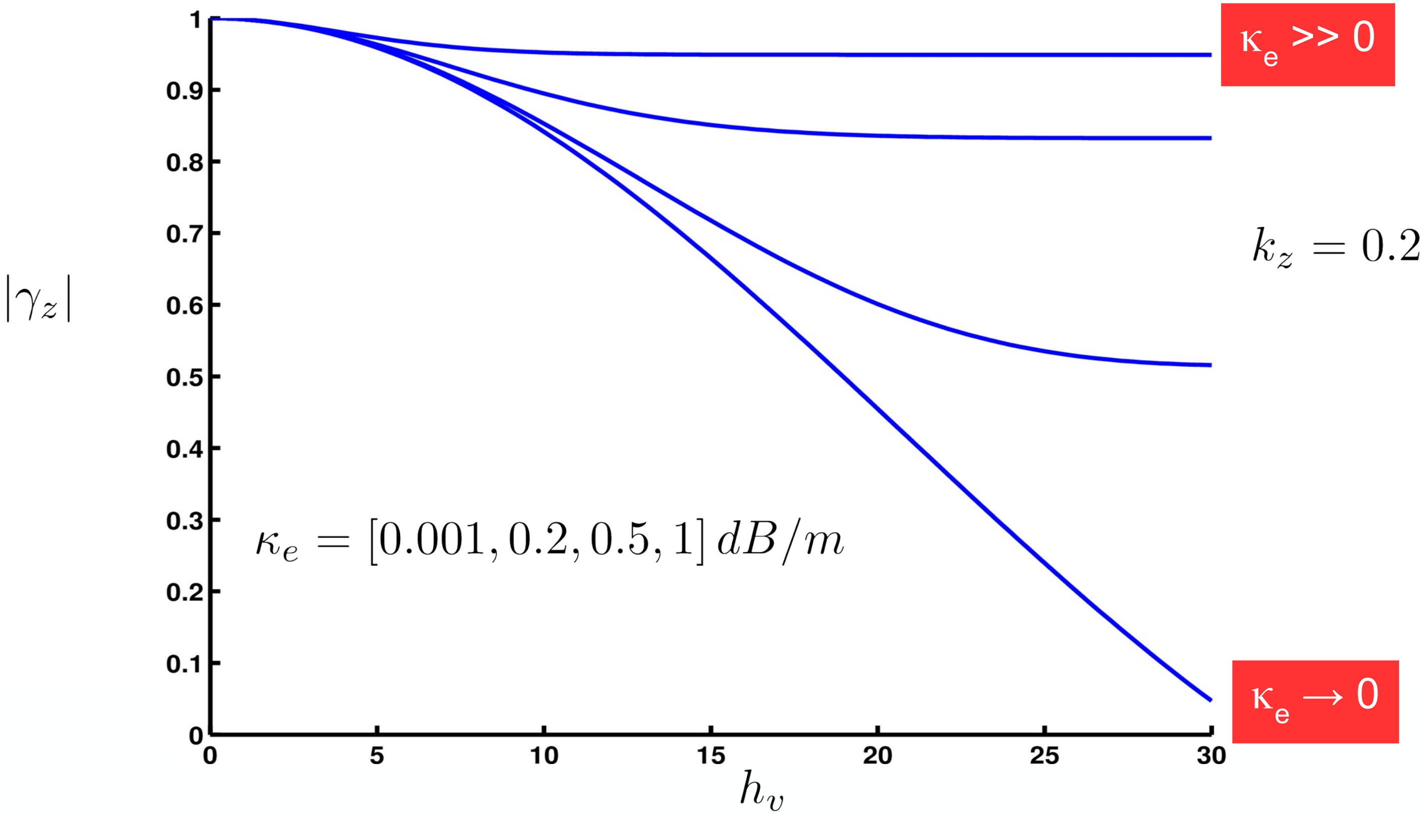

$$\gamma_{vol} = \gamma_z = e^{jk_z z_{v0}} \frac{p}{p_1} \left(\frac{e^{p_1 d} - 1}{e^{pd} - 1} \right) \qquad p = \frac{2\kappa_e}{\cos\theta} \qquad p_1 = \frac{2\kappa_e}{\cos\theta} + jk_z$$

InSAR $|\gamma_z| \rightarrow \hat{h}_v$ ambiguous estimation

InSAR RVOG analysis

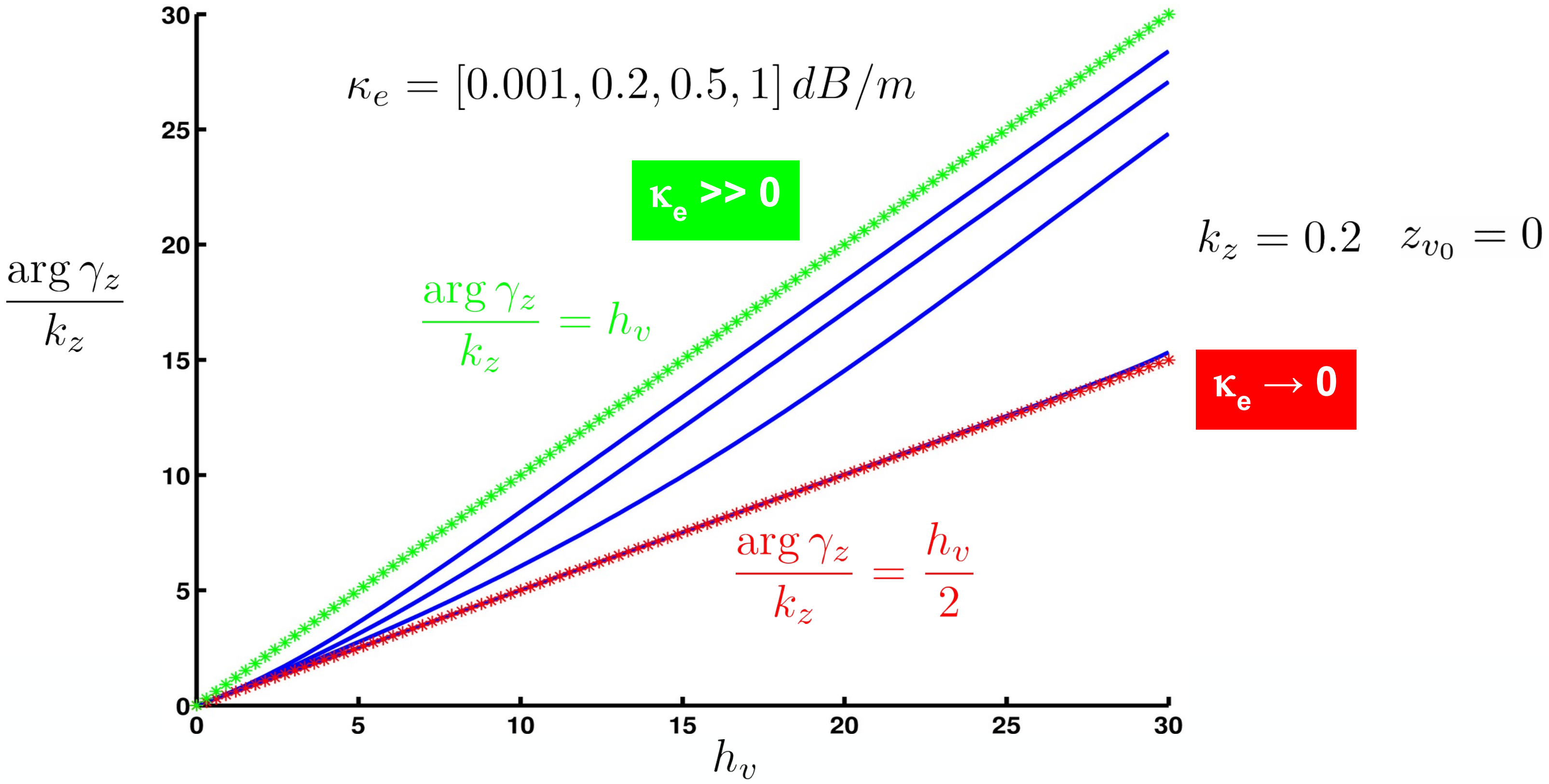

InSAR $\arg(\gamma_z) \rightarrow \hat{h}_v$ **ambiguous estimation**

Unambiguous solution for known $\sigma_{vol}(z)$ **shape :** $|\gamma_z|, \arg(\gamma_z) \rightarrow \hat{h}_v$

InSAR RVOG analysis

Attenuating random volume and ground

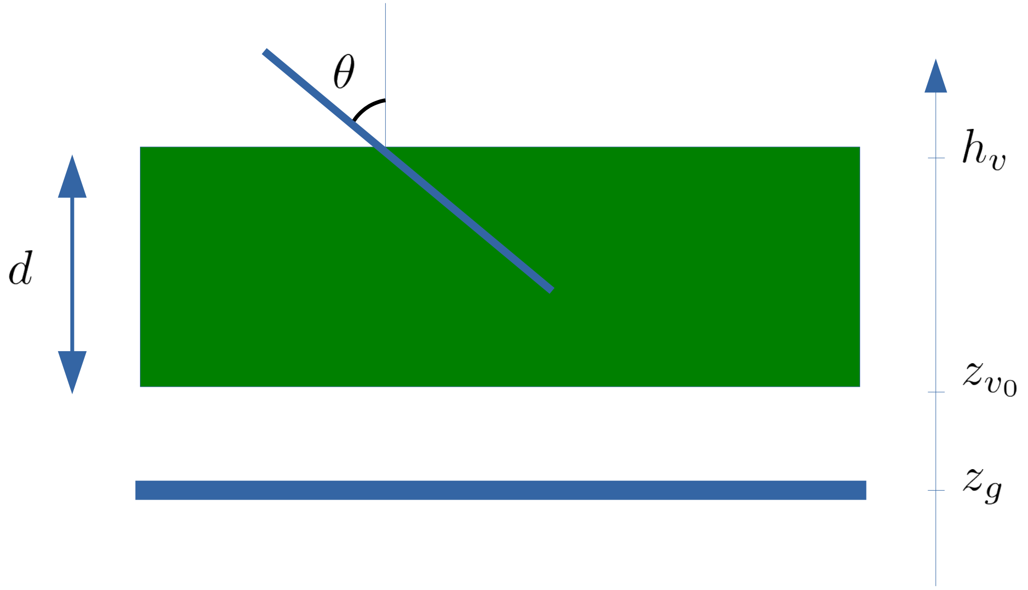

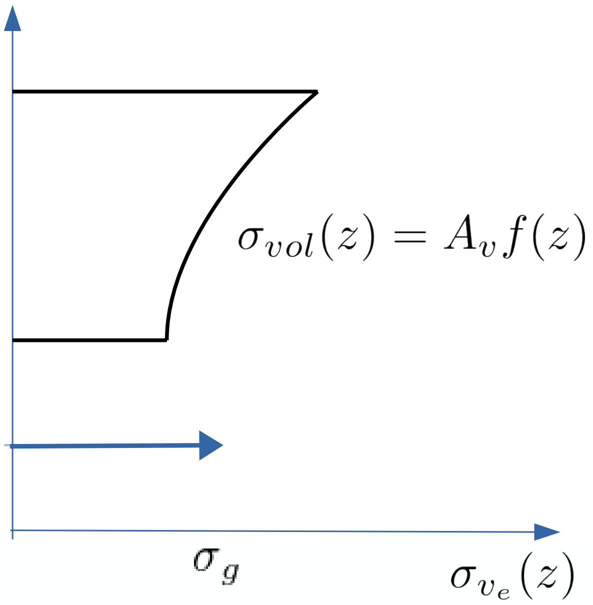

Backscattered volume intensity $I_v = \int_{z_{v0}}^{h_v} \sigma_{vol}(z) \mathrm{d}z = \int_{z_{v0}}^{h_v} A_v f(z) \mathrm{d}z$

Backscattered ground intensity $I_g = f(z_{v0}) \sigma_g = \mathrm{e}^{-2 \frac{\kappa_e}{\cos\theta} d} \sigma_g$

InSAR RVOG analysis

- Coherence formulation $\sigma_{v_e}(z) = \sigma_{vol}(z) + \delta(z - z_g) I_g$

$$\gamma_z = \frac{\int \sigma_{v_e}(z)\, \mathrm{e}^{jk_z z}\, \mathrm{d}z}{\int \sigma_{v_e}(z) \mathrm{d}z} = \frac{\int \sigma_{vol}(z)\, \mathrm{e}^{jk_z z}\, \mathrm{d}z + I_g\, \mathrm{e}^{jk_z z_g}}{\int \sigma_{vol}(z) \mathrm{d}z + I_g}$$

$$\boxed{\gamma_z = \frac{\gamma_{vol} + m\, \mathrm{e}^{jk_z z_g}}{1 + m}}$$

- Ground to volume intensity ratio $m = \dfrac{I_g}{I_v} \in \mathbb{R}^+$

- Coherence interpretation

$$m \rightarrow 0 \Rightarrow \left\{ \begin{array}{ll} \arg \gamma_z & \approx \arg \gamma_{vol} \\ |\gamma_z| & \leq 1 \end{array} \right. \qquad m \rightarrow +\infty \Rightarrow \left\{ \begin{array}{ll} \arg \gamma_z & \approx \phi_g \\ |\gamma_z| & = 1 \end{array} \right.$$

$$0 < m < +\infty \Rightarrow ?$$

InSAR based RVOG analysis: under-determined problem

→ another source of diversity is needed : polarization ?

Pol-InSAR RVOG analysis

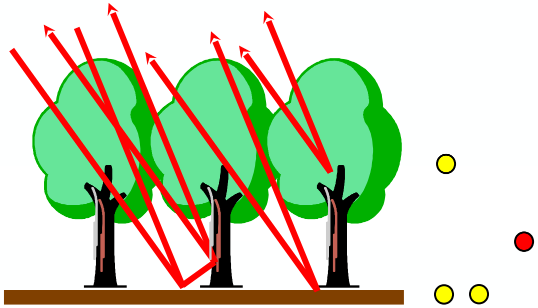

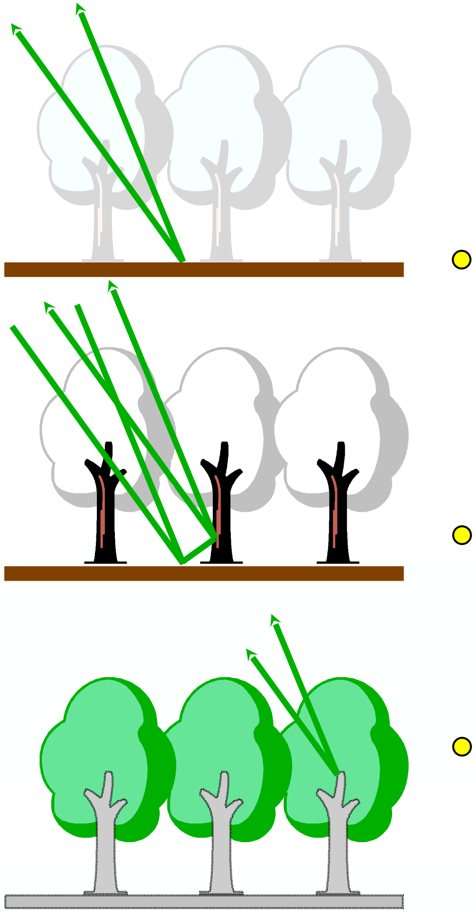

HH+VV

HH-VV

2HV

IN A PERFECT WORLD

Pol-InSAR RVOG analysis

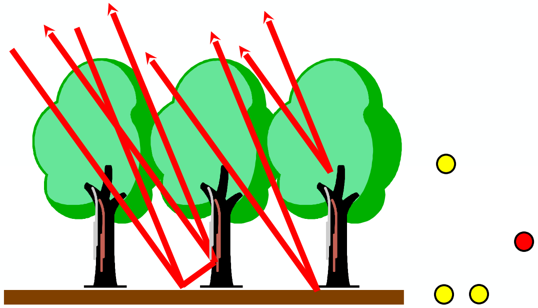

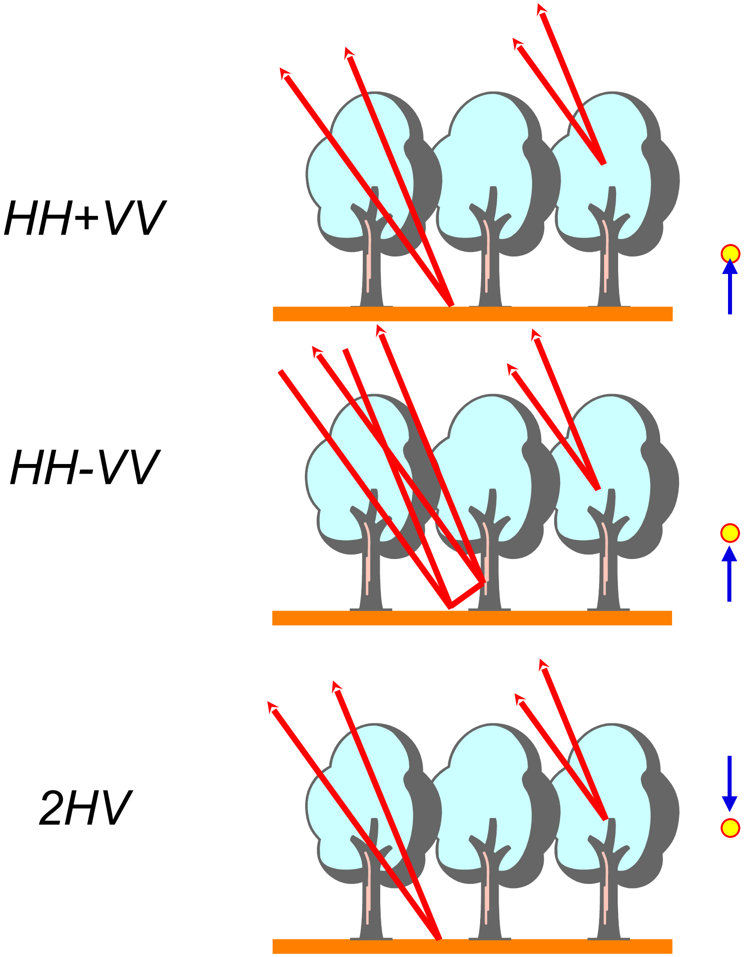

IN A REAL WORLD

Pol-InSAR RVOG analysis

Attenuating random volume and ground : polarimetric case

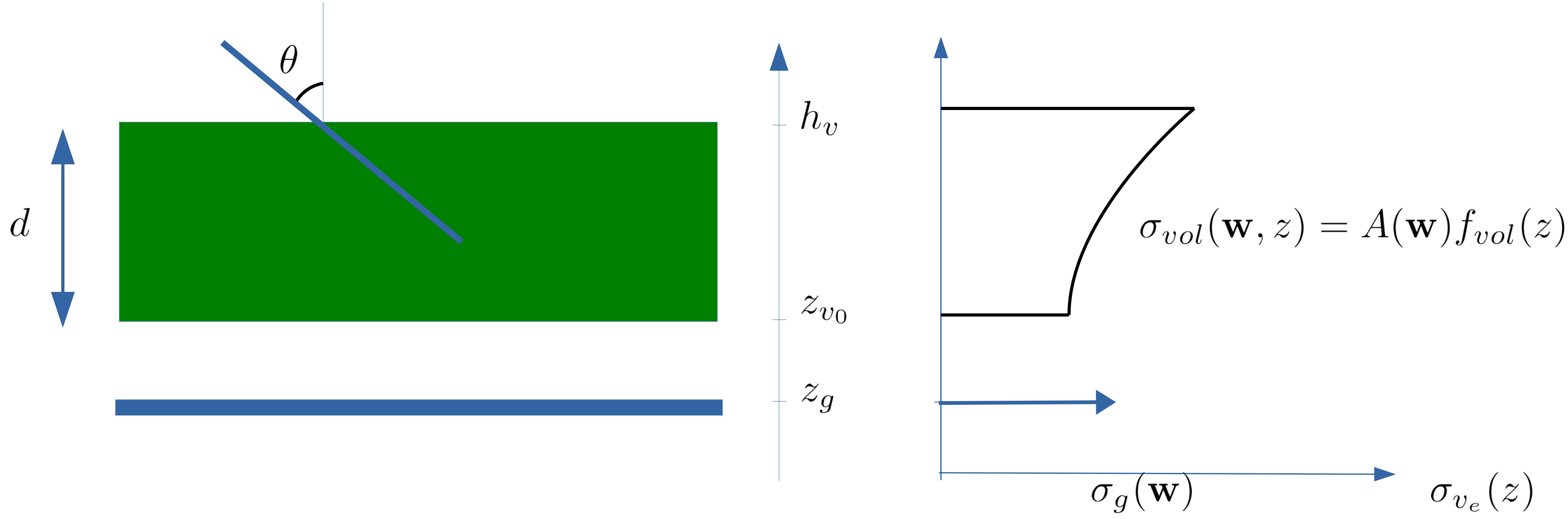

Unpolarized Linear differential extinction

$$\mathrm{d}I = -\kappa_e I \mathrm{d}s = -\frac{\kappa_e}{\cos\theta} I \mathrm{d}z$$

Effective reflectivity density:

$$\sigma_{vol}(\mathbf{w}, z) = A(\mathbf{w}) f_{vol}(z) = \mathbf{w}^H \mathbf{T}_{vol} \mathbf{w} f_{vol}(z)$$

Ground reflectivity

$$\sigma_g(\mathbf{w}, z) = \mathbf{w}^H \mathbf{T}_g \mathbf{w}\, \delta(z - z_g)$$

Attenuating random volume and ground : polarimetric case

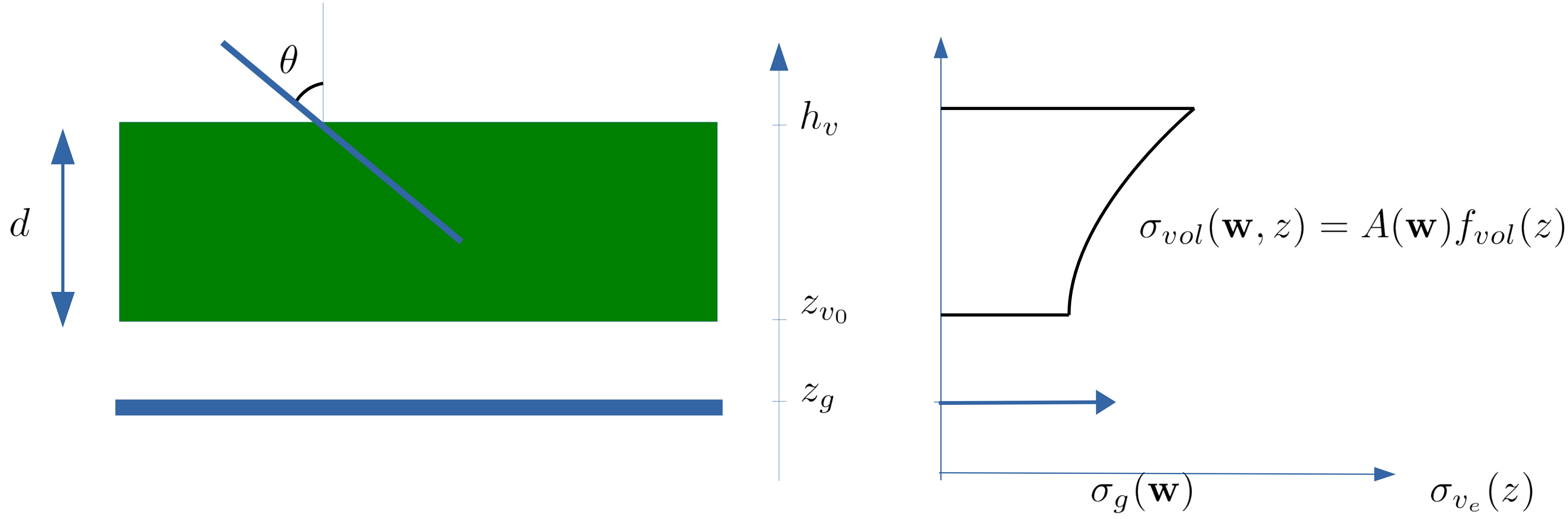

Unpolarized Linear differential extinction

$$\mathrm{d}I = -\kappa_e I \mathrm{d}s = -\frac{\kappa_e}{\cos\theta} I \mathrm{d}z$$

$$I_{vol}(\mathbf{w},z) = \mathbf{w}^H \mathbf{T}_{vol} \mathbf{w} \int_{z_{v0}}^{h_v} f_{vol}(z) \mathrm{d}z$$

$$I_g(\mathbf{w},z) = f_{vol}(z_{v0}) \mathbf{w}^H \mathbf{T}_g \mathbf{w} = \mathrm{e}^{-2\frac{ke}{\cos\theta}d}\, \mathbf{w}^H \mathbf{T}_g \mathbf{w}$$

Pol-InSAR RVOG analysis

Unpolarized volume coherence

$$\gamma_{vol}(\mathbf{w}) = \frac{\int A(\mathbf{w}) f(z)\, \mathrm{e}^{jk_z z}\, \mathrm{d}z}{\int A(\mathbf{w}) f(z) \mathrm{d}z} = \gamma_{vol}$$

- Polarized GVR

$$m(\mathbf{w}) = \frac{I_g(\mathbf{w})}{I_{vol}(\mathbf{w})}$$

- PolinSAR coherence

$$\gamma_z(\mathbf{w}) = \frac{\gamma_{vol} + m(\mathbf{w})\, \mathrm{e}^{jk_z z_g}}{1 + m(\mathbf{w})}$$

- Coherence interpretation : find a polarisation vector so that

Plausible

$$m \to 0 \Rightarrow \begin{cases} \arg \gamma_z & \approx \arg \gamma_{vol} \\ |\gamma_z| & \leq 1 \end{cases}$$

Unlikely

$$m \to +\infty \Rightarrow \begin{cases} \arg \gamma_z & \approx \phi_g \\ |\gamma_z| & = 1 \end{cases}$$

$$0 < m < +\infty \Rightarrow ?$$

RVOG COHERENCE MODEL : LINE MODEL

$$\gamma_z(\mathbf{w}) = \frac{\gamma_{vol} + m(\mathbf{w})\,\mathrm{e}^{jk_z z_g}}{1 + m(\mathbf{w})}$$

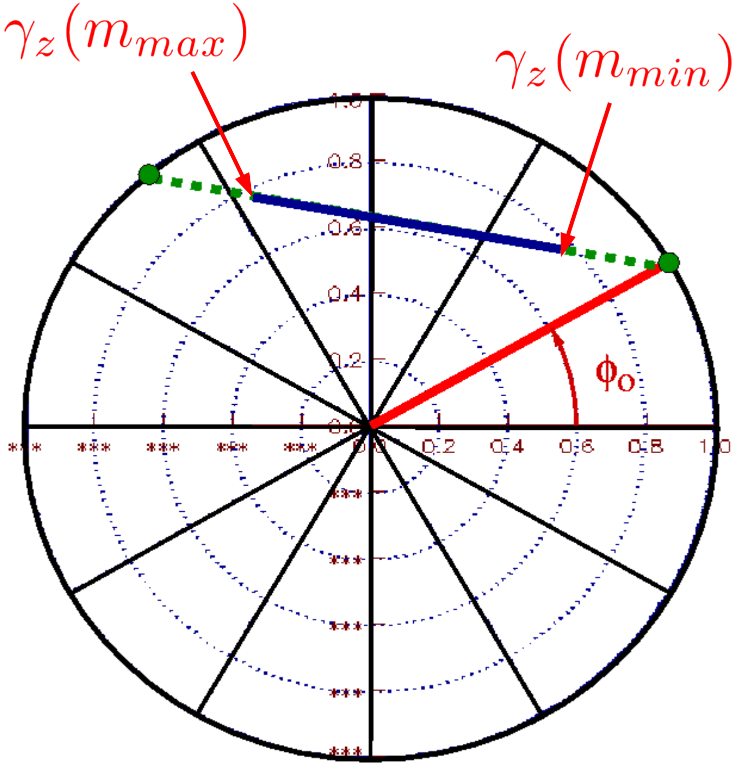

Equation of a straight line in the complex plane

Ground estimation through interpolation

PolinSAR RVOG solution :

- **some estimates remain ambiguous, requires phase diversity**
- **assumes a shape for volume extinction**

TomoSAR (MB-Pol-InSAR) RVOG analysis

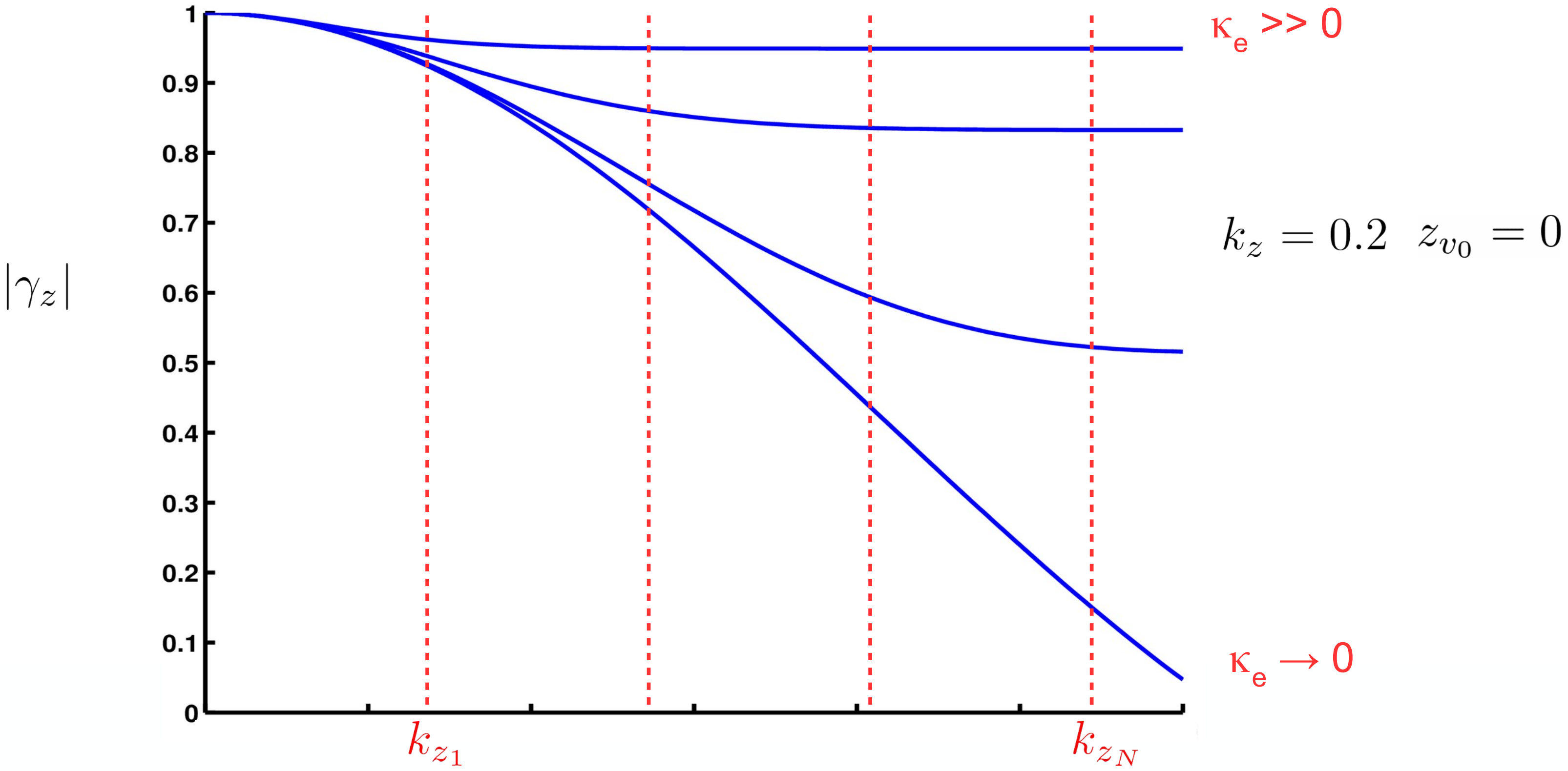

Additional spatial diversity

$\{\gamma_z(k_{z_n})\}_{n=1}^{N} \longrightarrow$

- Unambiguous height estimation for known f(z) shape
- Estimation of f(z) or **non-parametric analysis**
- PolTomoSAR (MB-Pol-InSAR) : $\{\gamma_z(k_{z_n}), \mathbf{w}\}_{n=1}^{N}$

InSAR phases, polarization & TomoSAR

L-band BIOSAR2, Capon tomograms

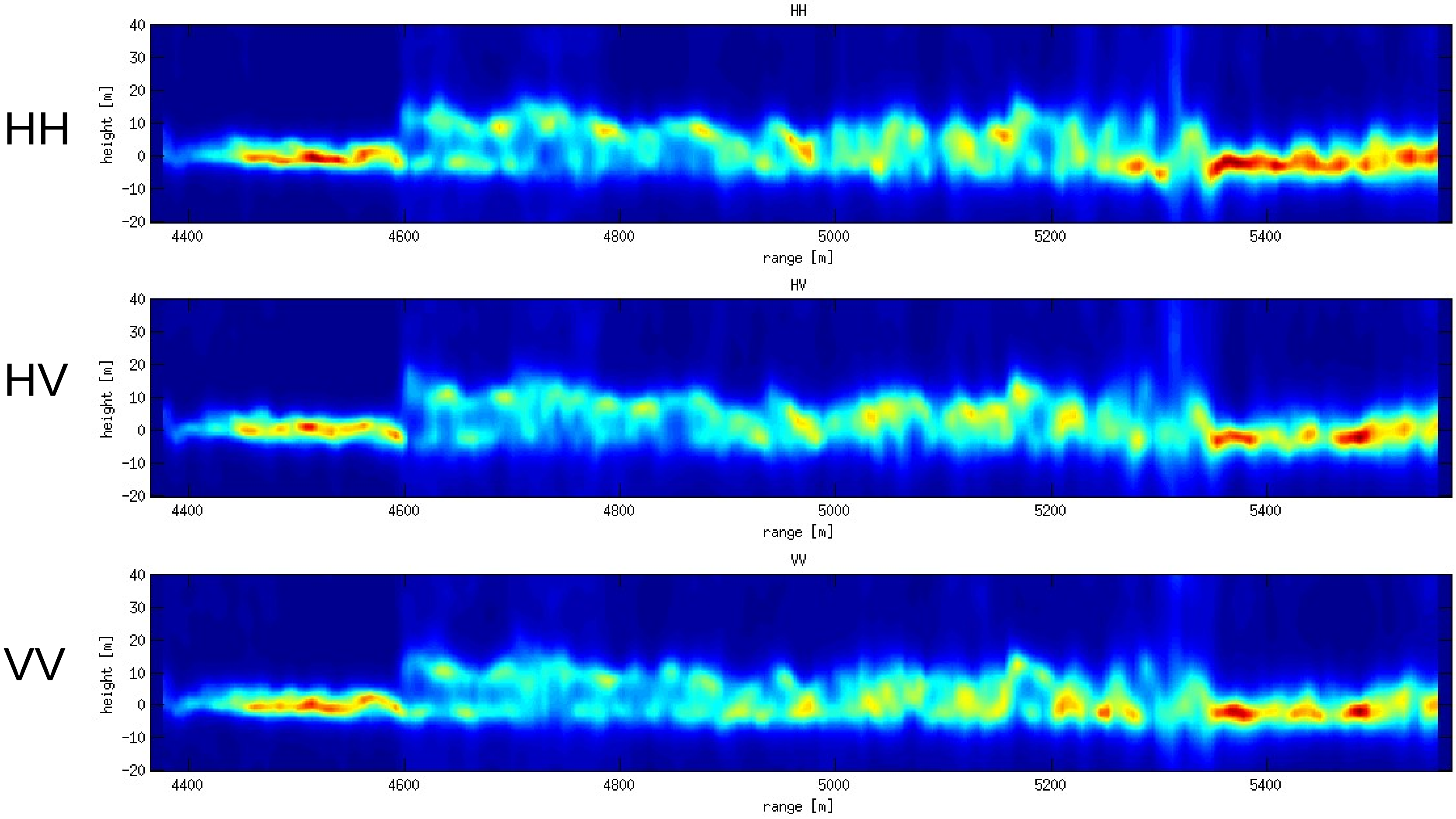

InSAR phases, polarization & TomoSAR

Polarimetric diversity POL-InSAR phase center heights

$h(\phi_{12})$

$h(\phi_{16})$

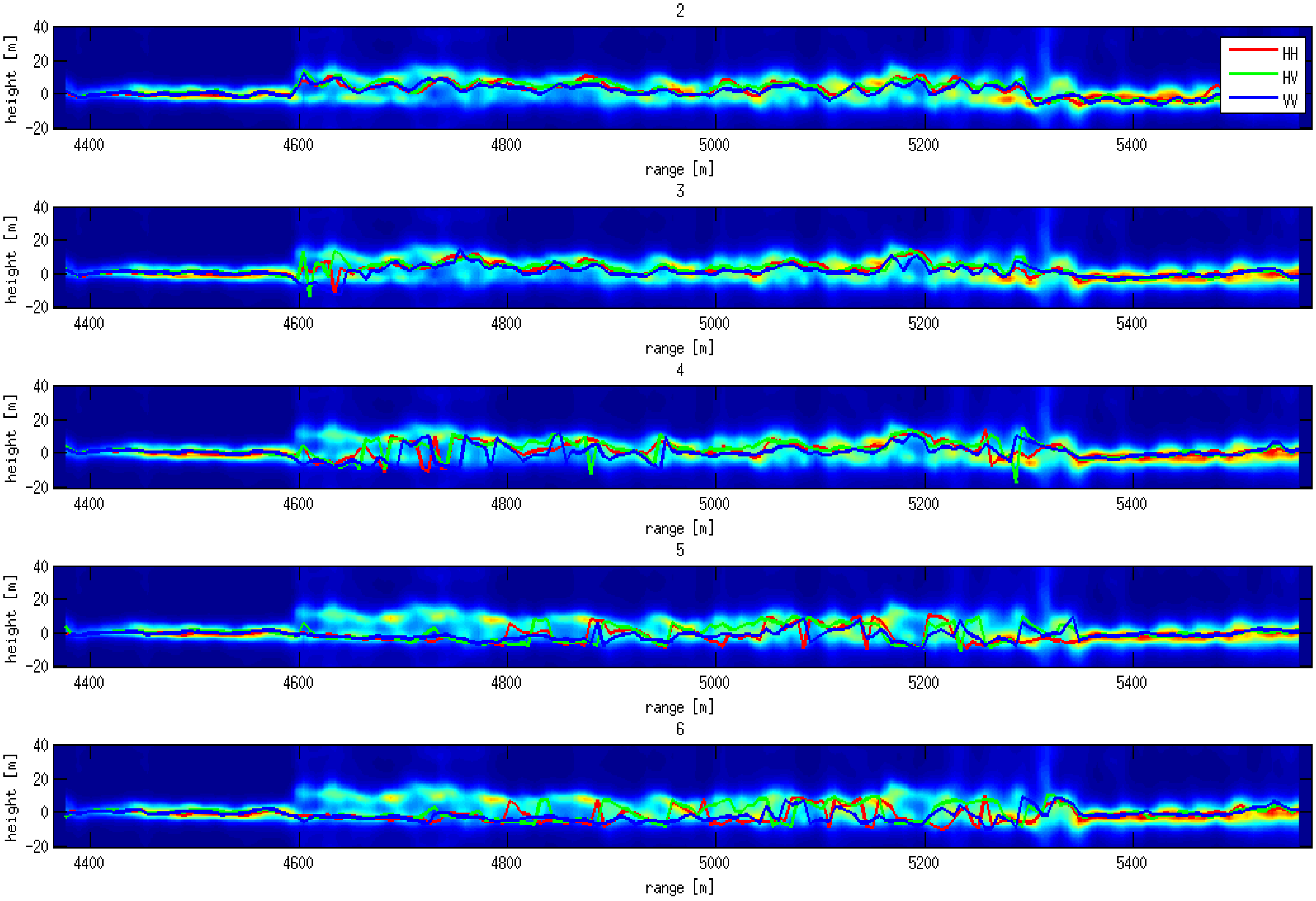

InSAR phases, polarization & TomoSAR

Polarimetric diversity

POL-InSAR phase center heights

$h(\phi_{12})$

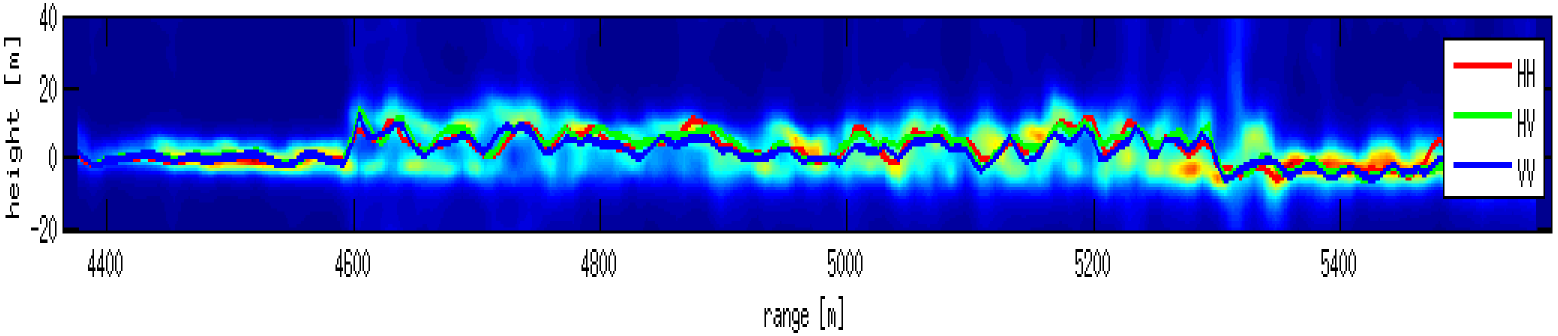

$h(\phi_{16})$

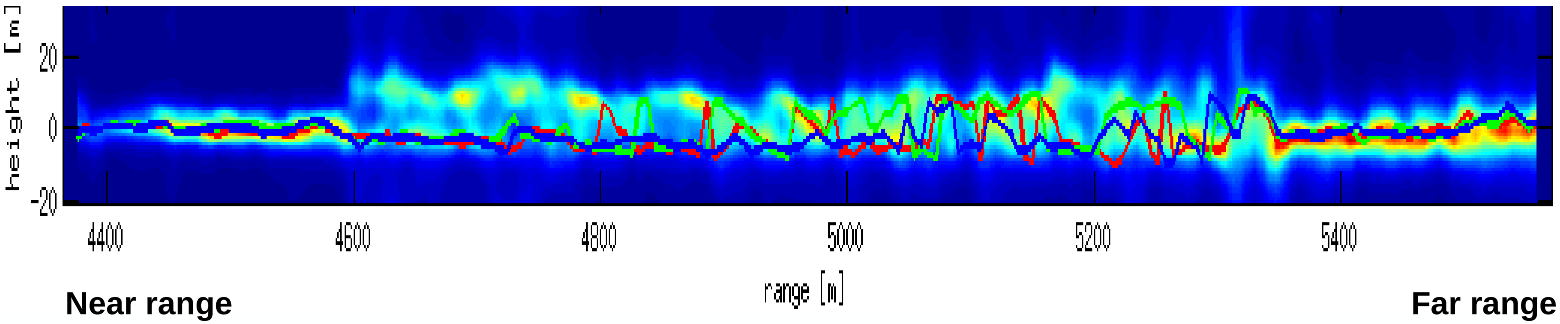

Near range **Far range**

Single-baseline PolinSAR:

- Phase Center height diversity not always guaranteed
- Requires **specific k_z** (baseline) values: **adequate volume decorrelation**

InSAR phases, polarization & TomoSAR

Spatial diversity MB-InSAR phase center heights

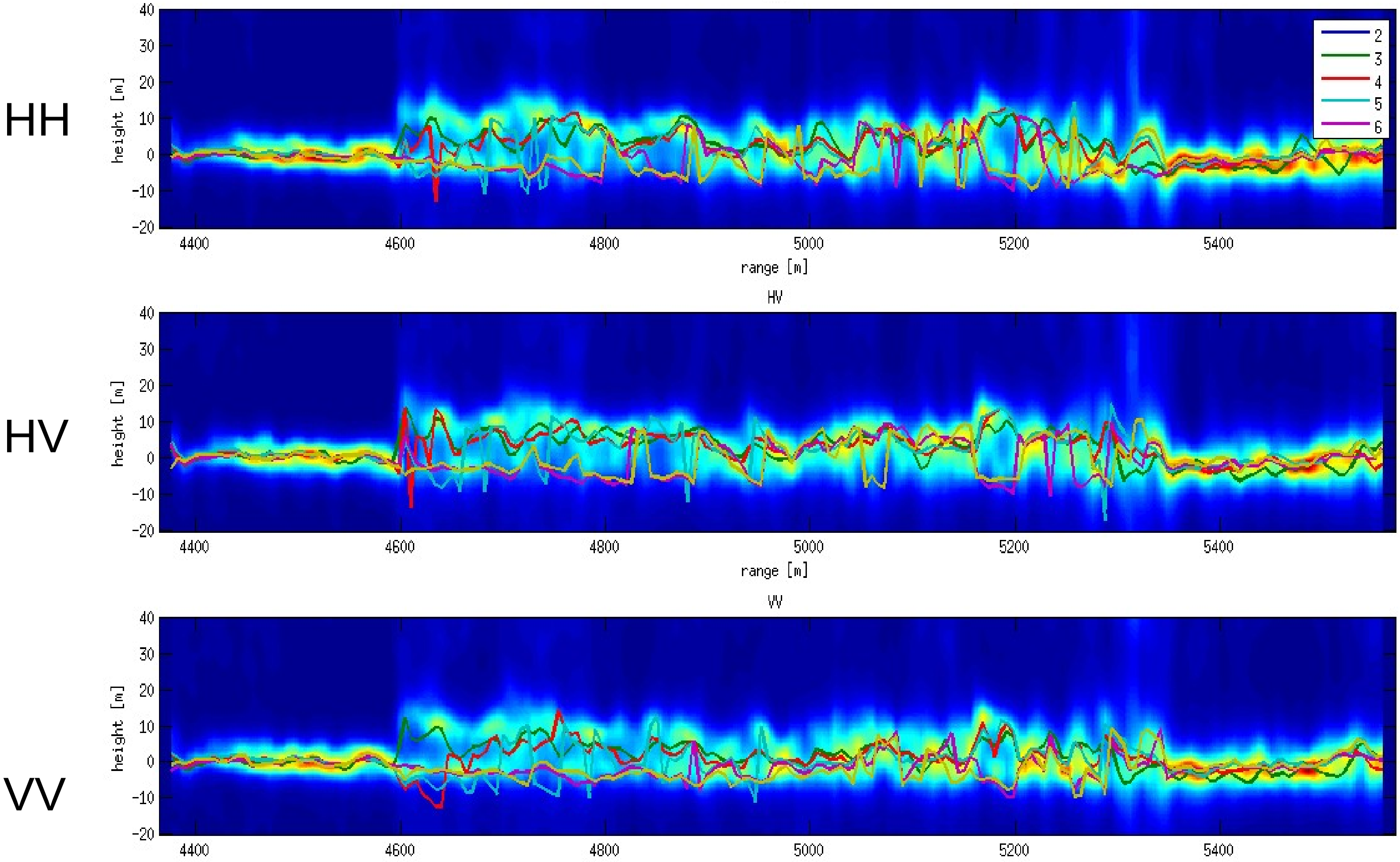

Tomography

Phase Center height diversity through baseline agility

Polarimetric SAR imaging of 3-D scenes

Multibaseline InSAR (MB-InSAR) tomography

Several mixed scatterers → many across-track positions

Acquisition geometry

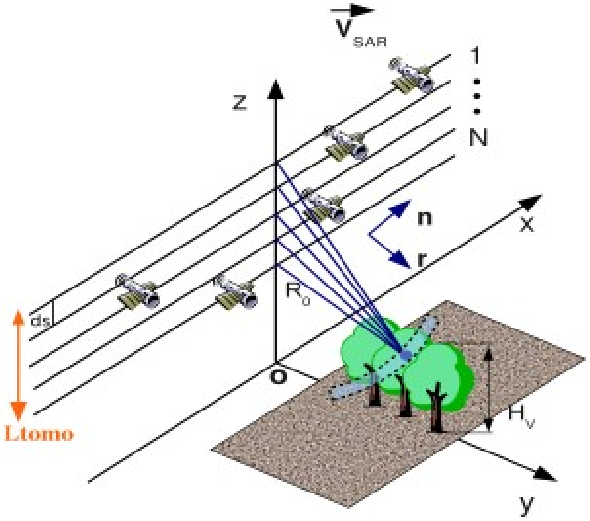

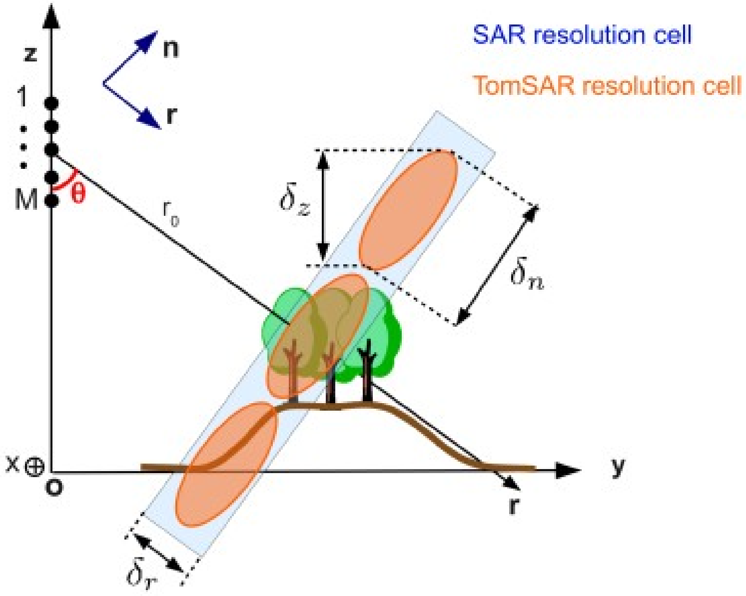

Processing options

- Direct 3-D imaging: coherent combination of M SAR acquistions

- M x 2-D focusing & coherent processing of M-InSAR quantities

Polarimetric SAR imaging of 3-D scenes

Direct 3-D imaging of an Alpine glacier at L band

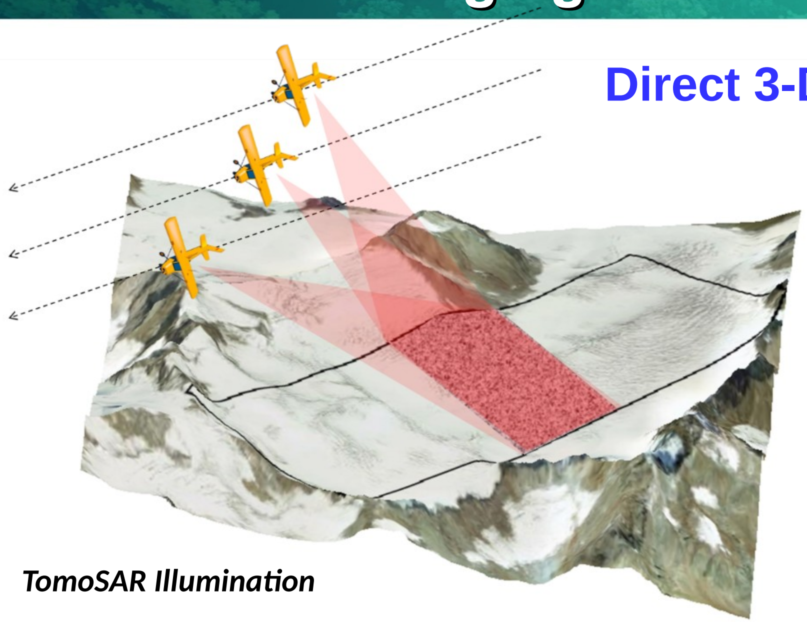

TomoSAR Illumination

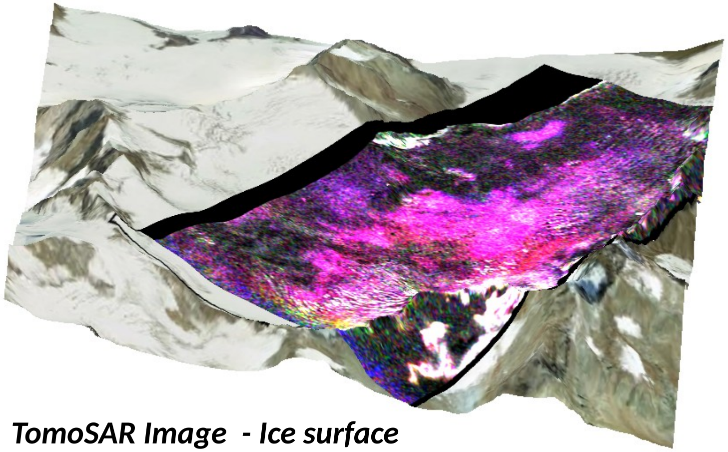

TomoSAR Image - Ice surface

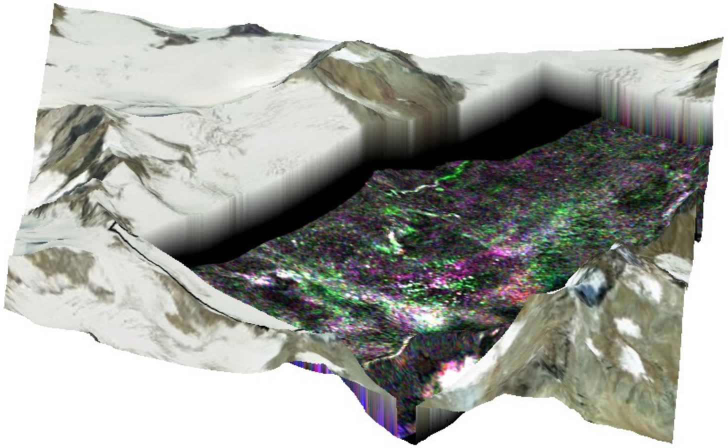

TomoSAR Image - 25 m below the Ice surface

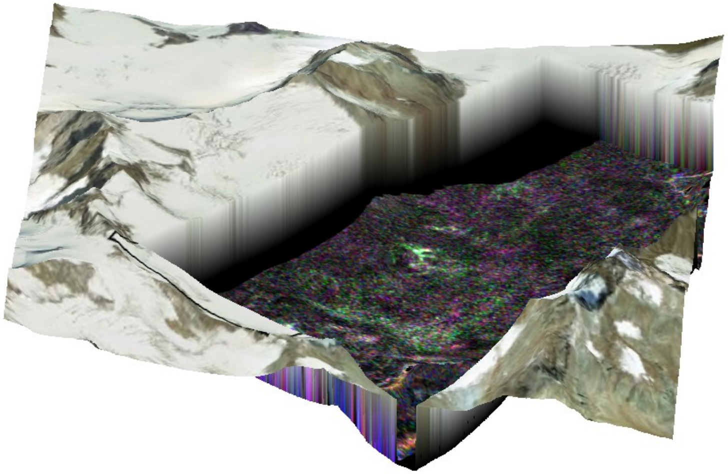

TomoSAR Image - 50 m below the Ice surface

L. Ferro-Famil & S.Tebaldini

Polarimetric SAR imaging of 3-D scenes

BIOSAR II, Boreal forest, L band

Forest height [m]

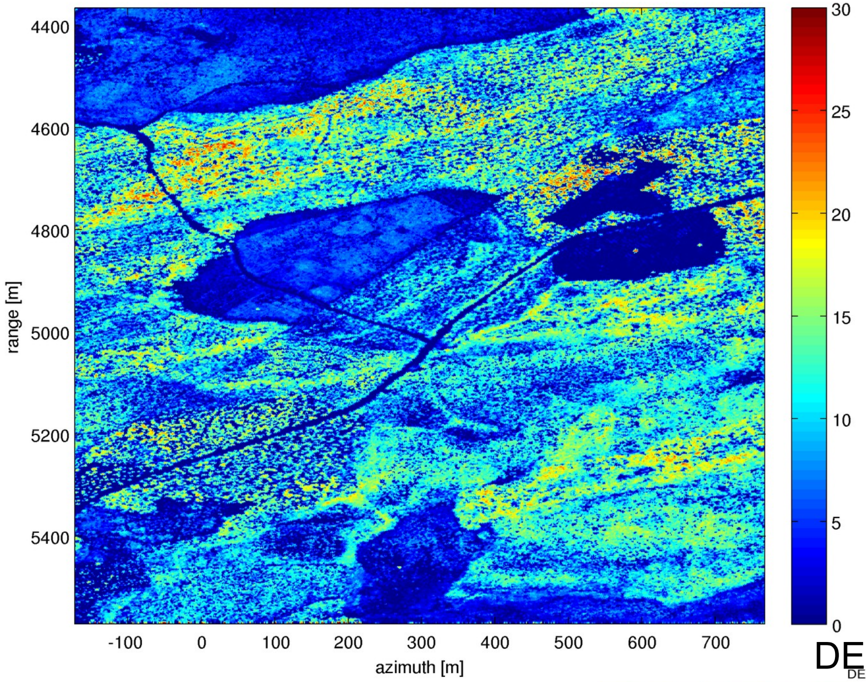

HH intensity [dB]

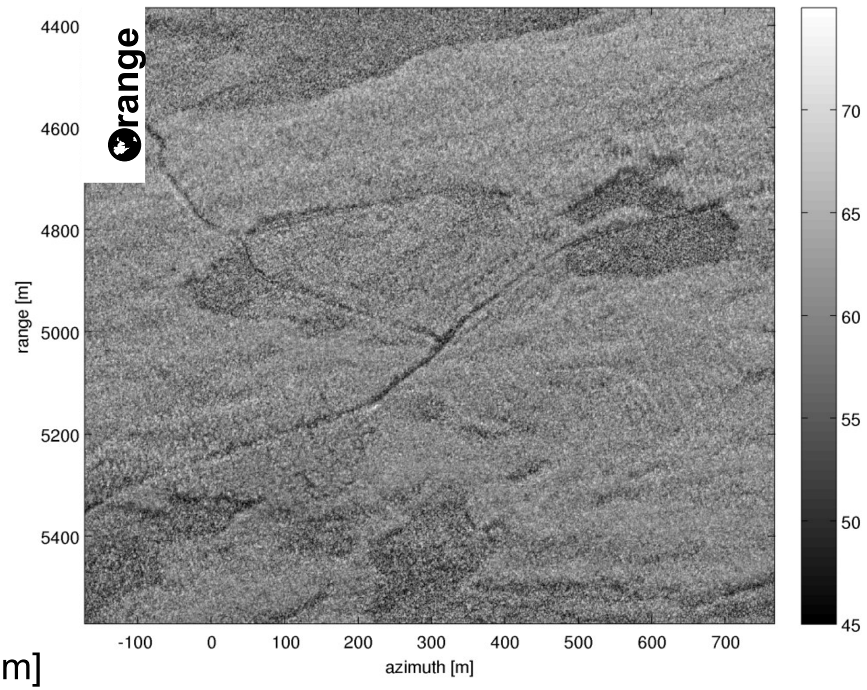

DEM [m]

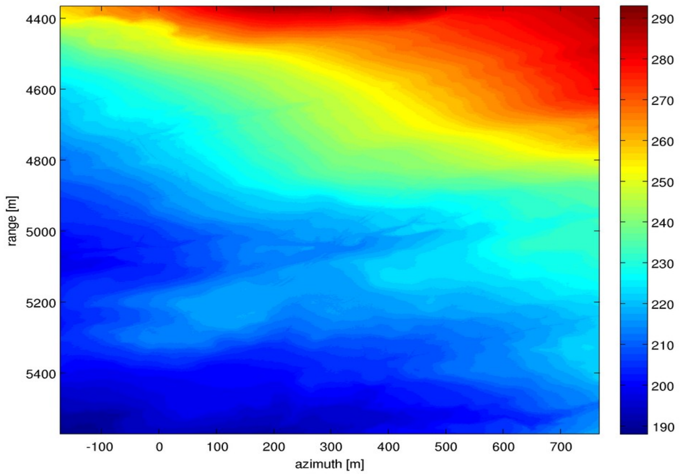

Polarimetric SAR imaging of 3-D scenes

M x 2-D imaging of a Boreal forest at L band

SAR: 2D Imaging

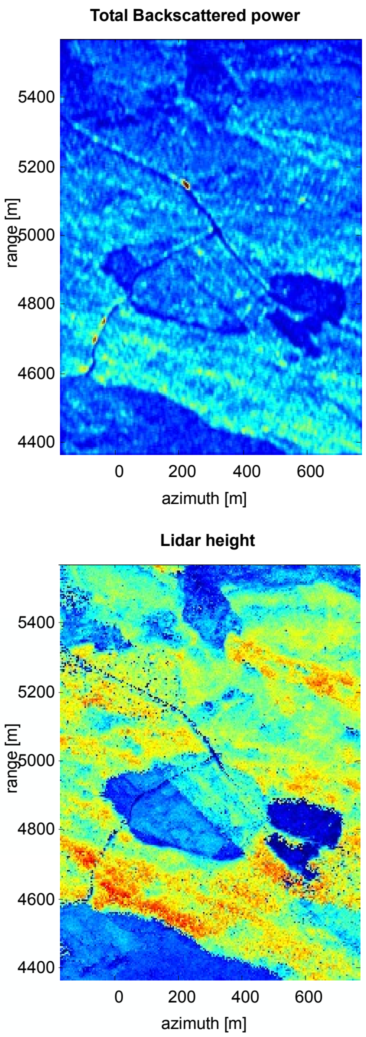
Total Backscattered power

Lidar height

TomoSAR: 3D Imaging

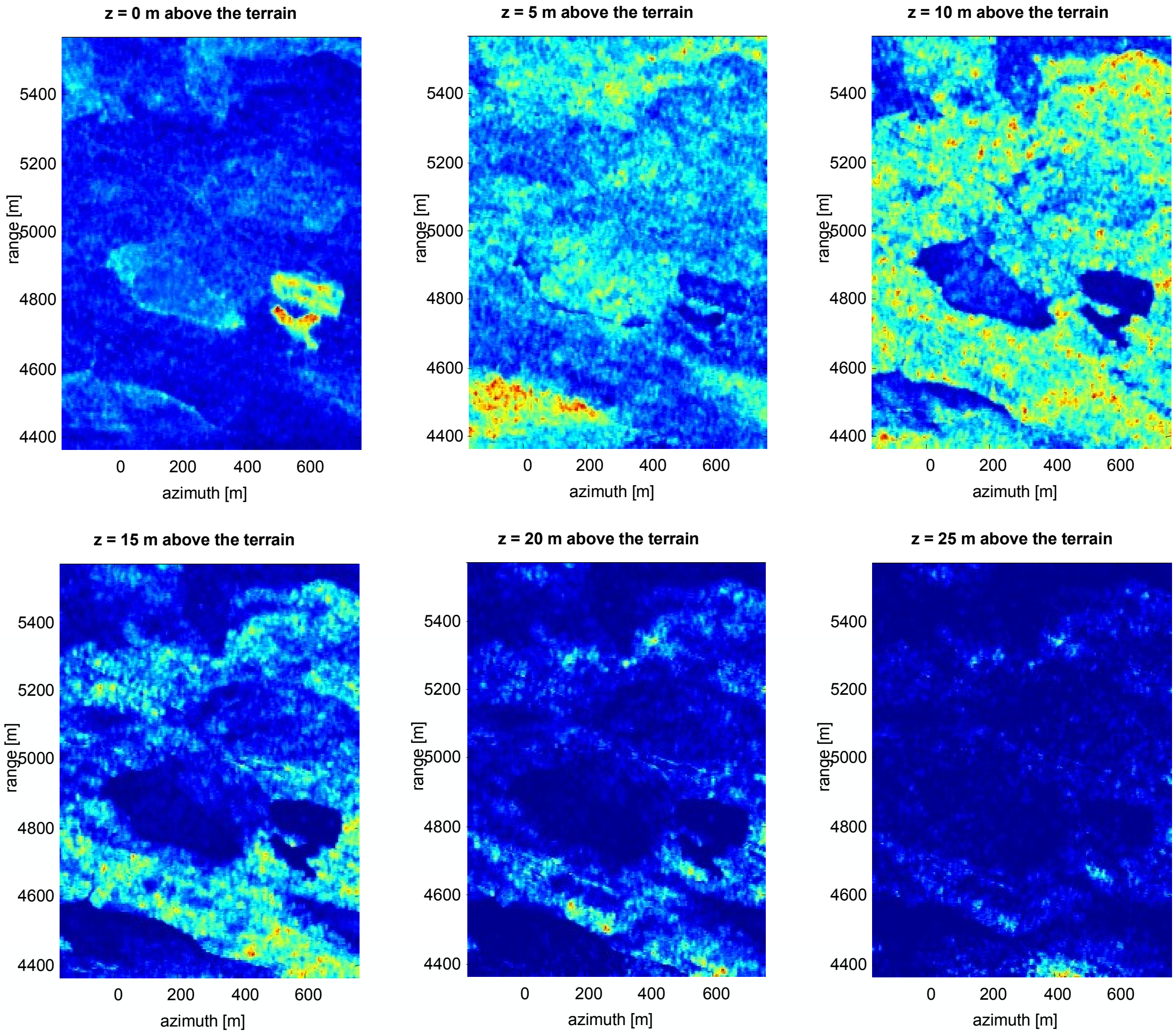
z = 0 m above the terrain

z = 5 m above the terrain

z = 10 m above the terrain

z = 15 m above the terrain

z = 20 m above the terrain

z = 25 m above the terrain

- ○ Power distribution in height direction
- ○ Full-resolution CAPON

L. Ferro-Famil & S.Tebaldini

Polarimetric SAR imaging of 3-D scenes

Tree height and ground topography estimation

Hybrid spectral approach

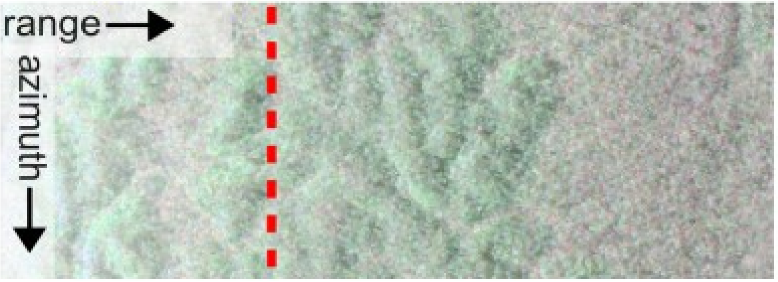

- Estimated profiles match LiDAR
- HH profiles : similar to FP case

LiDAR — TomSAR —

HH

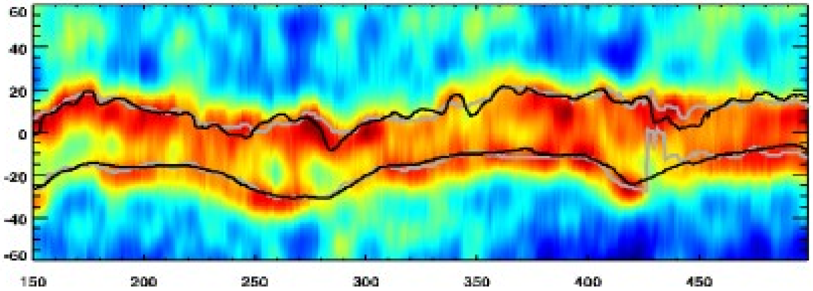

VV

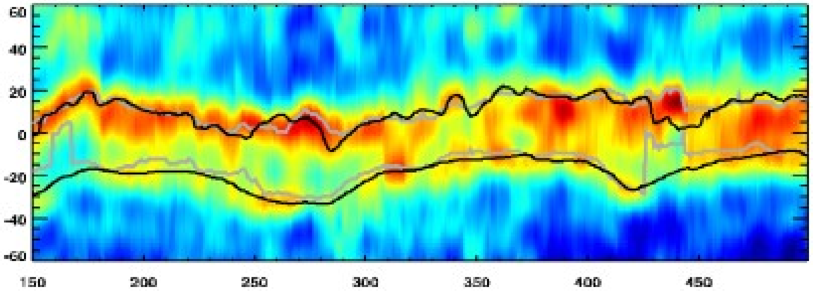

HV

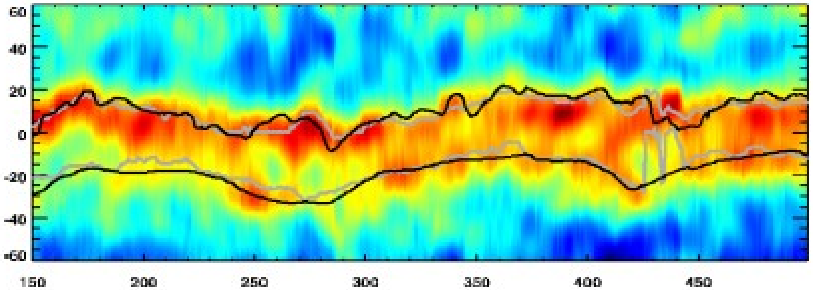

FP

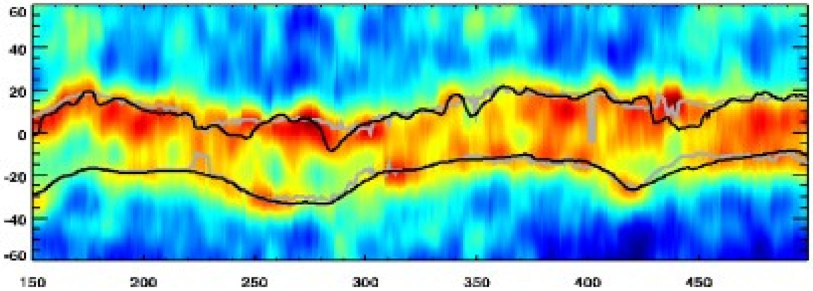

Polarimetric SAR imaging of 3-D scenes

Urban areas

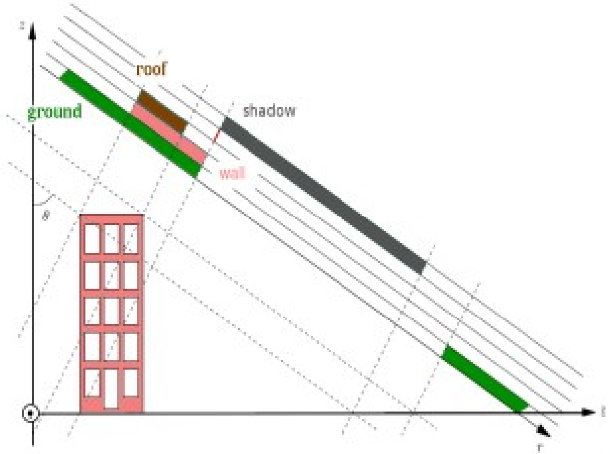

Mixture of several contributions in the elevation direction

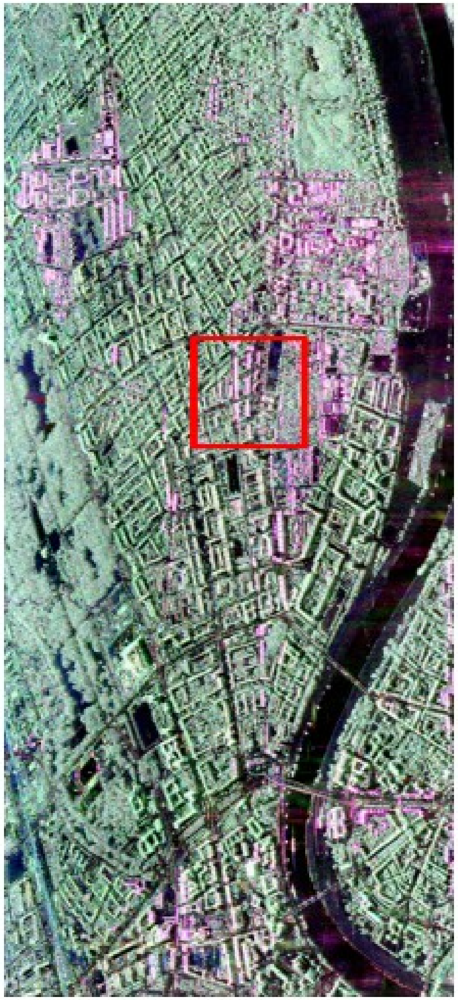

Pauli-coded SAR image

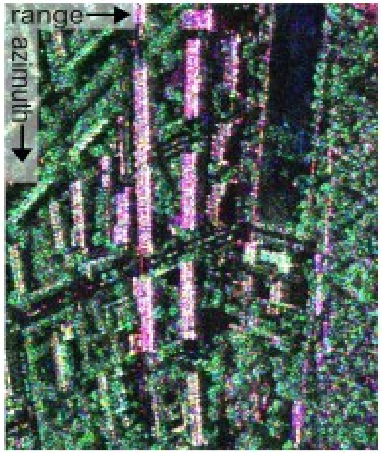

Optical image

Polarimetric SAR imaging of 3-D scenes

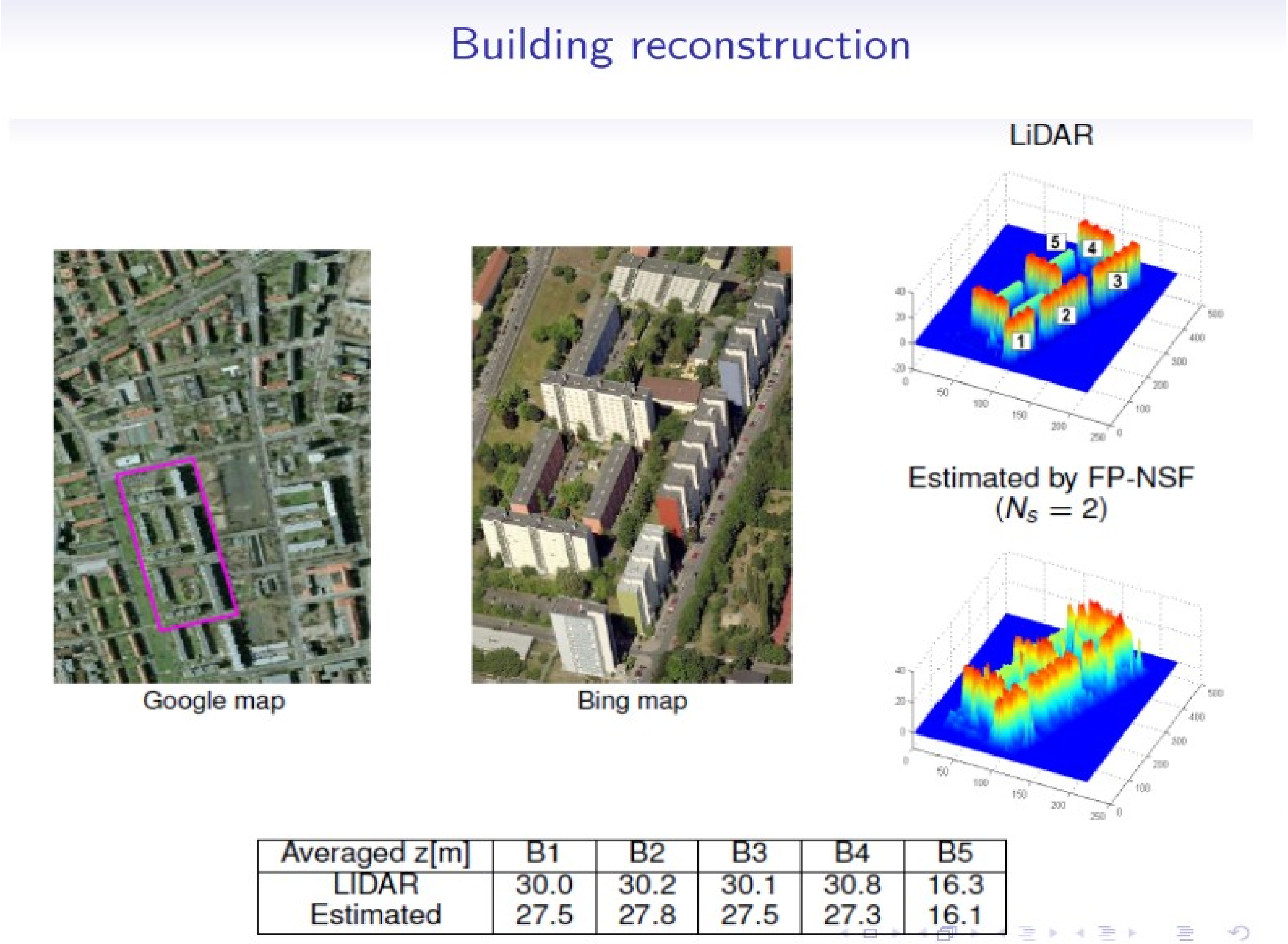

Building reconstruction

Google map

Bing map

LiDAR

Estimated by FP-NSF
$(N_s = 2)$

Averaged z[m]	B1	B2	B3	B4	B5
LIDAR	30.0	30.2	30.1	30.8	16.3
Estimated	27.5	27.8	27.5	27.3	16.1

From 3-D
Synthetic Aperture Imaging
To the Beamformer

2-D SAR impulse response

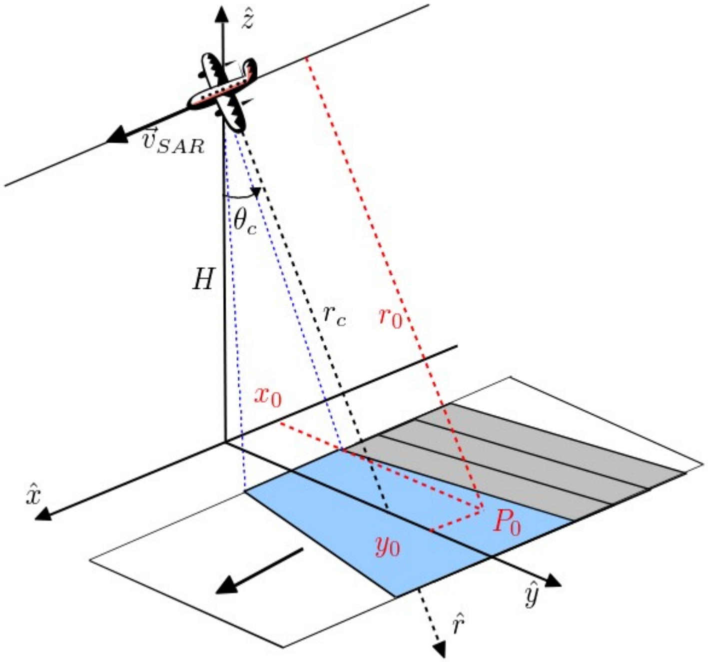

2-D focused signal (x-r domain)

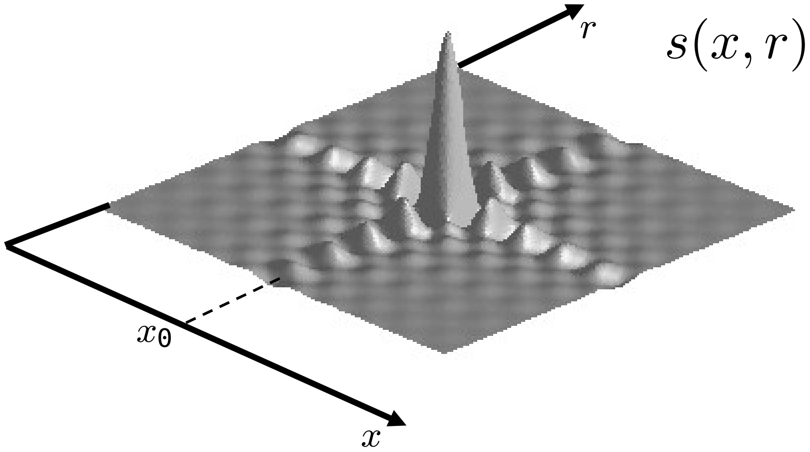

$s(x,r) =$	a_c	→ **complex reflection coefficient**
	$h_r(d - r_0)$	→ delayed range impulse response
	$h_a(x - x_0)$	→ delayed azimuth impulse response
	$\exp(-j\frac{4\pi}{\lambda_c} r_0)$	→ **two-way propagation phase**

2-D SAR imaging

SAR imaging: coherent integration of a reflectivity density

$$s(x,r) = \int a_c(x',r',\nu')h(x'-x,r'-r)\,\mathrm{e}^{-j\frac{4\pi}{\lambda_c}d(x'-x,r'-r)}\,\mathrm{d}x'\mathrm{d}r'\mathrm{d}\nu$$

$$s(x,r) \approx \int_{\mathcal{C}} a_c(x,r,\nu)\,\mathrm{e}^{-jk_c r(\nu)}\,\mathrm{d}\nu$$

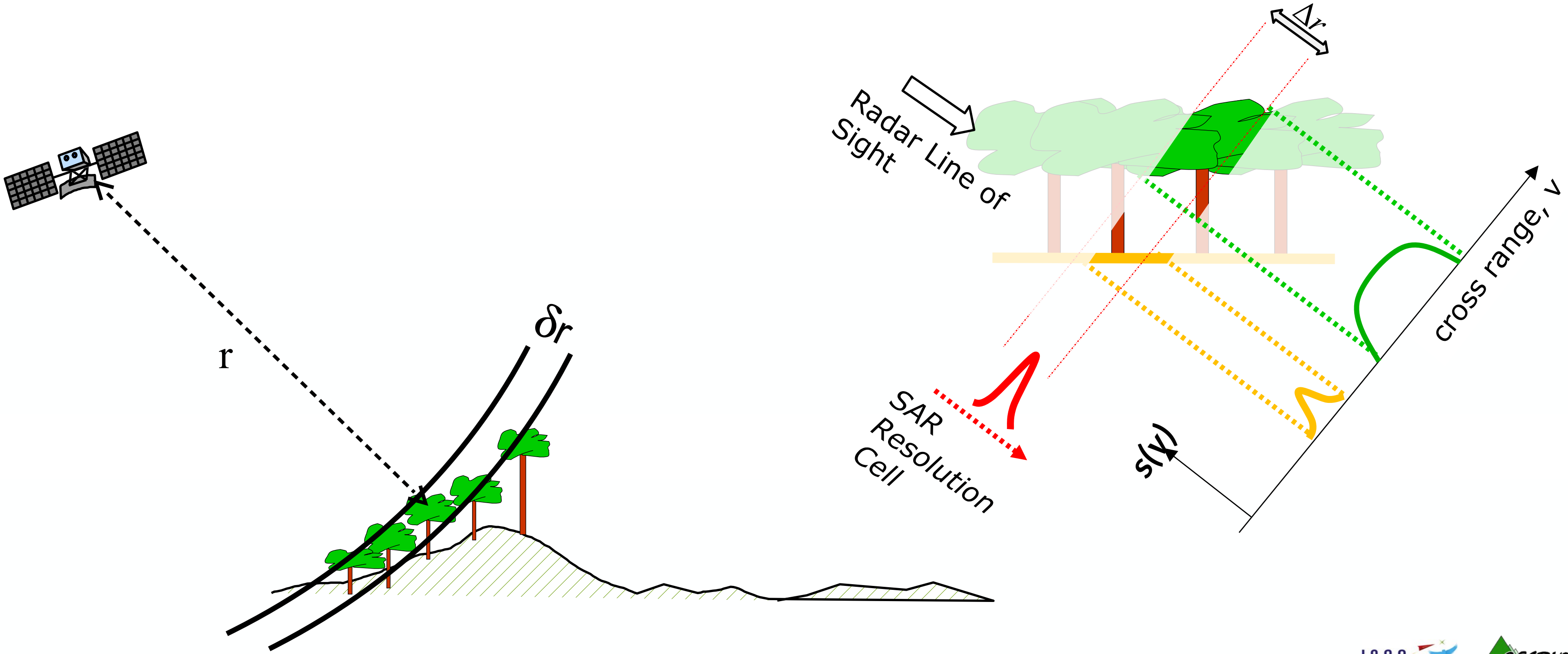

3-D SAR imaging

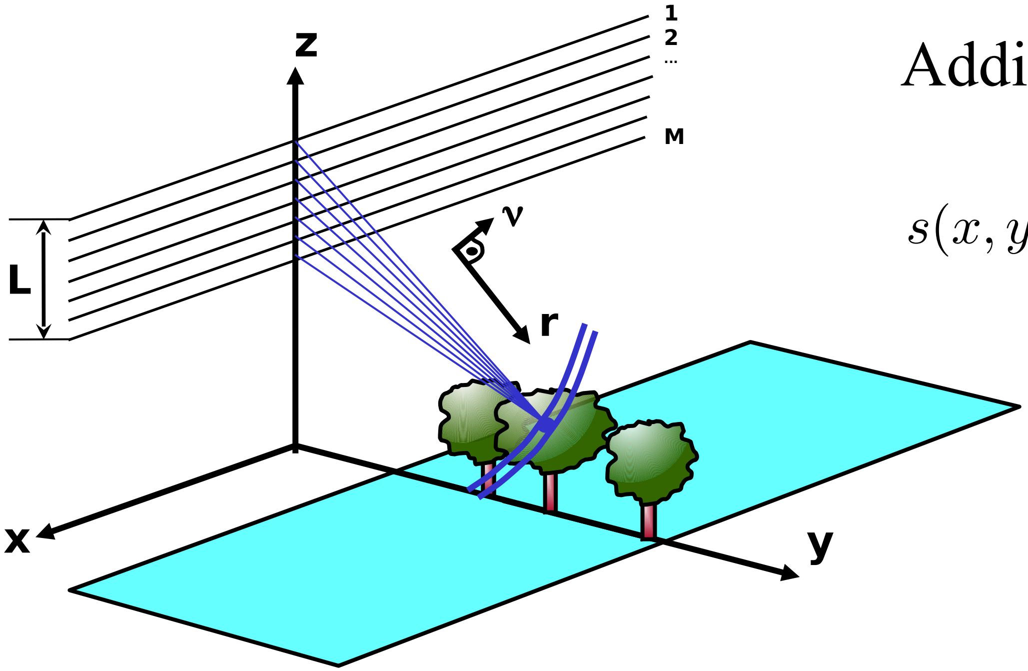

Additional aperture in elevation:

$$2\text{-D} \xrightarrow[M]{} 3\text{-D focusing}$$

$$s(x,y,z) = \sum_{i=1} s_i(x, r(y,z))\, \mathrm{e}^{jk_c r(y,z)}$$

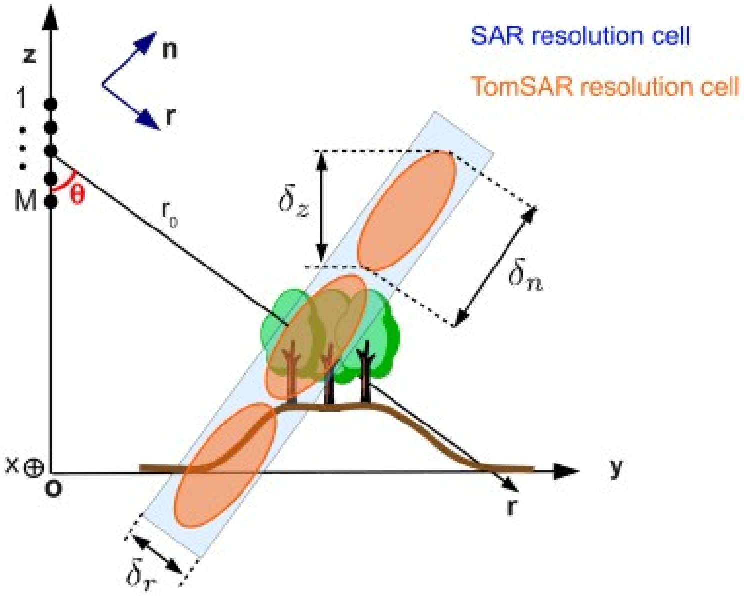

Vertical aperture : L_{tomo}

Resolution : $\delta_z = \delta_n \sin\theta$ with $\delta_n = \frac{\lambda R_0}{2L_{tomo}}$

3-D SAR imaging

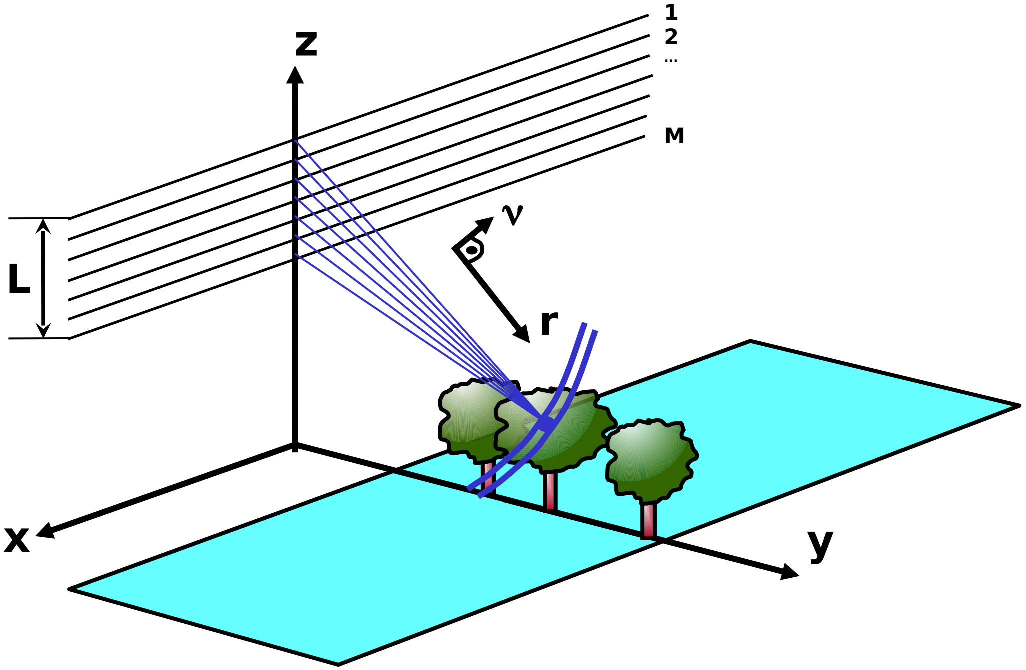

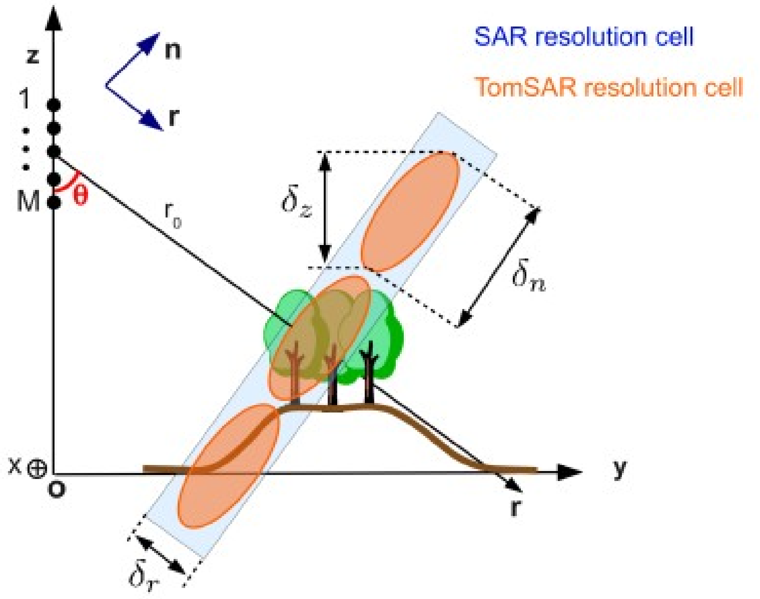

$$s(x,y,z) = \sum_{i=1}^{M} s_i(x, r(y,z))\, \mathrm{e}^{jk_c r(y,z)}$$

Interpolation

HF term

3-D SAR imaging

Co-registration on a reference plane

Valid for $z \in z_{ref} \pm \Delta z_{val}/2$

$$s(x,y,z) = \sum_{i=1}^{M} s_i(x, r(y,z))\, \mathrm{e}^{jk_c r(y,z)}$$

Discretization

NN-interp.

$$s(x,y,z) = \sum_{i=1}^{M} s_i(x, r_{i_{ref}})\, \mathrm{e}^{jk_c r_i}$$

$$r_i \approx r_{i_{ref}} + k_{z_i} z$$

Flat earth

Elevation

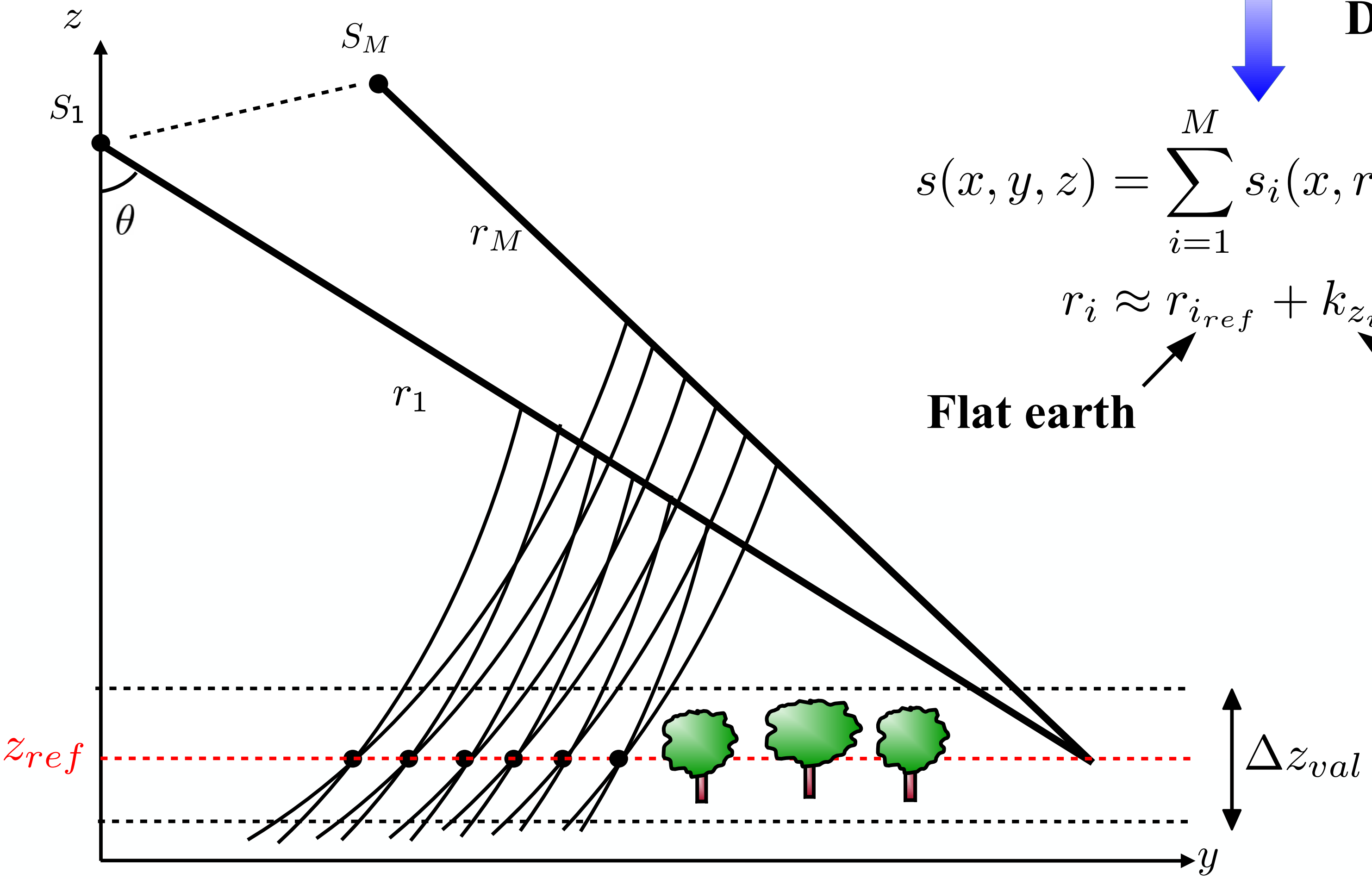

3-D SAR imaging

Co-registration on a reference plane

Valid for $z \in z_{ref} \pm \Delta z_{val}/2$

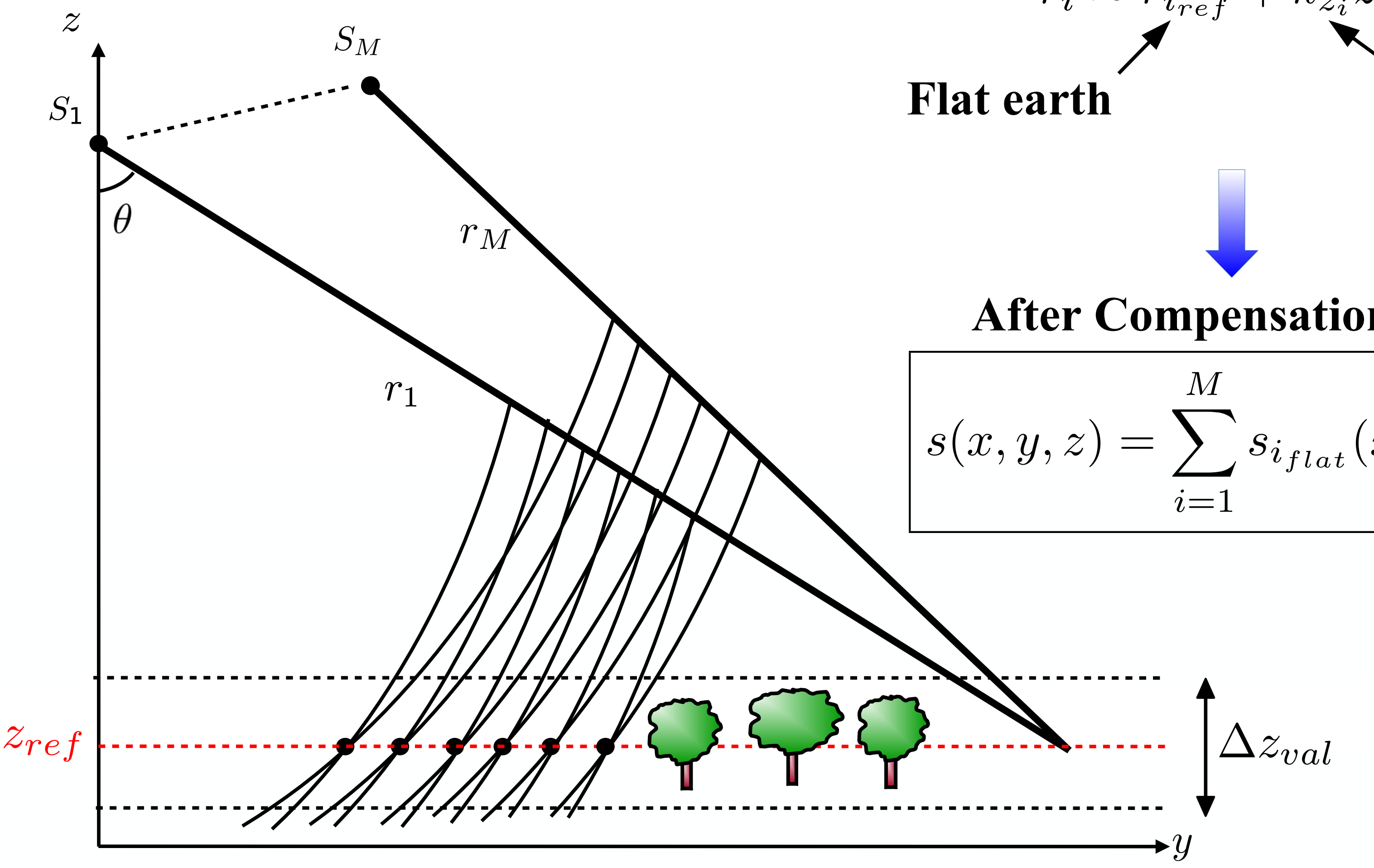

$$s(x,y,z) = \sum_{i=1}^{M} s_i(x, r_{i_{ref}})\, e^{jk_c r_i}$$

$$r_i \approx r_{i_{ref}} + k_{z_i} z$$

Flat earth **Elevation**

After Compensation

$$\boxed{s(x,y,z) = \sum_{i=1}^{M} s_{i_{flat}}(x, r_{i_{ref}})\, e^{jk_{z_i} z}}$$

3-D SAR imaging: 2D + 1D processing

3-D Synthetic Aperture imaging

$$s(x,y,z)=\sum_{i=1}^{M}s_i(x,r_{i_{ref}})\,\mathrm{e}^{jk_{z_i}z}$$

Filter-like formulation for a given 2-D resolution cell

Coregistered
Resampled
Flattened
Single Look Complex
(SLC) data

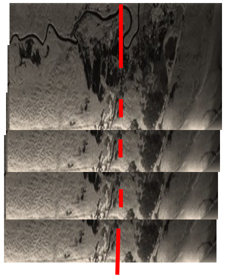

$$\Rightarrow\ \mathbf{y}=\begin{bmatrix}y_1\\ \vdots\\ y_M\end{bmatrix}=\begin{bmatrix}s_1(x,r_{1_{ref}})\\ \vdots\\ s_M(x,r_{M_{ref}})\end{bmatrix}$$

1D Linear filter

$$\boxed{s(z)=\sum_{i=1}^{M}y_i\,\mathrm{e}^{-jk_{z_i}z}=\mathbf{a}^H(z)\mathbf{y}}$$

Steering vector

$$\mathbf{a}=[1,\mathrm{e}^{jk_{z_2}z},\ldots,\mathrm{e}^{jk_{z_M}z}]^T$$

TomoSAR imaging using Monodimensional Spectral Analysis Techniques

Interferometric phase variations with height

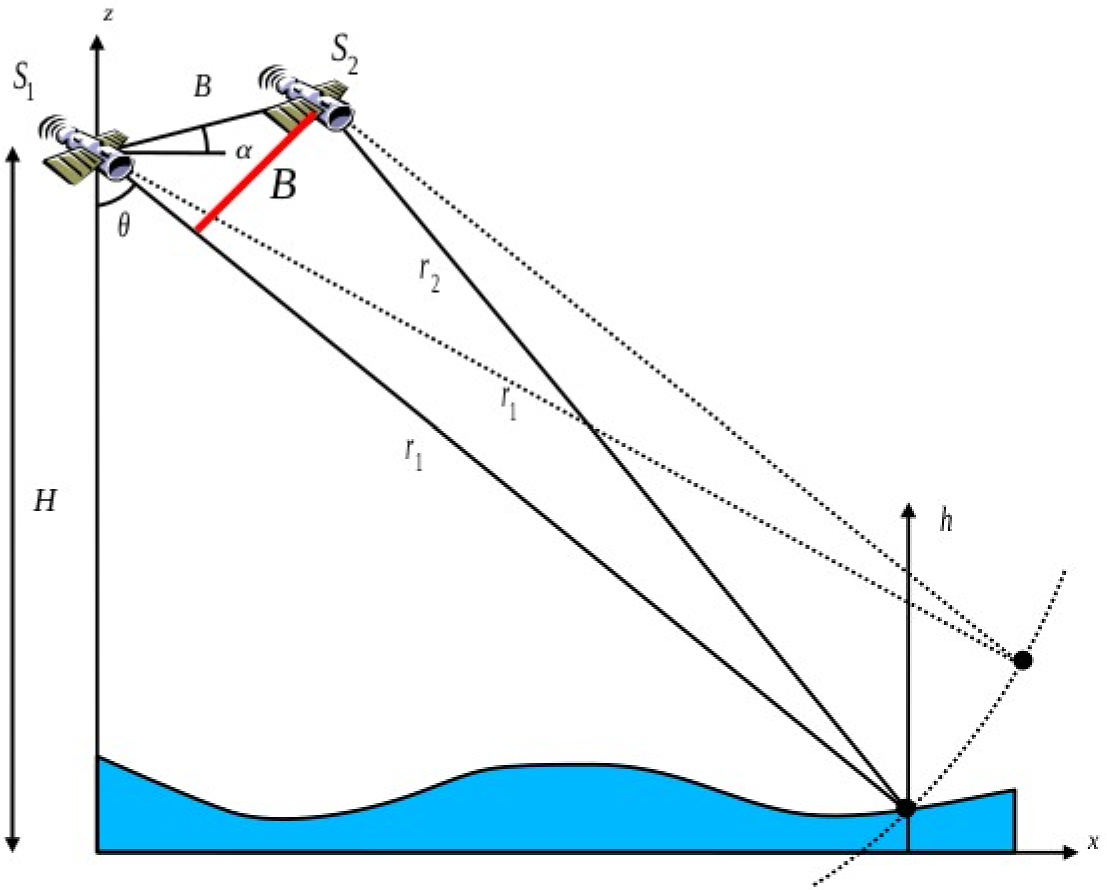

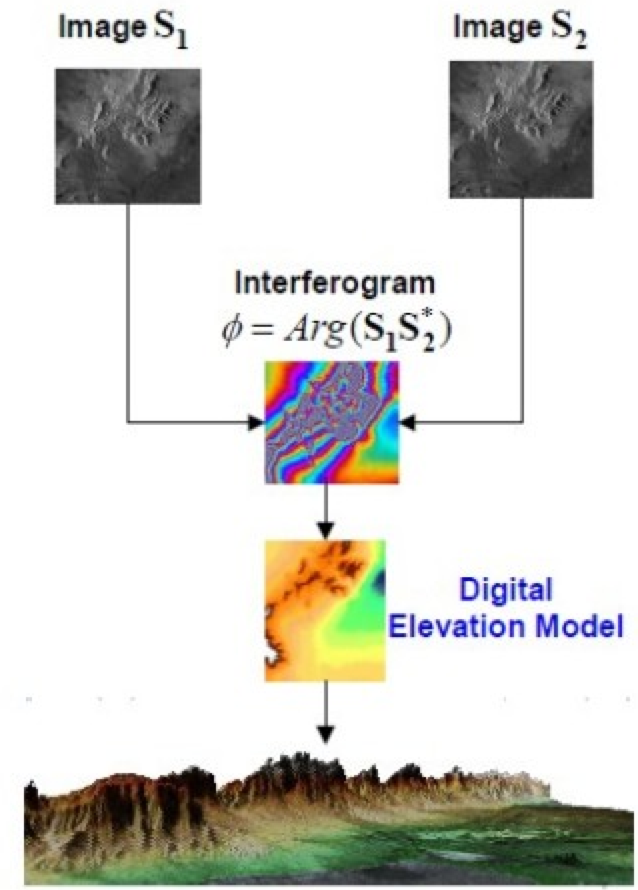

Image $\mathbf{S}_1$

Image $\mathbf{S}_2$

Interferogram

$\phi = Arg(\mathbf{S}_1\mathbf{S}_2^*)$

Digital Elevation Model

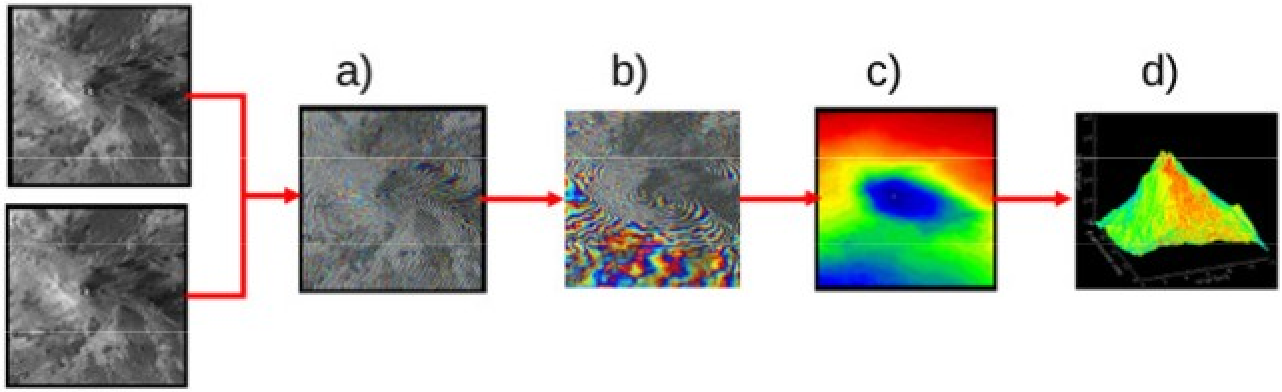
a)
b)
c)
d)

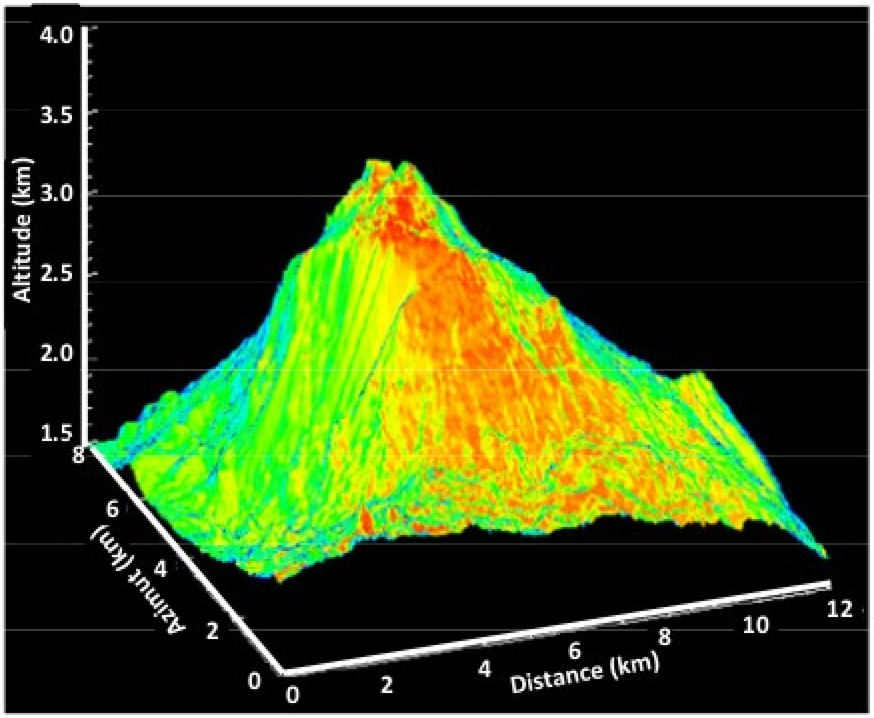
Altitude (km)
4.0
3.5
3.0
2.5
2.0
1.5
Azimut (km)
8
6
4
2
0
Distance (km)
0
2
4
6
8
10
12

Estimation of a single scatterer, M=2 images

InSAR way

$$\begin{aligned} s_1 &= a_c\, \mathrm{e}^{j\xi} \\ s_2 &= a_c\, \mathrm{e}^{j\xi + \Delta\phi} \end{aligned} \Rightarrow \begin{cases} \Delta\hat{\phi} = \arg(s_2 s_1^*) \\ \hat{I} = \frac{|s_1|^2 + |s_2|^2}{2} \end{cases}$$

Linear filtering way

$$\mathbf{y} = \begin{bmatrix} s_1 \\ s_2 \end{bmatrix} = a_c\, \mathrm{e}^{j\xi} \begin{bmatrix} 1 \\ \mathrm{e}^{j\Delta\phi} \end{bmatrix}, \mathbf{a}(\phi) = \begin{bmatrix} 1 \\ \mathrm{e}^{j\phi} \end{bmatrix}$$

$$\boxed{f(\phi) = \frac{\mathbf{a}^H(\phi)\mathbf{y}}{2} = \frac{s_1 + s_2\, \mathrm{e}^{-j\phi}}{2} = a_c\, \mathrm{e}^{j\xi} \frac{1 + \mathrm{e}^{-j(\Delta\phi - \phi)}}{2}}$$

$$\Rightarrow \begin{cases} \Delta\hat{\phi} = \arg\max_{\phi} |f(\phi)|^2 \\ \hat{I} = |f(\Delta\hat{\phi})|^2 \end{cases}$$

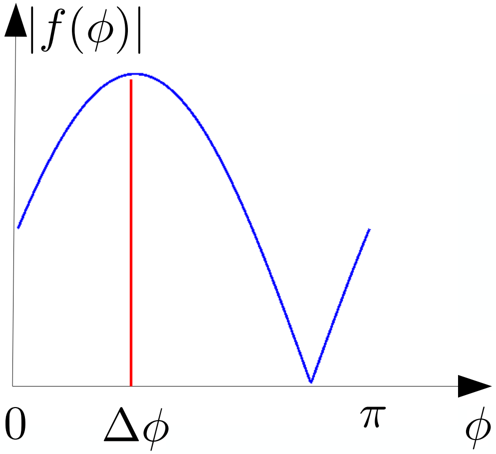

Phase estimation → linear filtering & search

Filter output: reflectivity

$\mathbf{a}(\phi)$ steering vector: **matched filter**

Estimation of several scatterers, M>2 images

Estimation of several scatterers: MB InSAR way

$$\{s_1, \ldots, s_M\}, \quad s_m = \sum_{t=1}^{N_t} a_{c_t}\, \mathrm{e}^{j\xi_t}\, \mathrm{e}^{jk_{z_m} z_t} \quad \Rightarrow \quad ???$$

Estimation of several scatterers: linear filtering way

$$\mathbf{y} = \begin{bmatrix} s_1 \\ \vdots \\ s_M \end{bmatrix}, \mathbf{a}(z) = \begin{bmatrix} 1 \\ \vdots \\ \mathrm{e}^{jk_{z_M} z} \end{bmatrix}$$

$$\boxed{f(z) = \frac{\mathbf{a}^H(z)\mathbf{y}}{M} = \frac{\sum_m s_m\, \mathrm{e}^{-jk_{z_m} z}}{M}}$$

$$\Rightarrow \begin{cases} \hat{z}_t = \arg\max_{loc} |f(z)|^2 \\ \hat{I}_t = |f(\hat{z}_t)|^2 \end{cases}$$

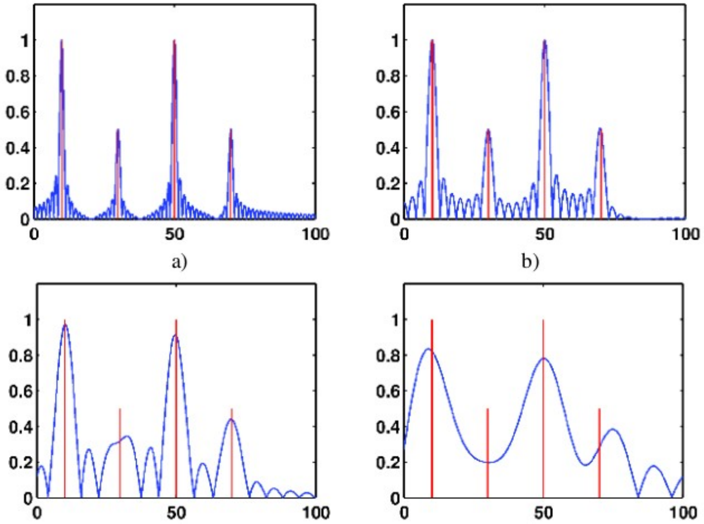

Matched filter: **Discrete Fourier Transform**

Tomographic focusing: spectral estimation problem

Estimation quality: depends on MB-inSAR configuration

L. Ferro-Famil & S.Tebaldini

Tomographic imaging using specan

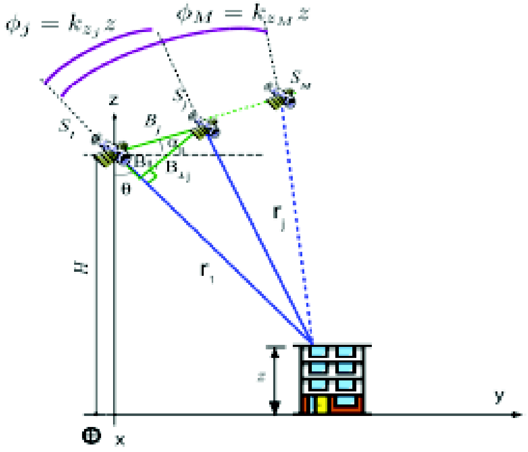

Ideal acquired signal (single scatterer)

$$\mathbf{y} = a_c \, \mathbf{a}(z_0)$$

$$\text{with} \quad \mathbf{a}(z_0) = [1, e^{jk_{z_2} z_0}, \ldots, e^{jk_{z_M} z_0}]^T$$

Uniform baseline distribution

$$B_{\perp_i} = (i-1) B_\perp \Rightarrow k_{z_i} = (i-1) \mathrm{d}k_z$$

$$\mathbf{a}(z) = [1, e^{j \mathrm{d}k_z z}, \ldots, e^{j(M-1)\mathrm{d}k_z z}]^T$$

Spectral sampling: $\mathrm{d}k_z = \dfrac{k_c B_\perp}{r \sin\theta}$

Spectral bandwidth: $\Delta k_z = M \mathrm{d}k_z$

$$|f(z)| = |a_c| \frac{|\mathbf{a}^H(z)\mathbf{a}(z_0)|}{M} = \frac{|a_c|}{M} \frac{|\sin(\pi \Delta k_z (z - z_0))|}{|\sin(\pi \mathrm{d}k_z (z - z_0))|}$$

Fast

M times Slower

Periodic oscillating filter output

Tomographic imaging using specan

Uniform baseline sampling $\mathbf{a}(z) = [1, \mathrm{e}^{j\mathrm{d}k_z z}, \ldots, \mathrm{e}^{j(M-1)\mathrm{d}k_z z}]^T$

$$|f(z)| = |a_c| \frac{|\mathbf{a}^H(z)\mathbf{a}(z_0)|}{M} = \frac{|a_c|}{M} \frac{|\sin(\pi \Delta k_z (z - z_0))|}{|\sin(\pi \mathrm{d}k_z (z - z_0))|}$$

Fast → resolution

Slow→ ambiguity

Spatial features of a tomogram

- **rapid oscillations: resolution**
- **band-limited: sidelobes**
- **sampled spectrum :**
  spatial ambiguities

$$\boxed{\delta z = \frac{2\pi}{\Delta k}, z_{amb} = \frac{2\pi}{\mathrm{d}k}, \delta z = \frac{z_{amb}}{M}}$$

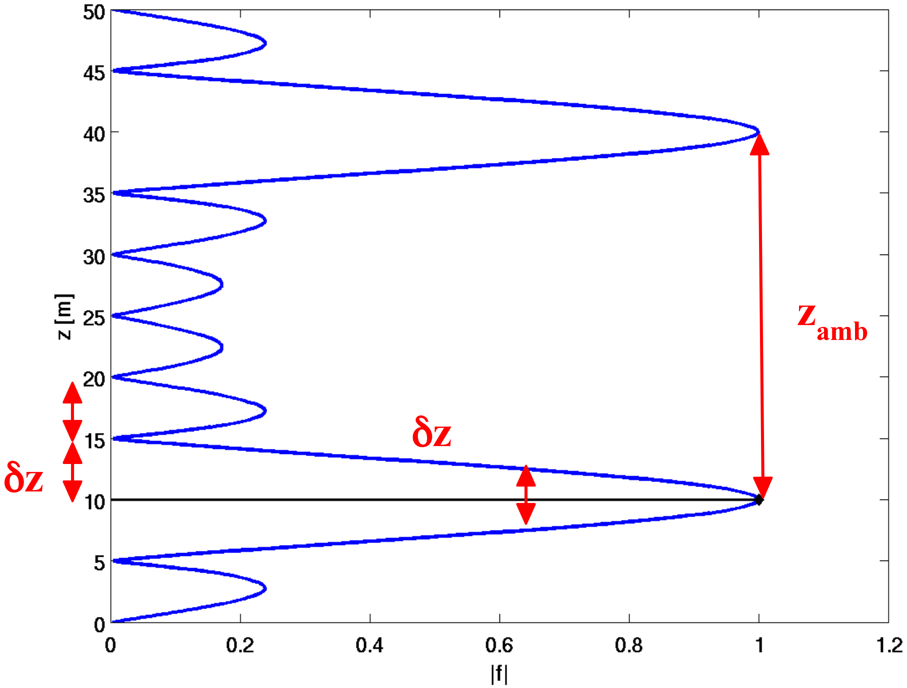

M=6

Tomographic imaging using specan

M=6

$$\boxed{\begin{aligned}\Delta k_z &\propto M B_\perp \\ \mathrm{d}k_z &= \frac{\Delta k_z}{M}\end{aligned}}$$

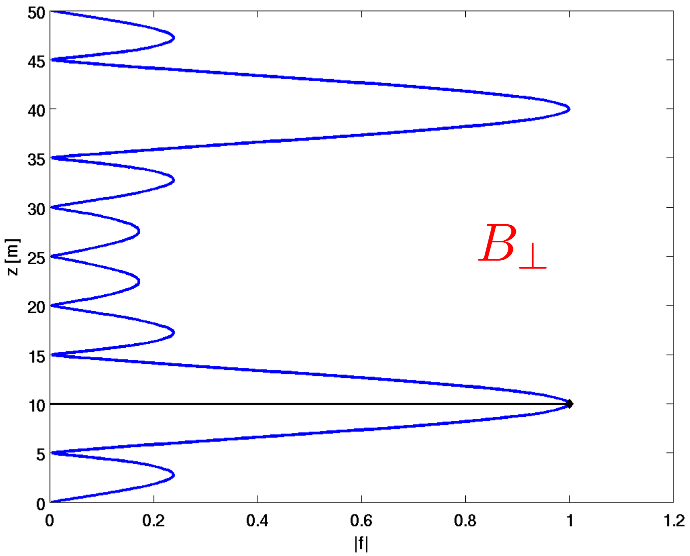

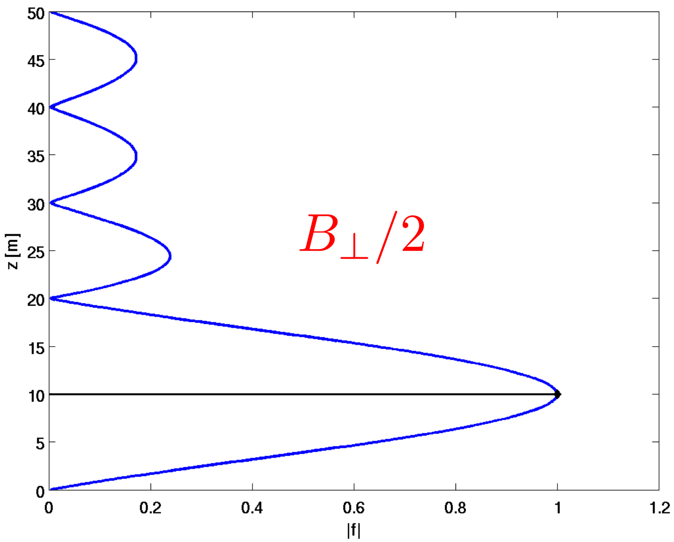

Reduced resolution

Improved ambiguity

Tomographic imaging using specan

M=6

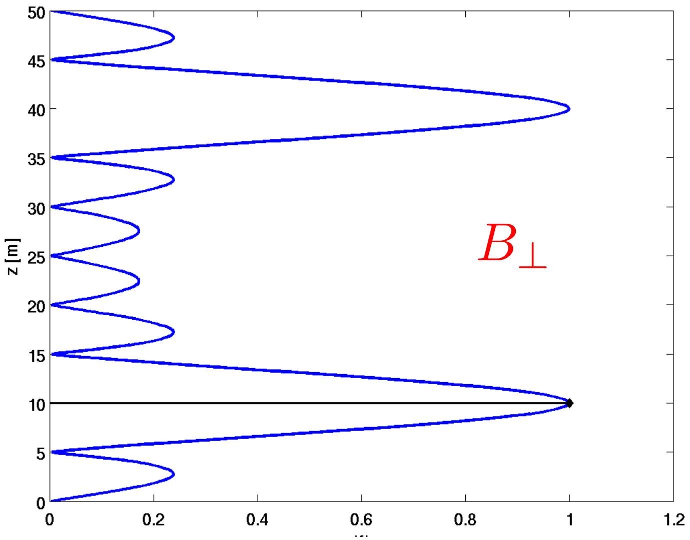

$$\boxed{\begin{array}{c}\Delta k_z \propto M B_\perp \\ \mathrm{d}k_z = \dfrac{\Delta k_z}{M}\end{array}}$$

M=12

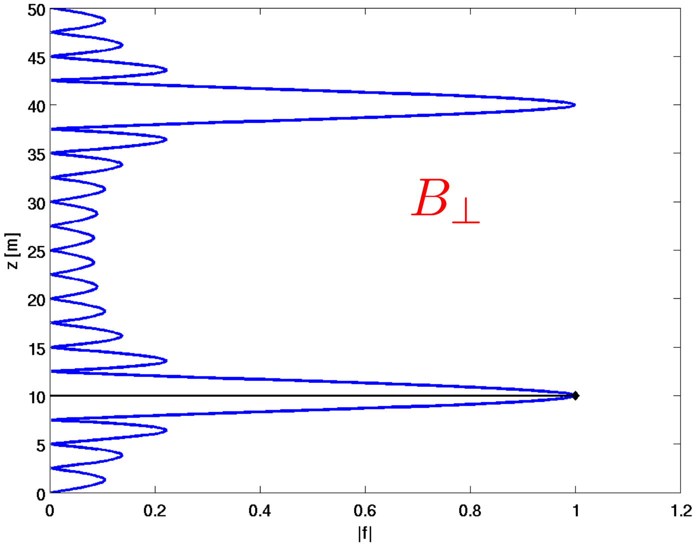

Improved resolution

Unchanged ambiguity

Tomographic imaging using specan

M=6

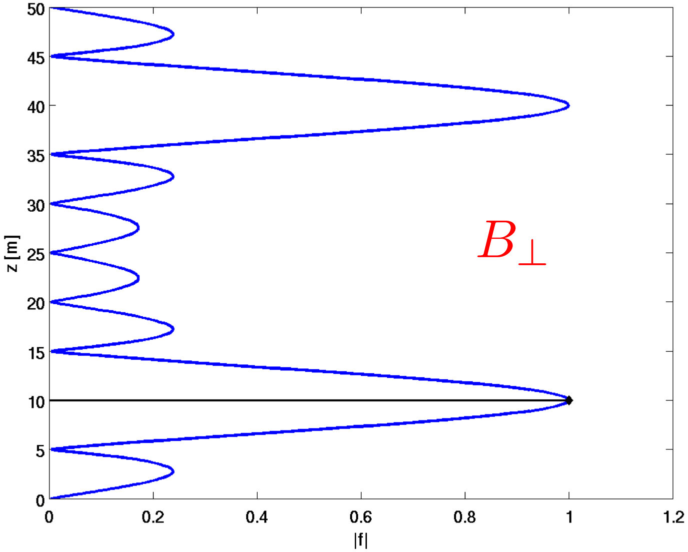

$$\boxed{\begin{array}{l}\Delta k_z \propto M B_\perp \\ \mathrm{d}k_z = \dfrac{\Delta k_z}{M}\end{array}}$$

M=12

Unchanged resolution

Improved ambiguity

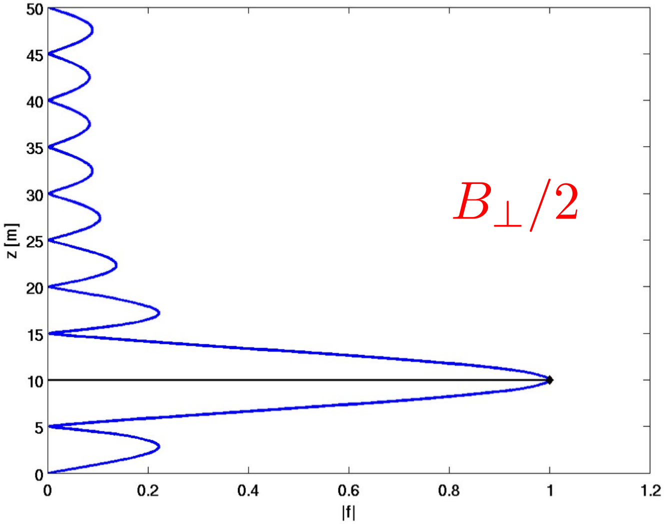

Tomographic imaging using specan

M=6

$$\boxed{\begin{aligned}\Delta k_z &\propto M B_\perp \\ \mathrm{d}k_z &= \frac{\Delta k_z}{M}\end{aligned}}$$

M=12

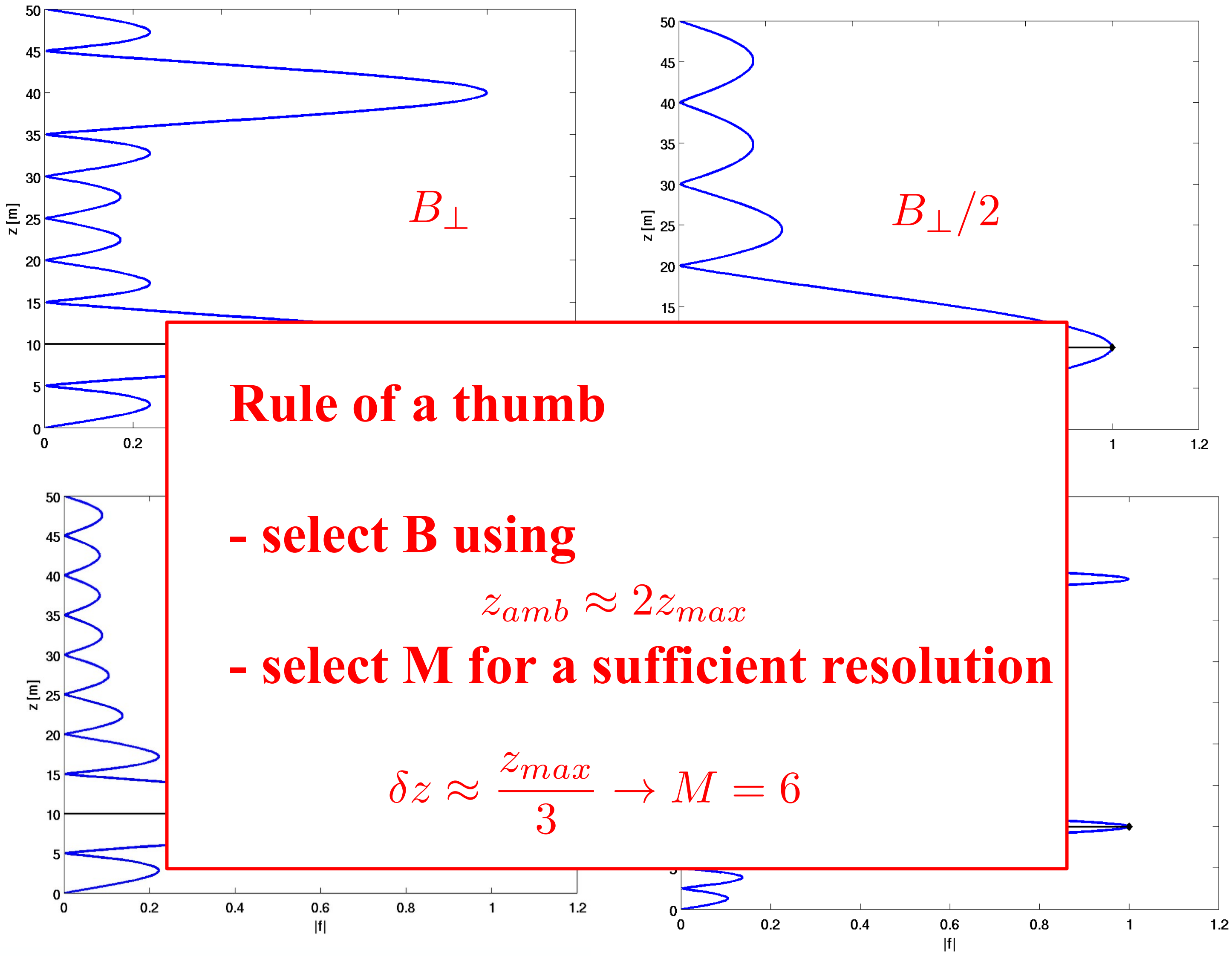

Rule of a thumb

- select B using

$$z_{amb} \approx 2 z_{max}$$

- select M for a sufficient resolution

$$\delta z \approx \frac{z_{max}}{3} \rightarrow M = 6$$

Tomographic imaging using specan

Single-look tomograms

$$\hat{I}(z) = \left| \frac{\mathbf{a}^H(z)\mathbf{y}}{M} \right|^2$$

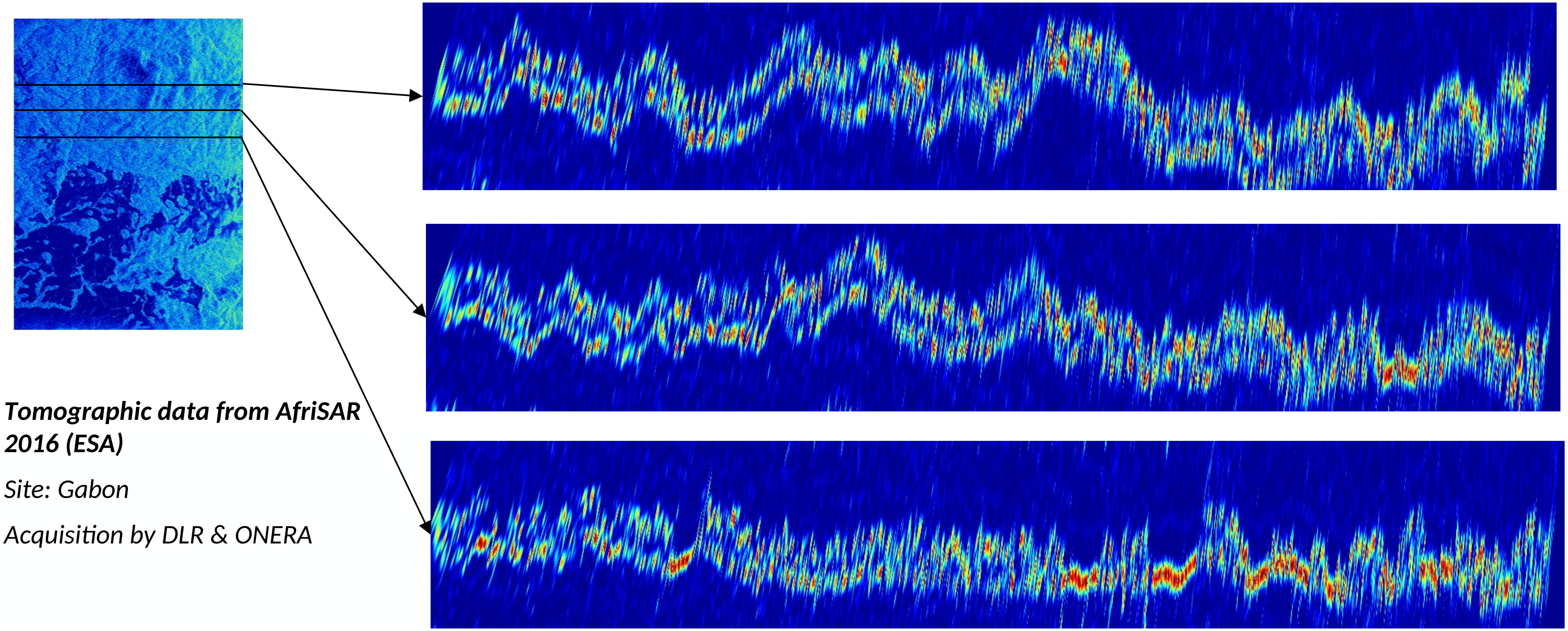

Tomographic data from AfriSAR 2016 (ESA)

Site: Gabon

Acquisition by DLR & ONERA

Noisy aspect due to speckle

TomoSAR imaging Using multilook Specan methods

Speckle effect

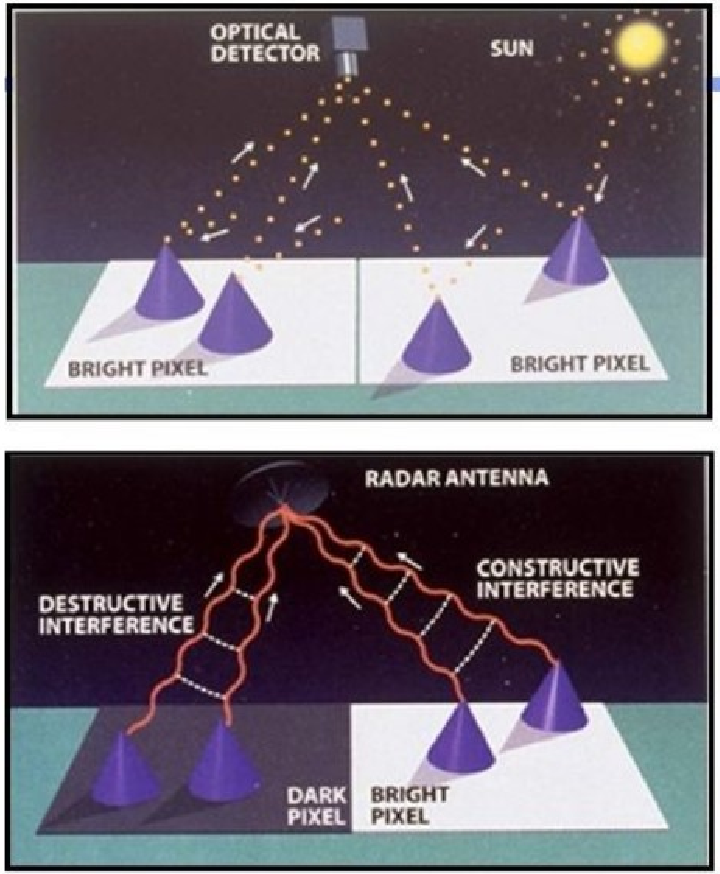

© Scientific American

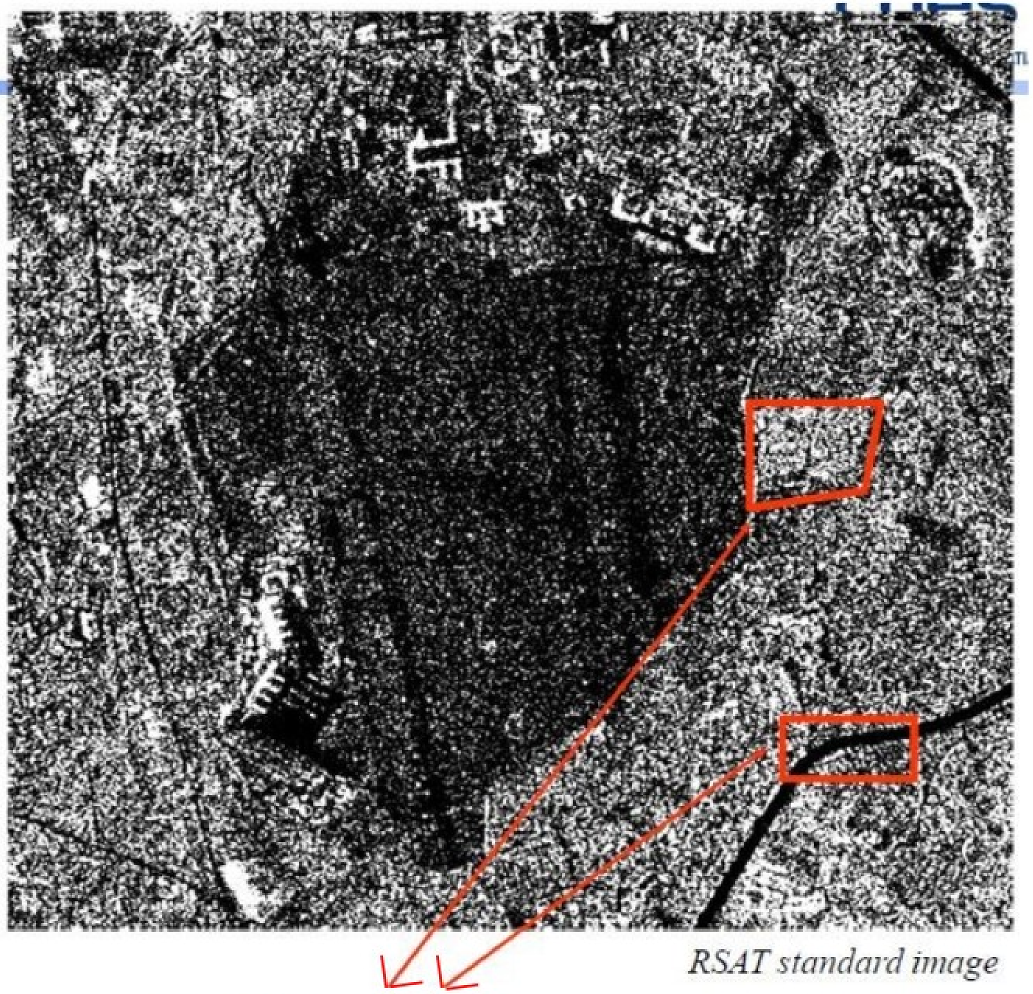

RSAT standard image

Speckle: coherent effect that appears as a Multiplicative noise

Speckle effect

$$s(x,r) \approx \int_{\mathcal{C}} a_c(x,r,\nu)\, \mathrm{e}^{-jk_c r(\nu)}\, \mathrm{d}\nu$$

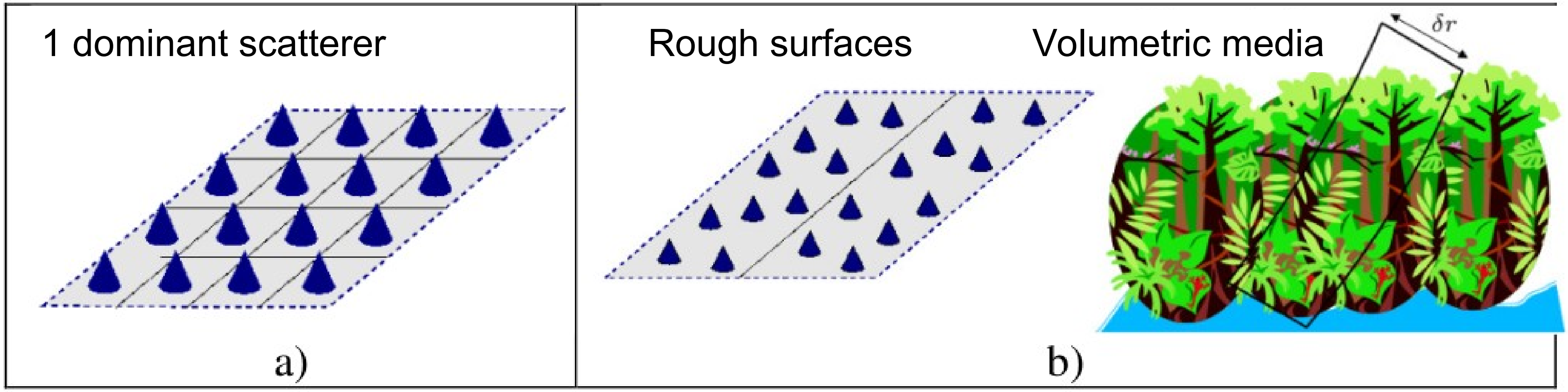

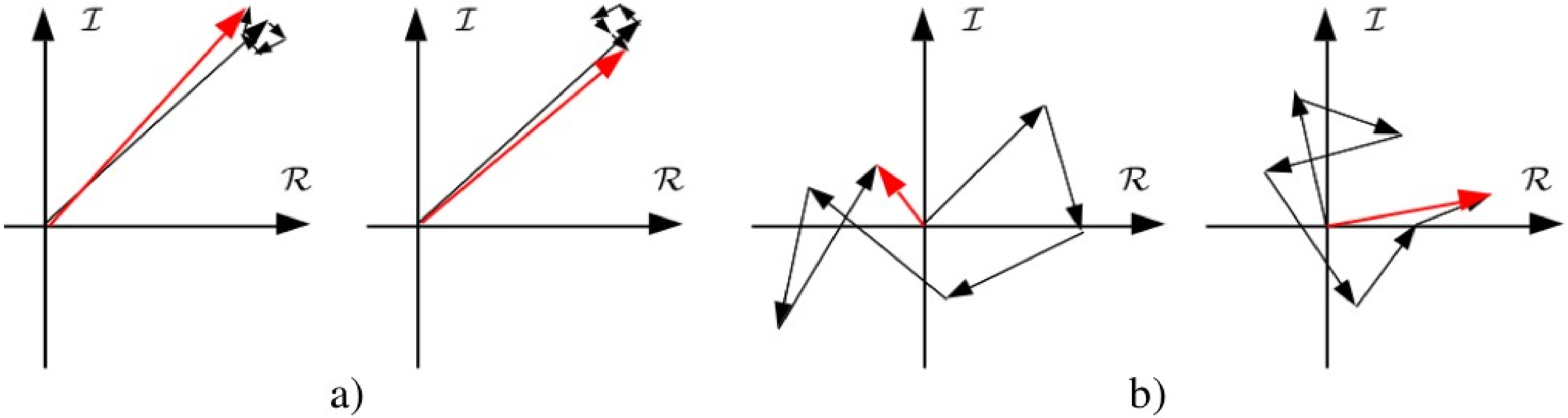

Two realizations in both cases

Speckle filtering

Unfiltered intensity image: exponential distribution

$$\hat{I} = |s(l)|^2, \quad \mathrm{E}(\hat{I}) = I, \quad \mathrm{var}(\hat{I}) = I^2$$

L independent samples (looks): ML estimate has chi2 distribution

$$\boxed{\hat{I} = \frac{1}{L}\sum_{l=1}^{L}|s(l)|^2}, \quad \mathrm{E}(\hat{I}) = I, \mathrm{var}(\hat{I}) = \frac{I^2}{L}$$

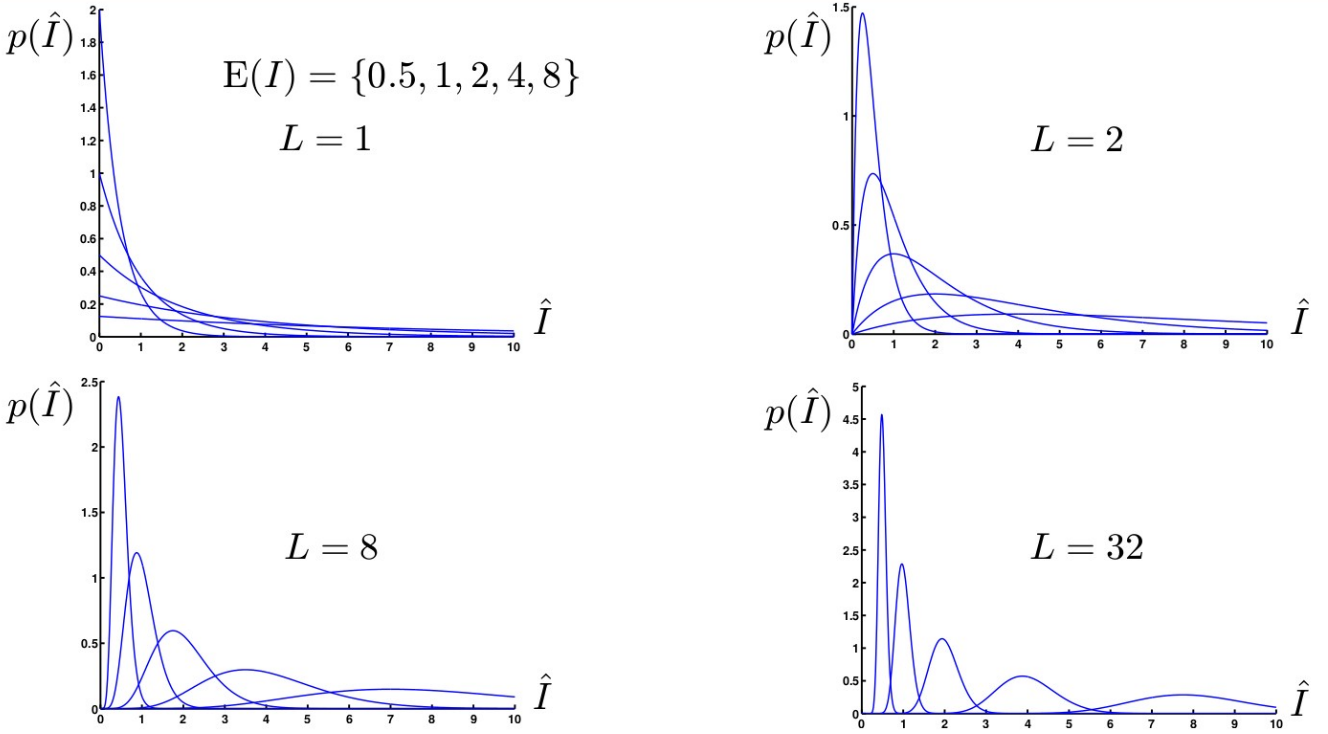

Speckle filtering

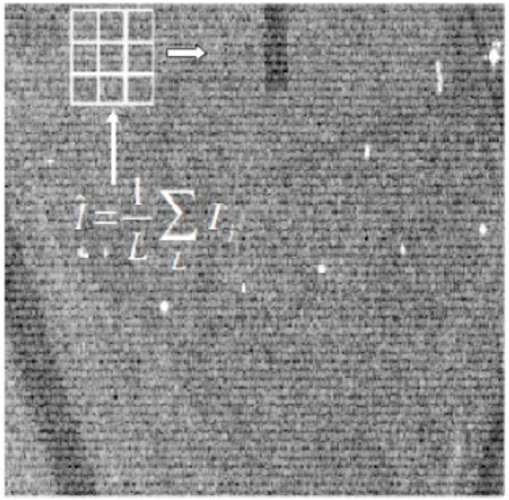

a)

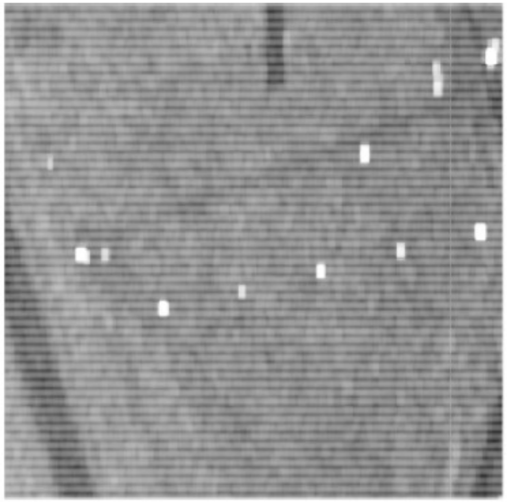

b)

Equivalent Number of Looks

$$ENL = \frac{\mathrm{E}(\hat{I})^2}{\mathrm{var}\,\hat{I}}$$

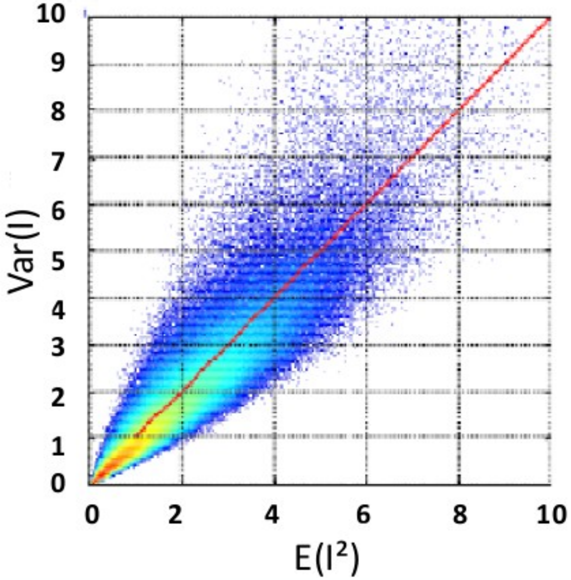

Speckle filtering

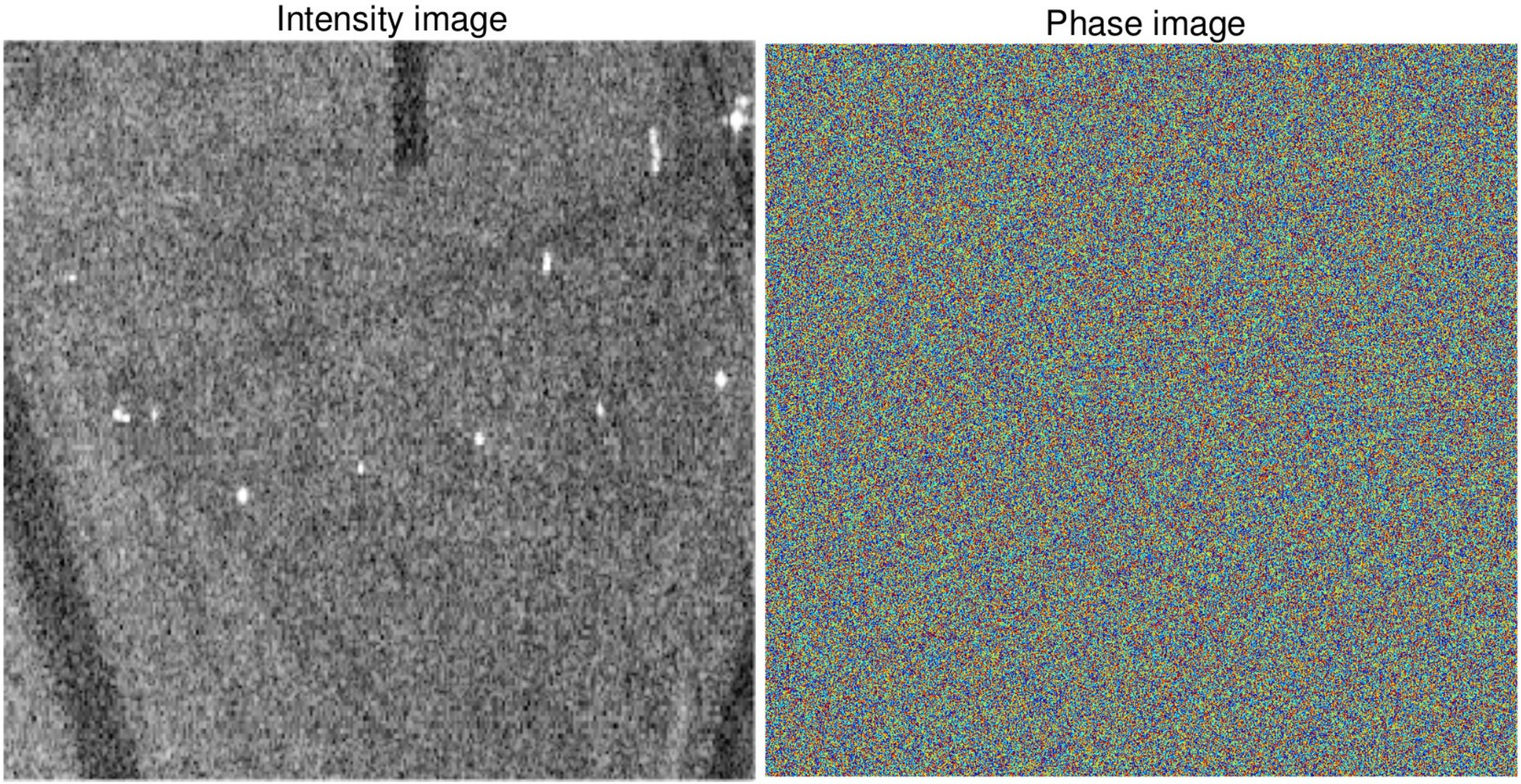

Speckle filtering

Intensity images

$$\hat{I} = \frac{1}{L}\sum_{L} I_i$$

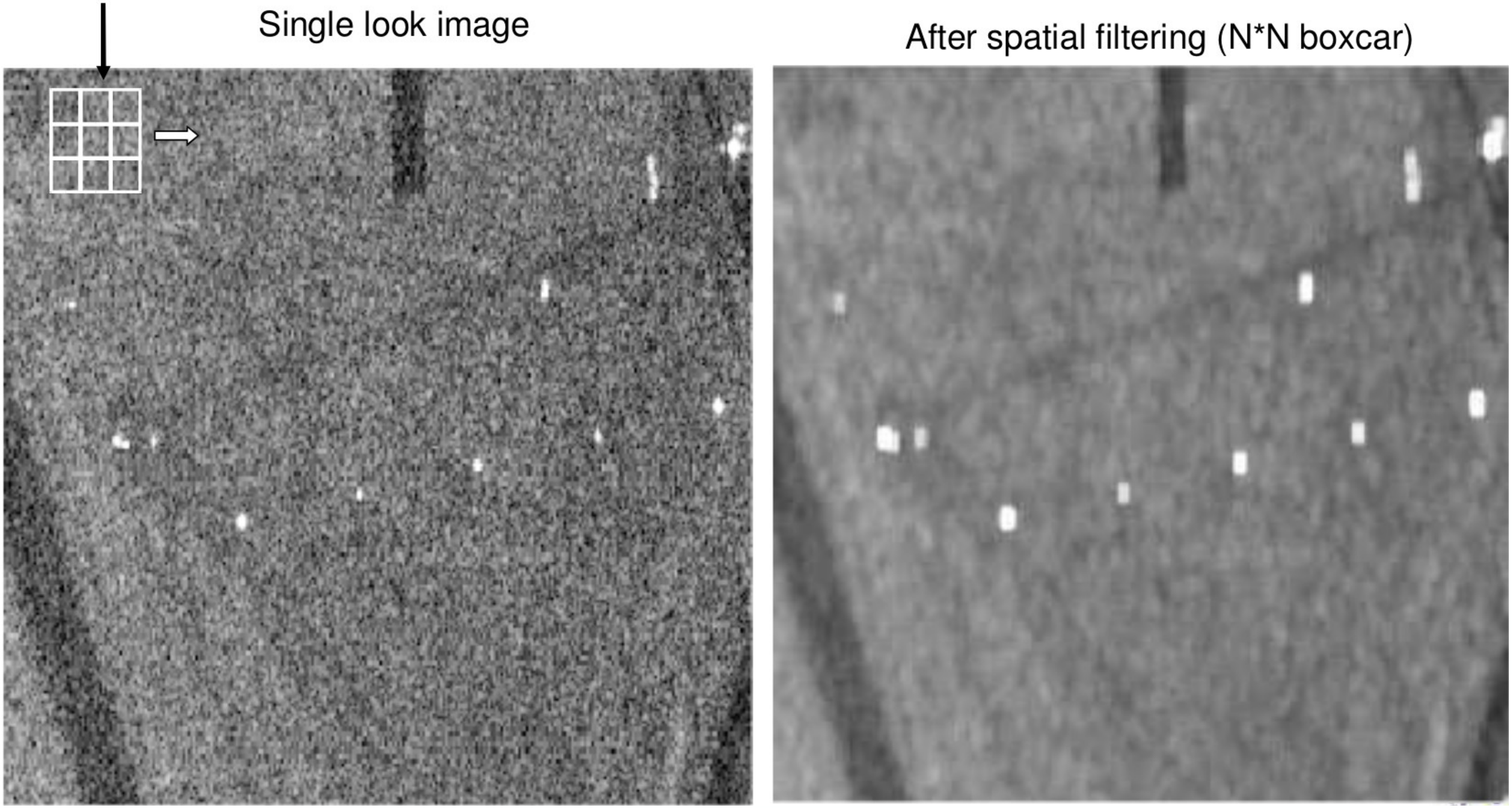

Single look image

After spatial filtering (N*N boxcar)

Speckle filtering

Single look image

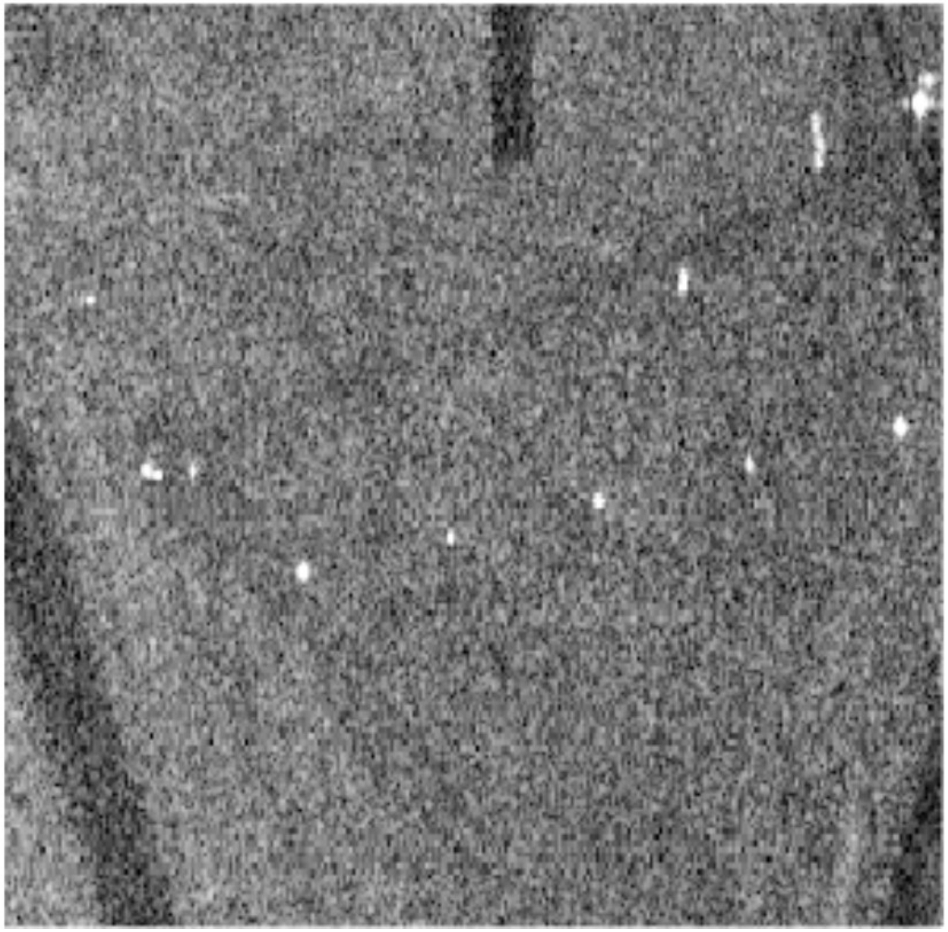

After spatial filtering (N*N Lee filter)

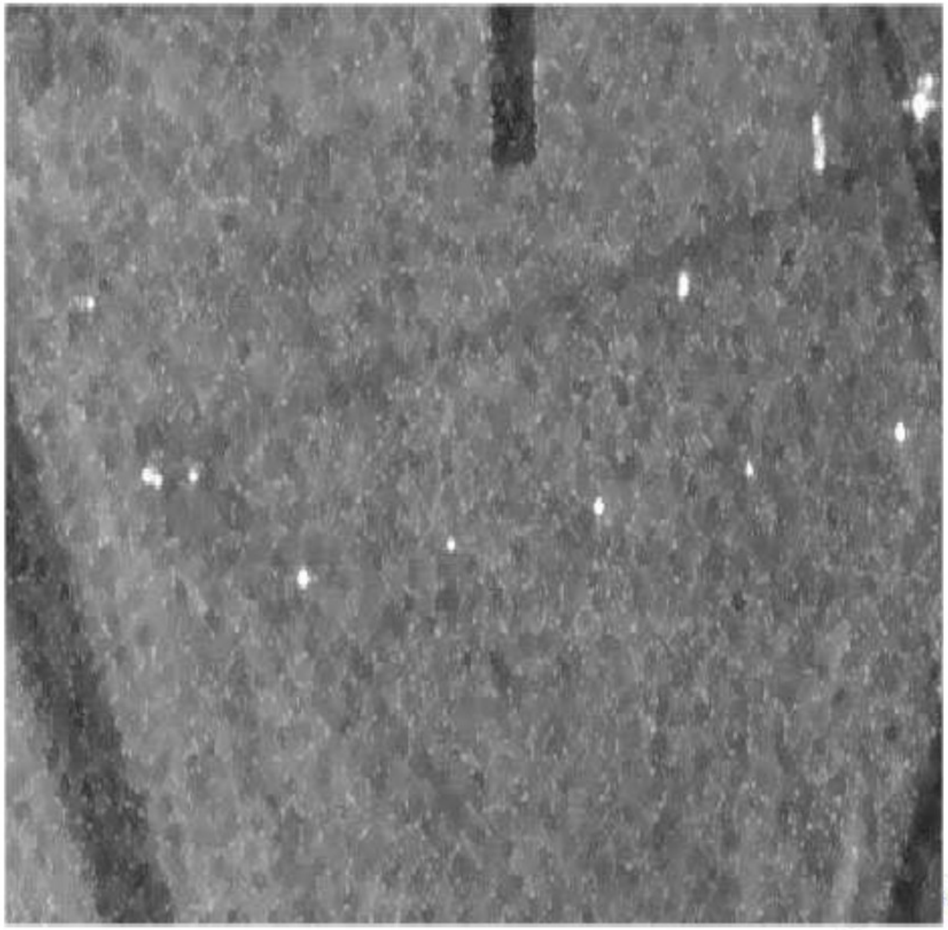

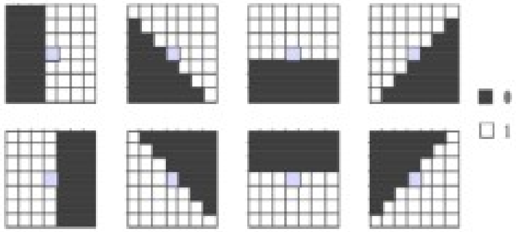

Speckle filtering

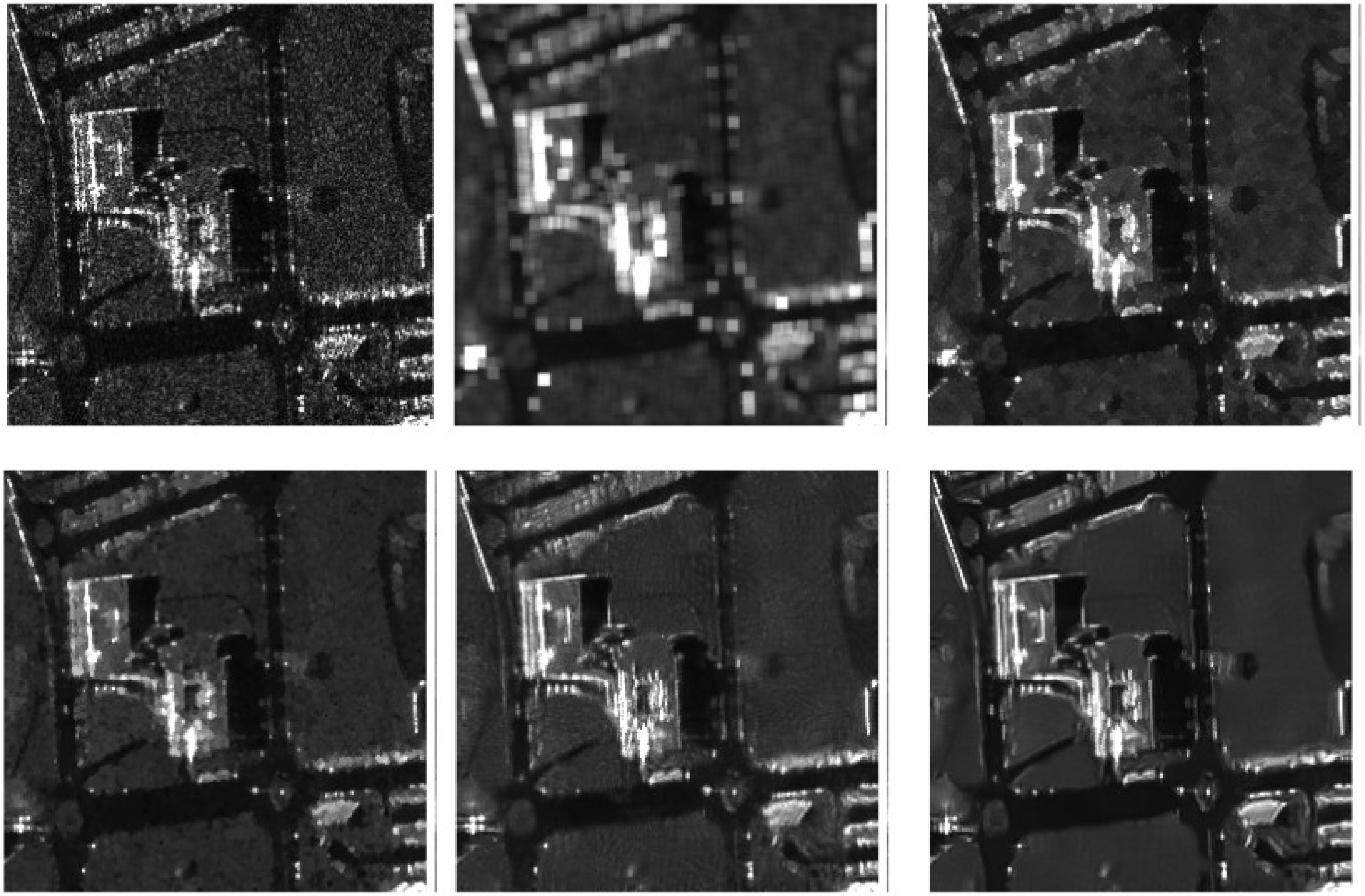

Non local speckle filtering

Speckle filtering with tomographic data

Speckle filtering for monovariate SLC SAR images

$$\boxed{\hat{I} = \frac{1}{L}\sum_{l=1}^{L}|s(l)|^2}, \quad \mathrm{E}(\hat{I}) = I, \quad \mathrm{var}(\hat{I}) = \frac{I^2}{L}$$

Speckle filtering for multivariate SLC MB-InSAR images

$$\mathbf{y} = \begin{bmatrix} s_1 \\ \vdots \\ s_M \end{bmatrix}, \mathbf{a}(z) = \begin{bmatrix} 1 \\ \vdots \\ e^{jk_{z_M}z} \end{bmatrix} \quad f(z) = \frac{\mathbf{a}^H(z)\mathbf{y}}{M} = \frac{1}{M}\sum_m s_m\, e^{-jk_{z_m}z}$$

$$\hat{I}(z) = \frac{1}{L}\sum_{l=1}^{L}|f(z,l)|^2 = \frac{1}{M^2}\mathbf{a}^H(z)\widehat{\mathbf{R}}\mathbf{a}(z)$$

L-look (ML) estimate of the TomoSAR covariance matrix

$$\boxed{\widehat{\mathbf{R}} = \frac{1}{L}\sum_{l=1}^{L}\mathbf{y}(l)\mathbf{y}^H(l) \quad \mathrm{E}(\widehat{\mathbf{R}}) = \mathbf{R}}$$

Speckle filtering with tomographic data

TomoSAR covariance matrix

$$\boxed{\widehat{\mathbf{R}} = \frac{1}{L}\sum_{l=1}^{L}\mathbf{y}(l)\mathbf{y}^{H}(l) \quad \mathrm{E}(\widehat{\mathbf{R}}) = \mathbf{R}}$$

$$\widehat{\mathbf{R}} = \frac{1}{L}\sum_{l=1}^{L}\mathbf{y}(l)\mathbf{y}^{H}(l) = \begin{bmatrix} R_{11} & R_{12} & \dots & R_{1M} \\ R_{12}^{*} & R_{22} & \dots & R_{2M} \\ & & \ddots & \\ R_{1M}^{*} & R_{2M}^{*} & \dots & R_{MM} \end{bmatrix}$$

$$\hat{R}_{ii} = \frac{1}{L}\sum_{l=1}^{L} y_i(l)y_i^{*}(l) = \hat{I}_i \qquad \hat{R}_{ij} = \frac{1}{L}\sum_{l=1}^{L} y_i(l)y_j^{*}(l) = \sqrt{\hat{I}_i\hat{I}_j}\,\hat{\gamma}_{ij}$$

Interferometric coherence estimate

$$\hat{\gamma}_{ij} = \frac{\hat{R}_{ij}}{\sqrt{\hat{I}_i\hat{I}_j}} \qquad \hat{\phi}_{ij} = \arg(\hat{\gamma}_{ij}) \qquad |\hat{\gamma}_{ij}| \leq 1$$

Tomographic imaging using specan

Beamformer is Fourier imaging

$$\boxed{\hat{I}_{BF}(z) = \frac{1}{M^2}\mathbf{a}^H(z)\widehat{\mathbf{R}}\,\mathbf{a}(z)}$$

- Excellent (optimal) statistical accuracy
- Fourier resolution: $\delta z = \dfrac{2\pi}{\Delta k}$
- Cannot handle closely spaced scatterers
- High sidelobes

Capon's solution: constrained beamformer

Objective: minimize output power, with unitary gain at the height of interest

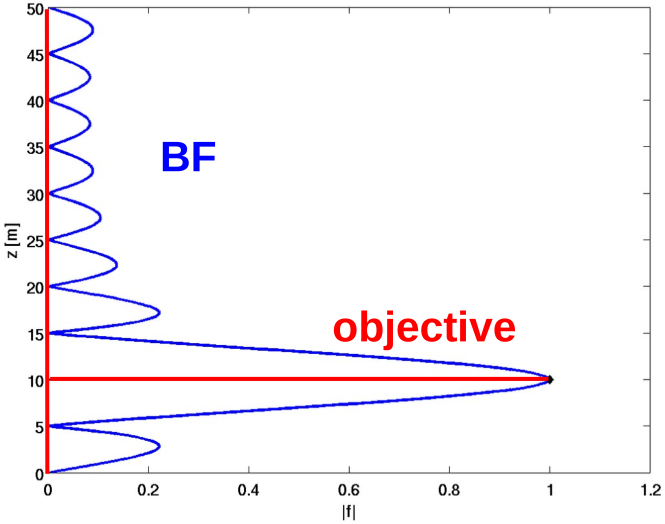

$$\mathbf{v}_{CP}(z) = \arg\min_{\mathbf{v}} \mathrm{E}(|\mathbf{v}^H\mathbf{y}|^2) \quad \text{s.t,} \quad \mathbf{v}^H\mathbf{a}(z) = 1$$

Solution:

$$\boxed{\hat{I}_{CP} = \frac{1}{\mathbf{a}^H(z)\widehat{\mathbf{R}}^{-1}\mathbf{a}(z)}}$$

Tomographic imaging using specan

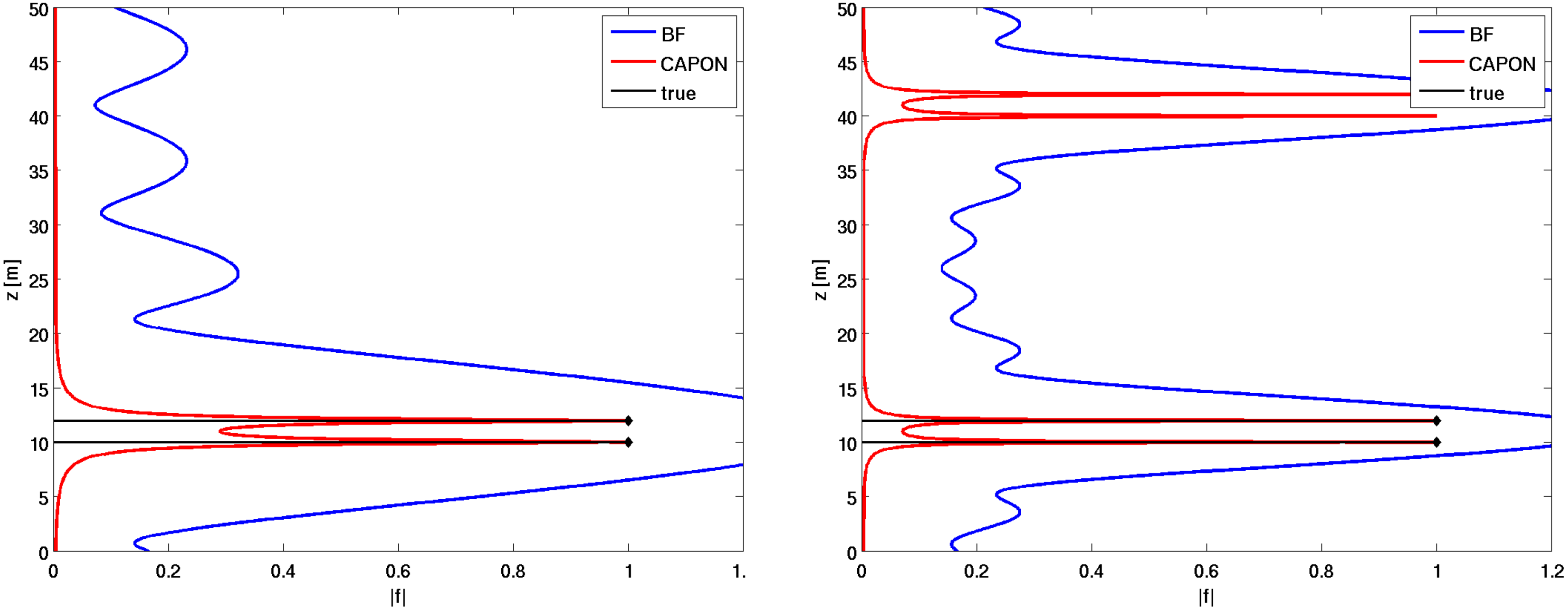

- **Capon: significantly improved resolution**
- **Resolution improvement is a function of the Signal to Noise Ratio (SNR)**
- **For regular baselines, BF & Capon are equally affected by ambiguities**

Tomographic imaging using specan

Irregular baseline sampling: logscale distribution

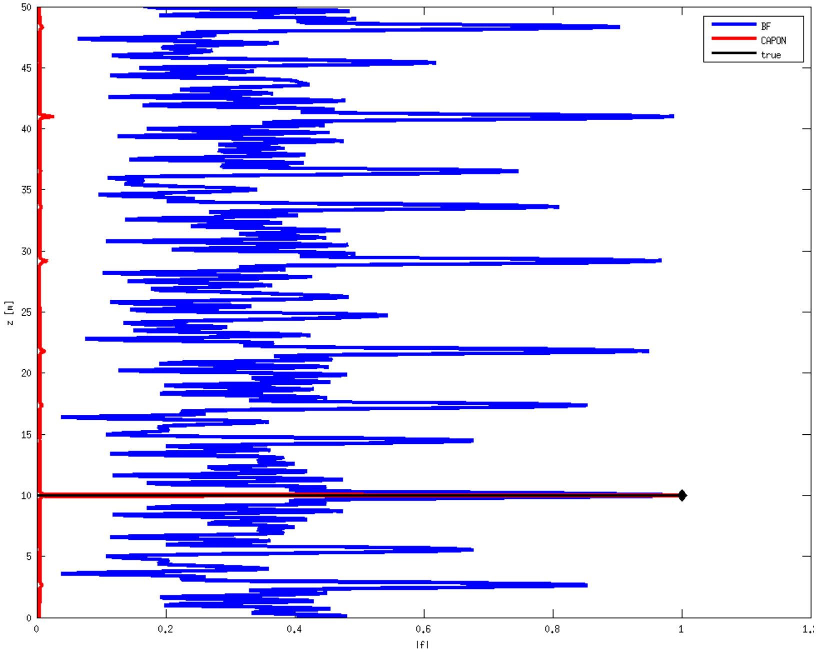

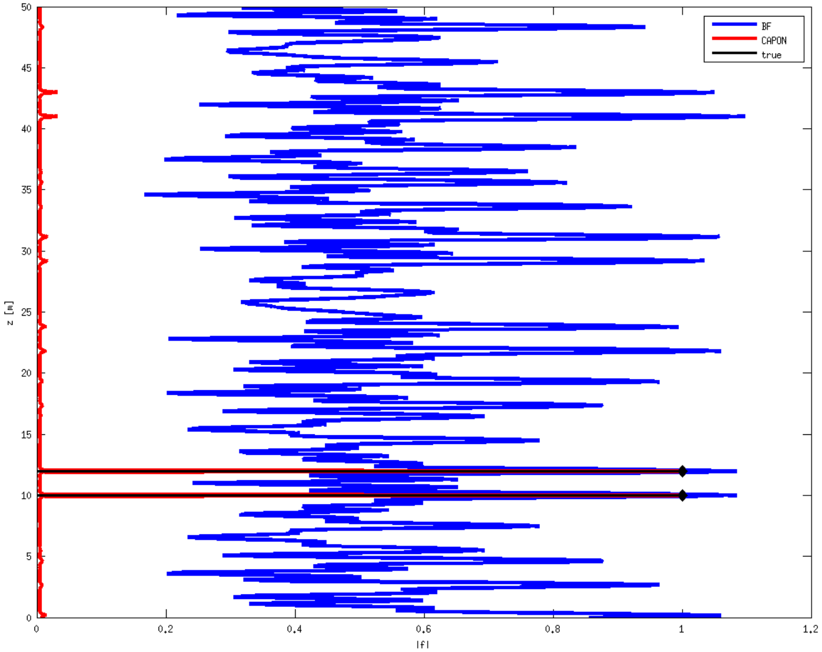

- BF: strongly affected by ambiguities
- CAPON: asynchronous ambiguities are considered as perturbations and filtered (may be dangerous!). Good resolution performance preserved

Tomographic imaging using specan

Practical implementation

- Asymptotic (L → +∞) estimators

$$\boxed{I_{BF}(z) = \frac{\mathbf{a}^H(z)\mathbf{R}\mathbf{a}(z)}{M^2}} \qquad \boxed{I_{CP}(z) = \frac{1}{\mathbf{a}^H(z)\mathbf{R}^{-1}\mathbf{a}(z)}}$$

- In practice, spatial averaging

$$\mathbf{R} \rightarrow \widehat{\mathbf{R}} = \frac{1}{L}\sum_{l=1}^{L}\mathbf{y}(l)\mathbf{y}^H(l)$$

- BF: quite stable w.r.t L

- Capon may suffer from a poor covariance matrix conditioning: sufficient ENL needed

⇒ Diagonal Loading $\widetilde{\mathbf{R}} = \widehat{\mathbf{R}} + \alpha\mathbf{I}_M, \quad \alpha \geq 0$

For large α (low SNR): CP → BF

Tomographic imaging using specan

Tropical forest profile at P band with residual phase errors

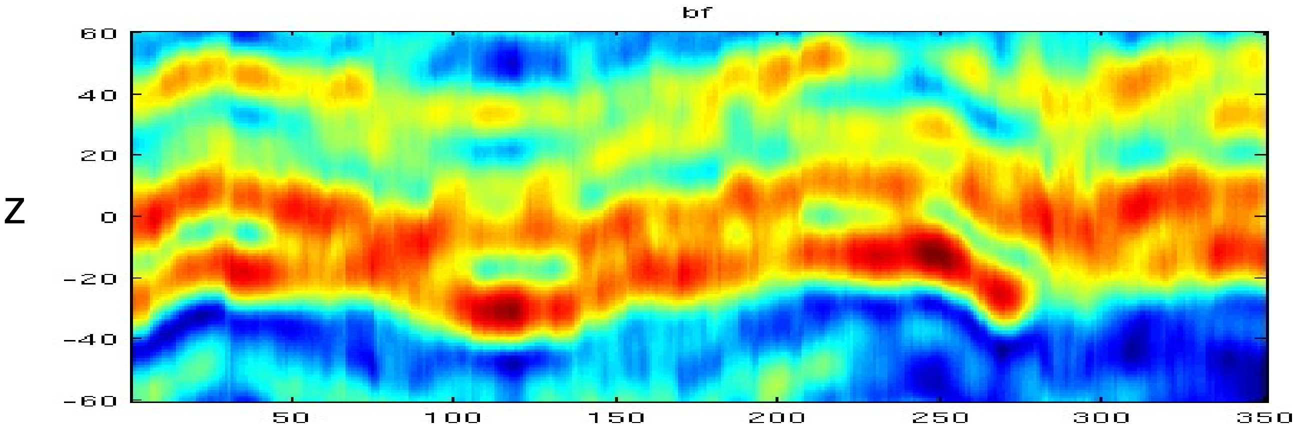

BF

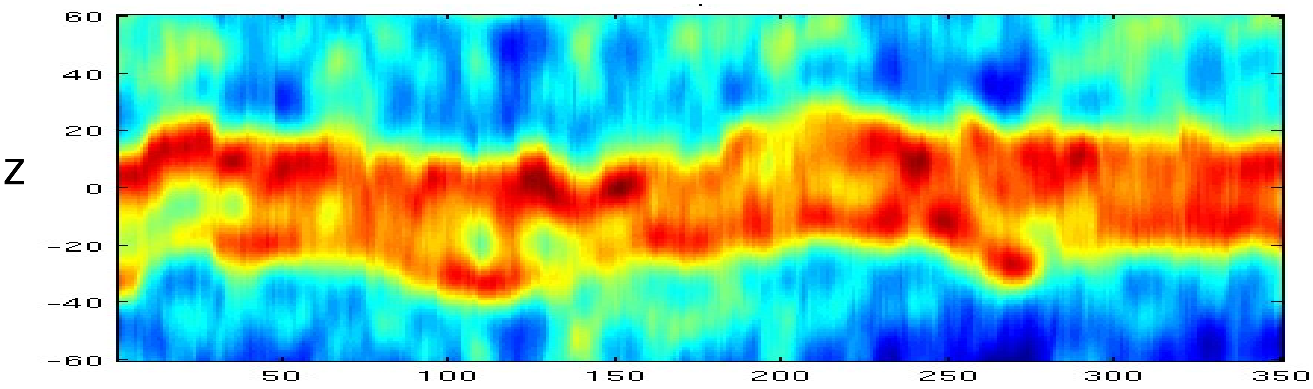

Capon

Tomographic imaging using specan

P band tomogram (Tomosense campaign) with residual phase errors

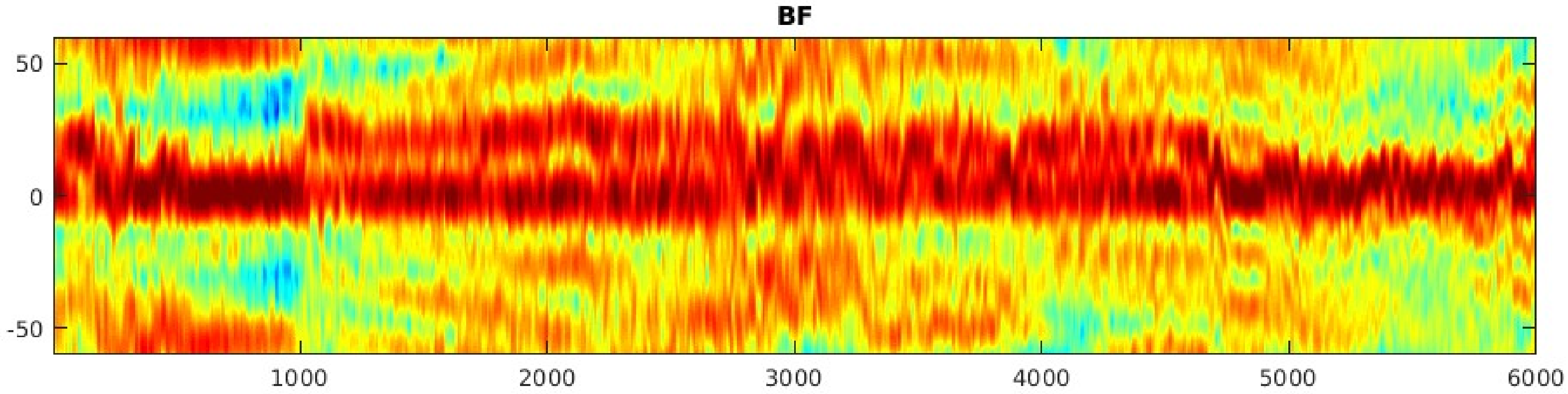

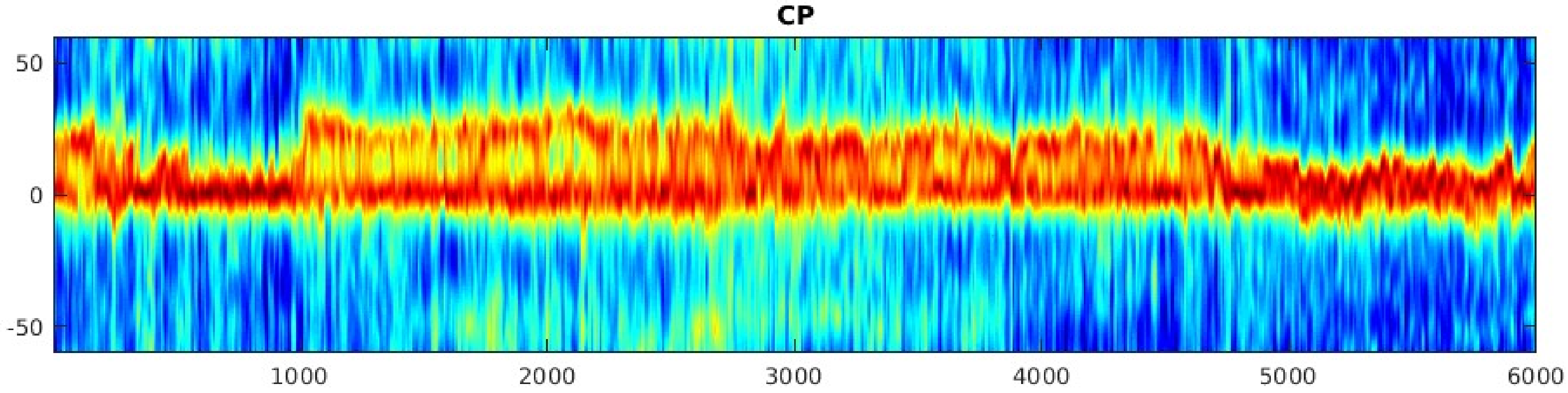

Case study: BIOSAR 2 data

Forest height

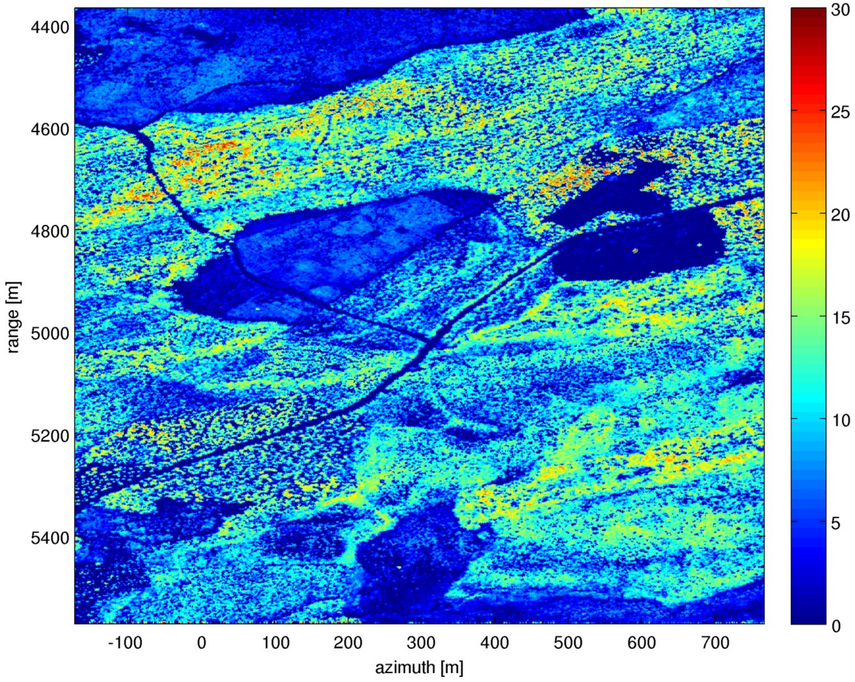

HH intensity

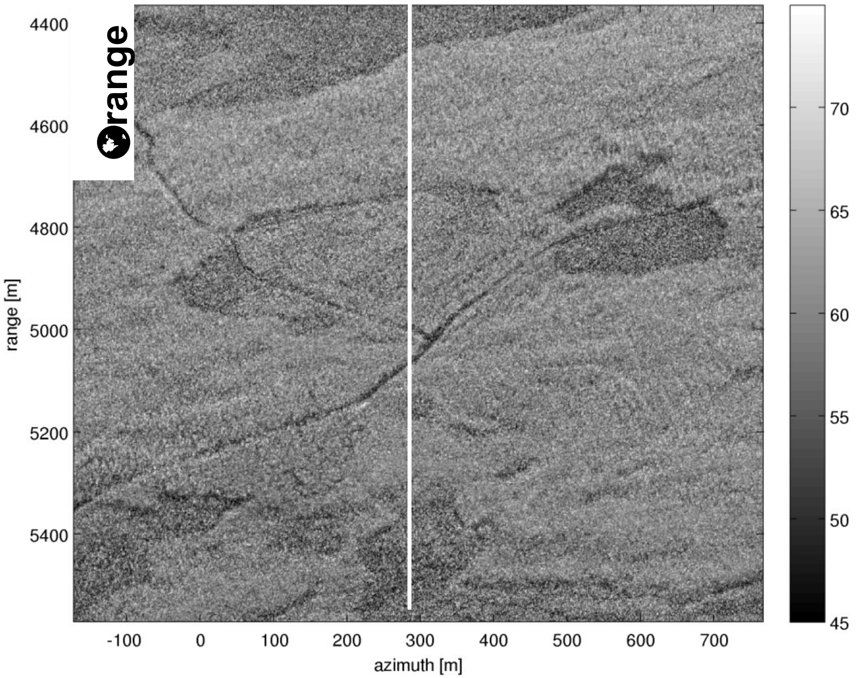

DEM

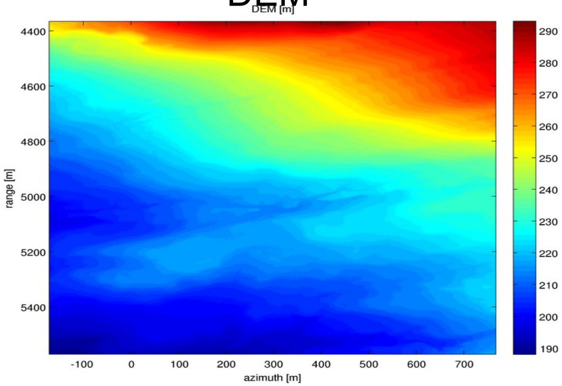

Case study: BIOSAR 2 data

BF

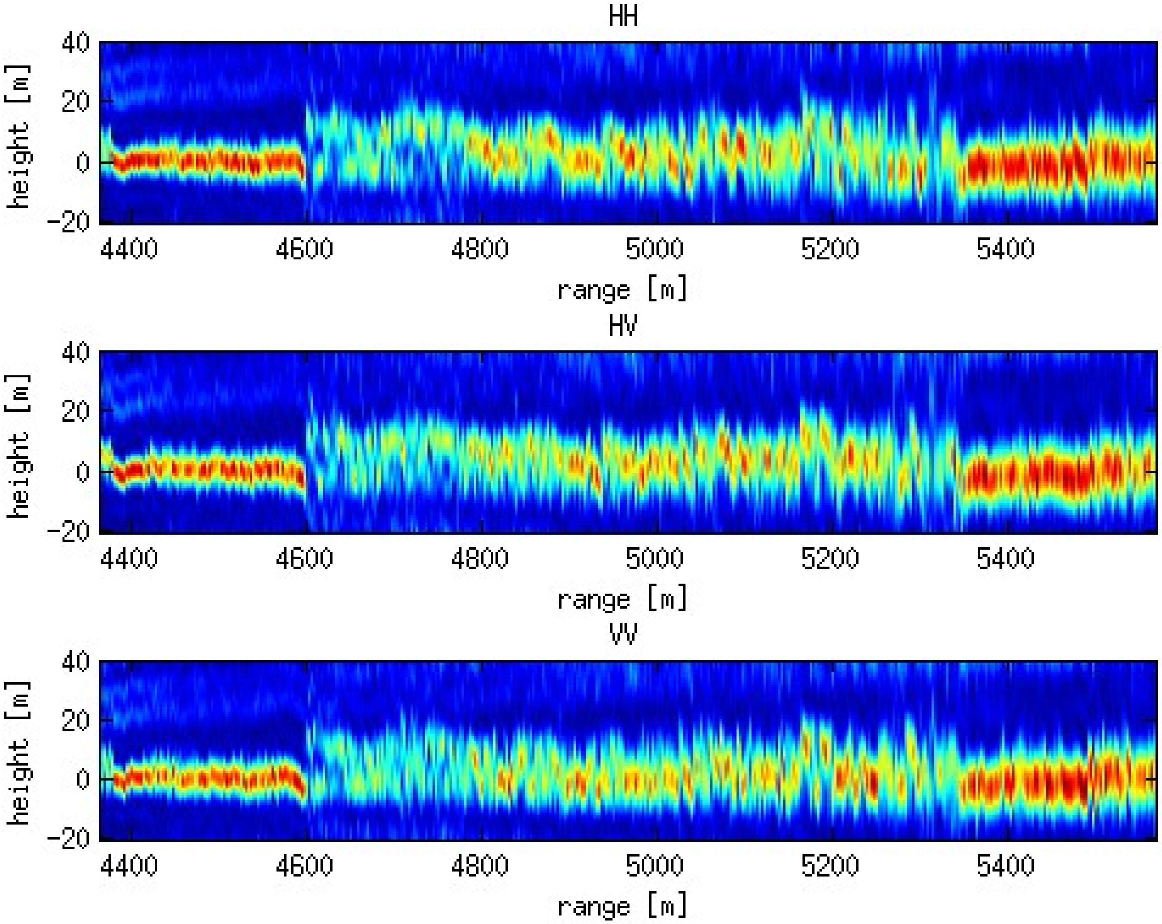

Case study: BIOSAR 2 data

CAPON: processing OK ?

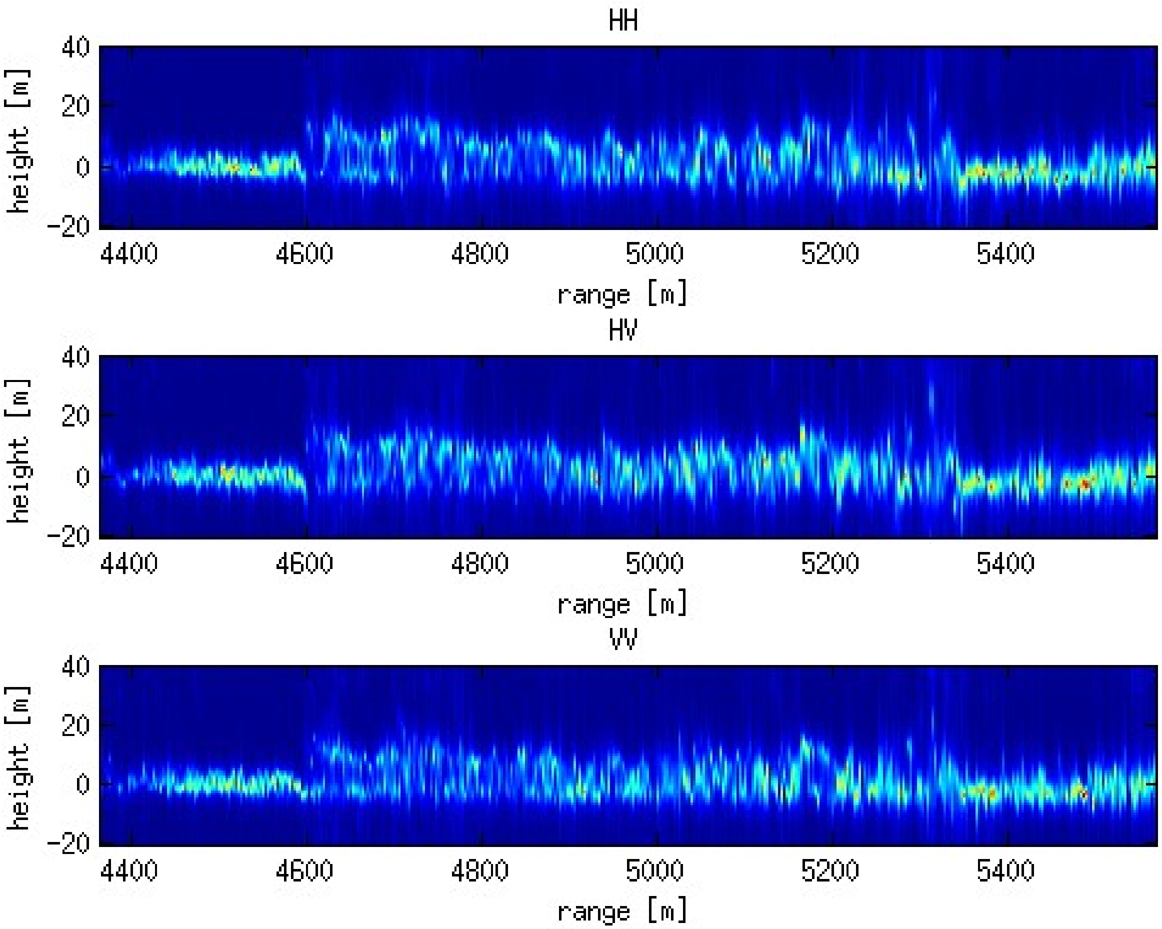

Advanced TomoSAR imaging Using Specan methods

Urban area test site

- Images over Dresden, 2000
- DLR's E-SAR at L-Band
- Resolution : 0.5 m × 2.5 m
- Fully polarimetric
- Dual-baseline InSAR

Baselines	H_{am}
10 m	55-73 m
40 m	14-18 m

3 PolSAR images

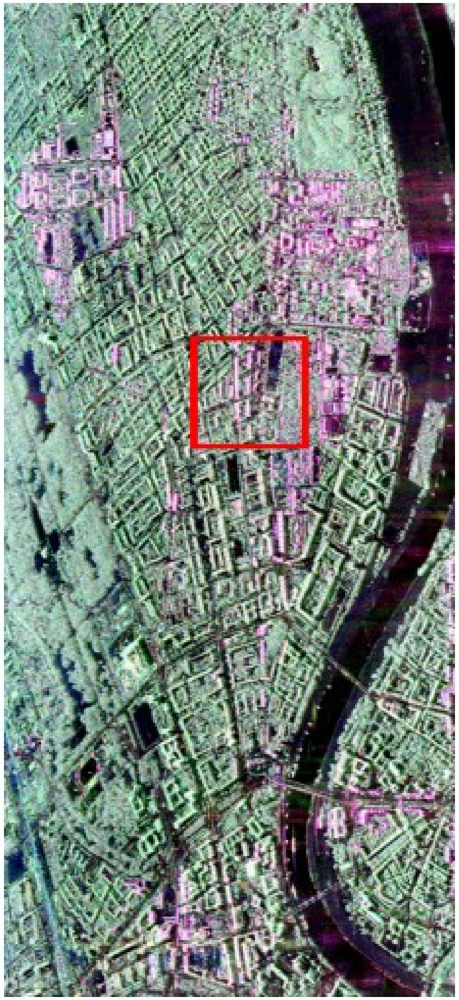

Pauli-coded SAR image

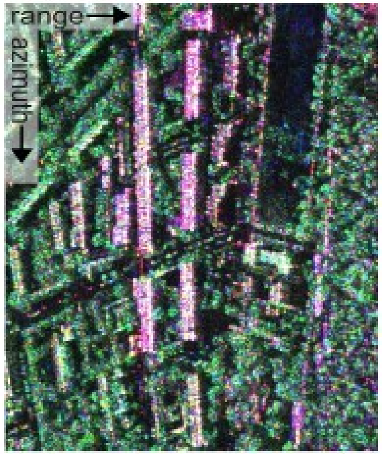

Optical image

SAR tomography over urban areas

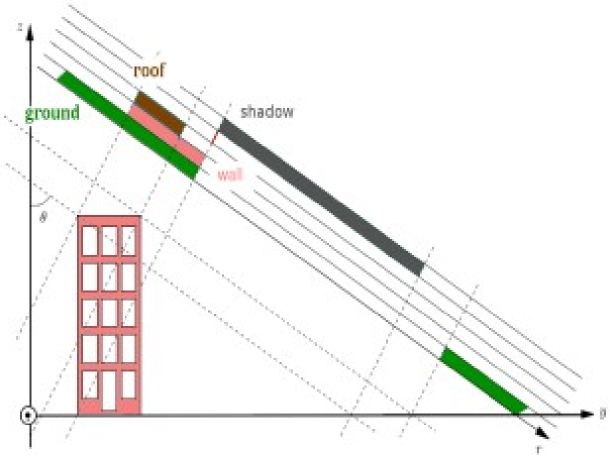

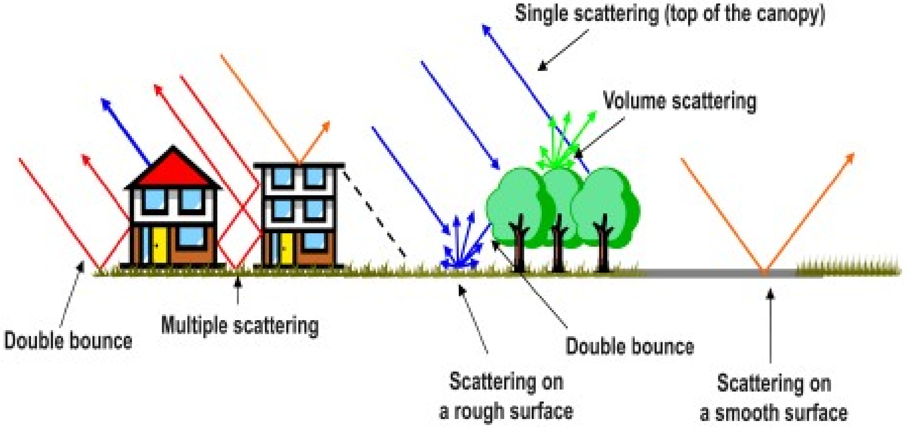

- L-band intermediate-resolution data sets
  $\Rightarrow$ High-Resolution (HR) tomographic estimators
- 3 images
  $\Rightarrow N_s = 2$

Tomographic imaging using specan

Critical configuration (3 images) in an urban environment at L band

(a) Optical image

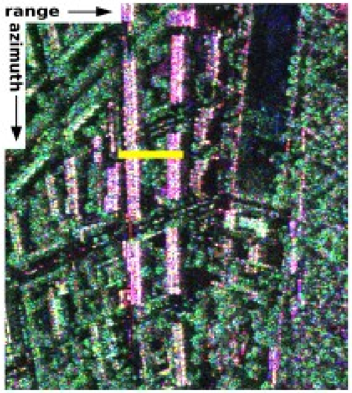

(b) SAR

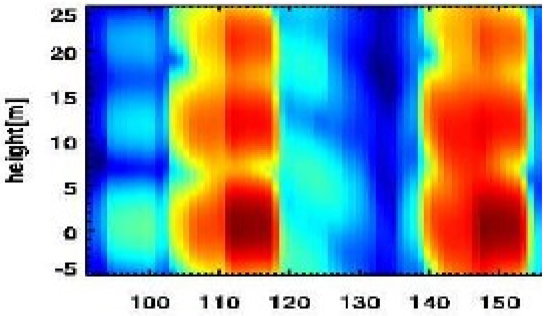

BF

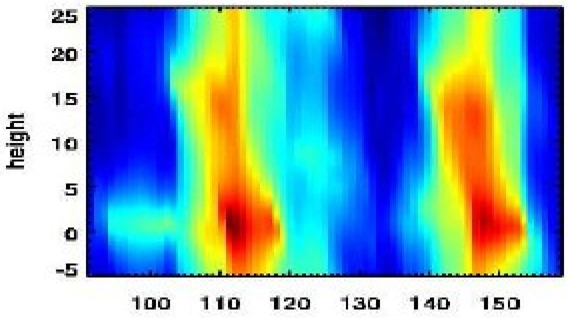

CAPON

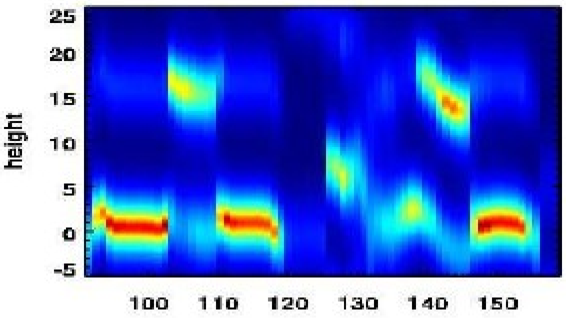

MUSIC

- Strictly speaking, Capon's technique is not HR, but is very convenient
- MUSIC (and some other techniques) is HR

Polarimetric SAR tomography over urban areas

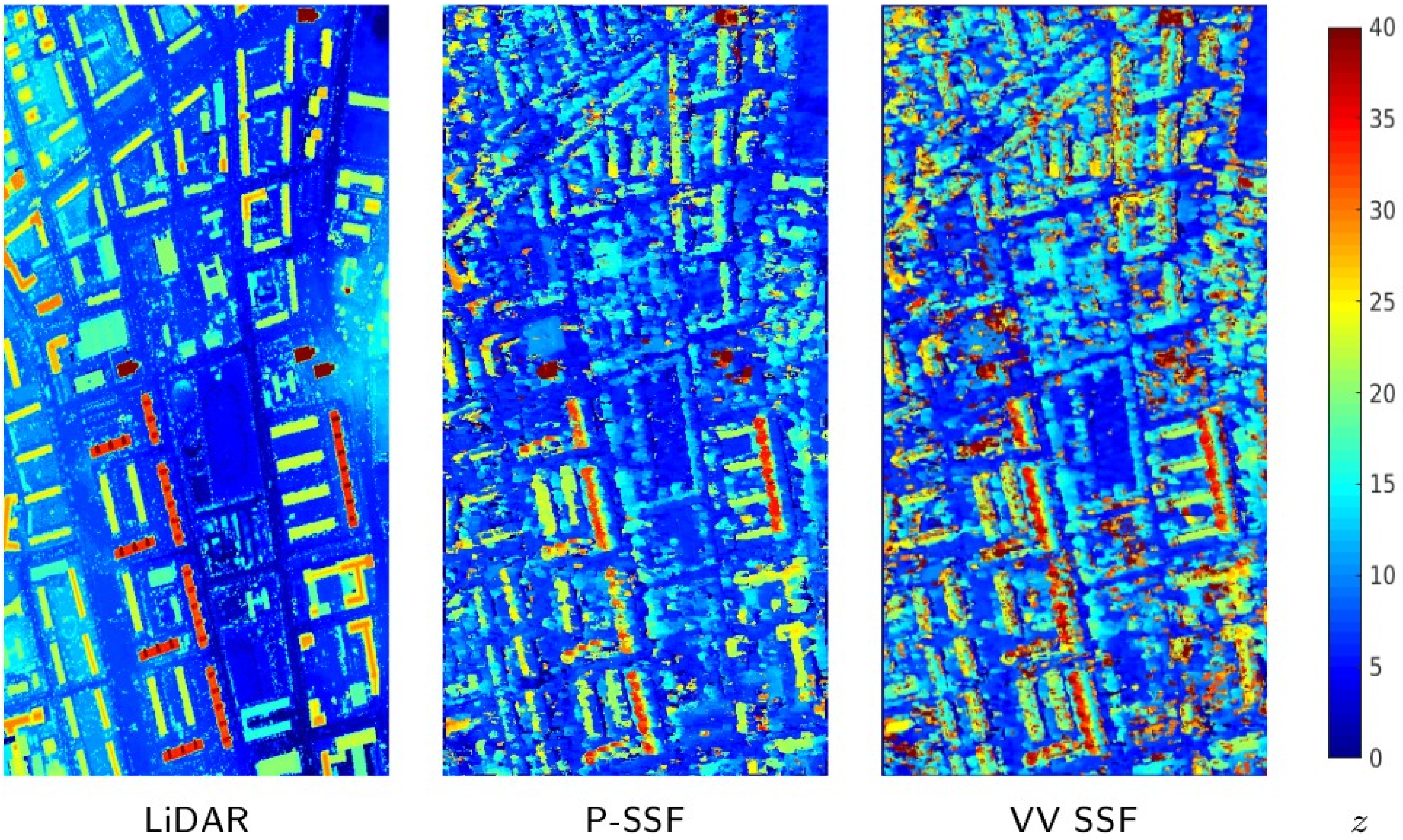

Polarimetric SAR tomography over urban areas

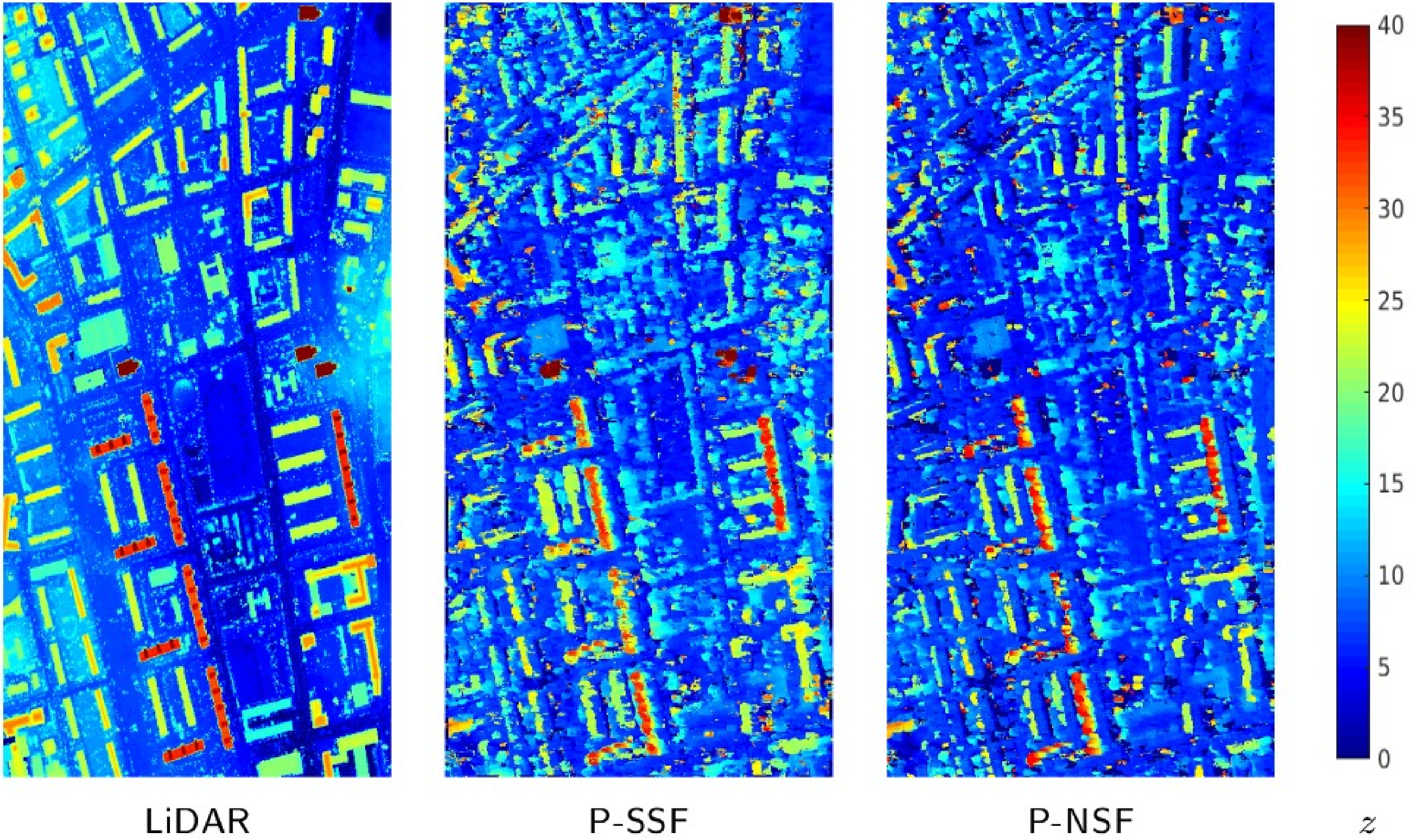

Polarimetric SAR tomography over urban areas

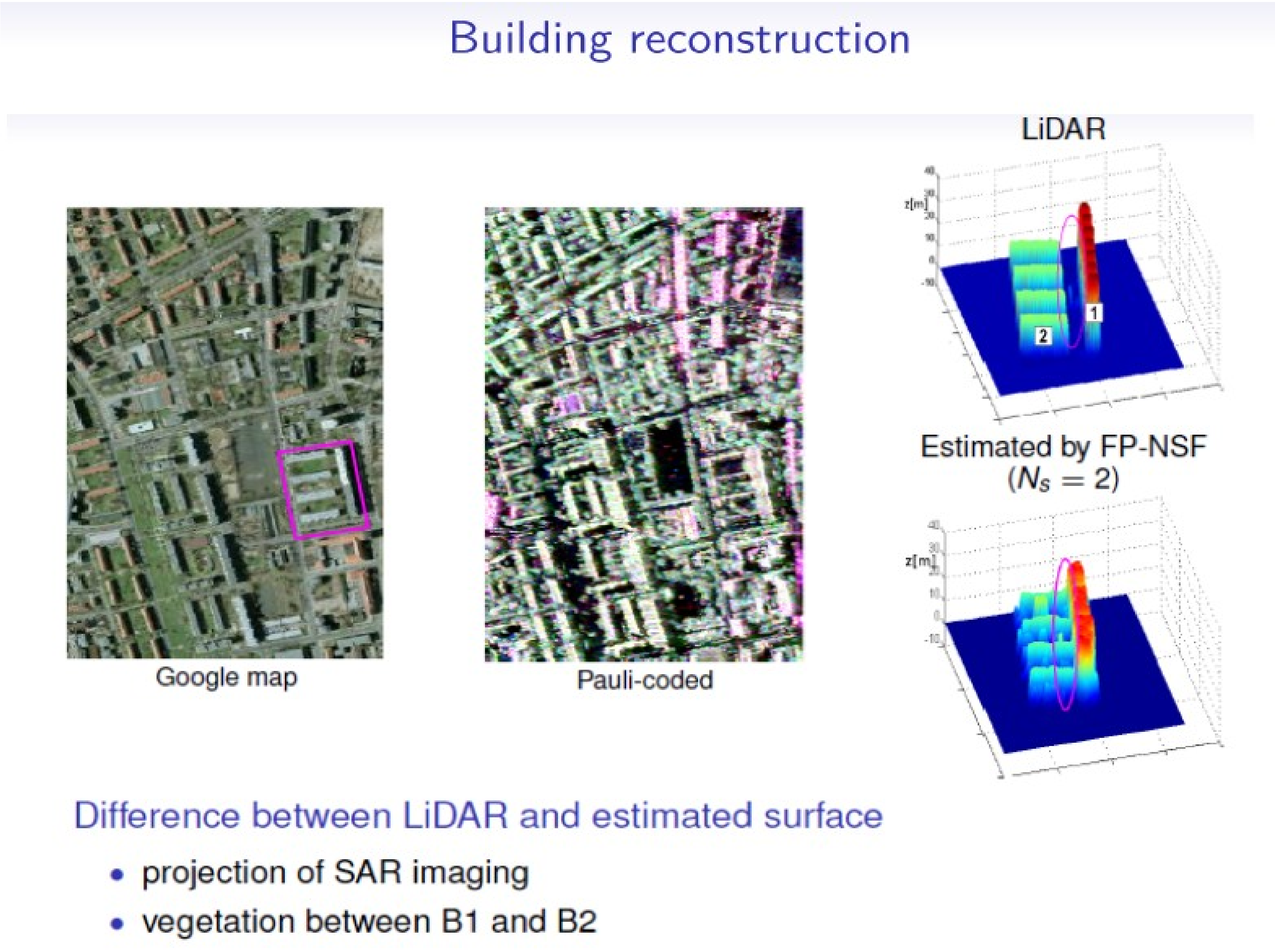

Building reconstruction

Google map

Pauli-coded

LiDAR

Estimated by FP-NSF ($N_s = 2$)

Difference between LiDAR and estimated surface

- projection of SAR imaging
- vegetation between B1 and B2

Polarimetric SAR tomography over urban areas

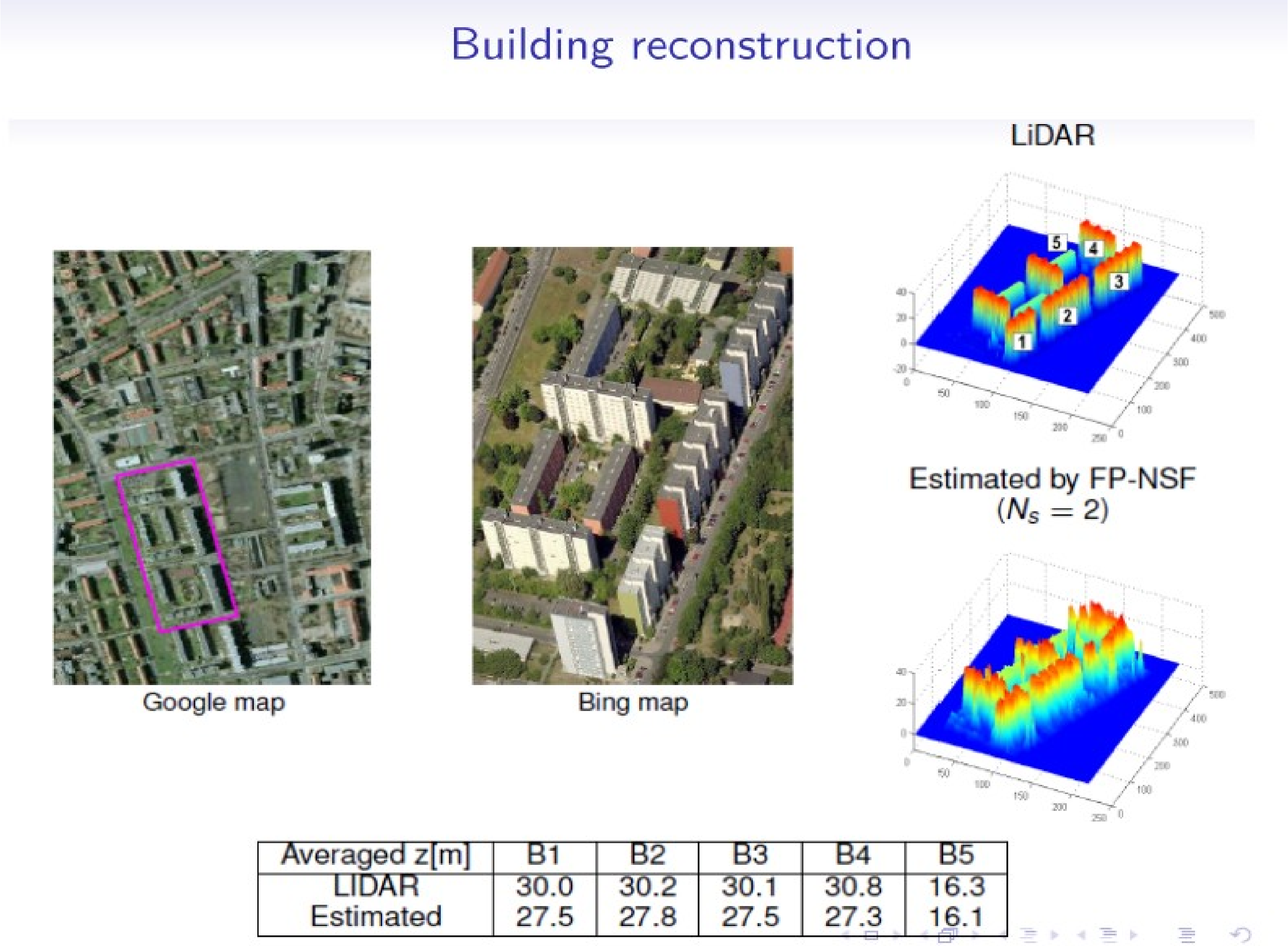

Building reconstruction

Google map

Bing map

LiDAR

Estimated by FP-NSF ($N_s = 2$)

Averaged z[m]	B1	B2	B3	B4	B5
LIDAR	30.0	30.2	30.1	30.8	16.3
Estimated	27.5	27.8	27.5	27.3	16.1

TomoSAR imaging of concealed objects

Above ground and under foliage objects observed at L band

- DLR E-SAR image over Dornstetten, Germany
- L-Band
- 21 tracks : average baseline 20m
- $\delta_z = 2\text{m}$

Horizontal baseline distribution

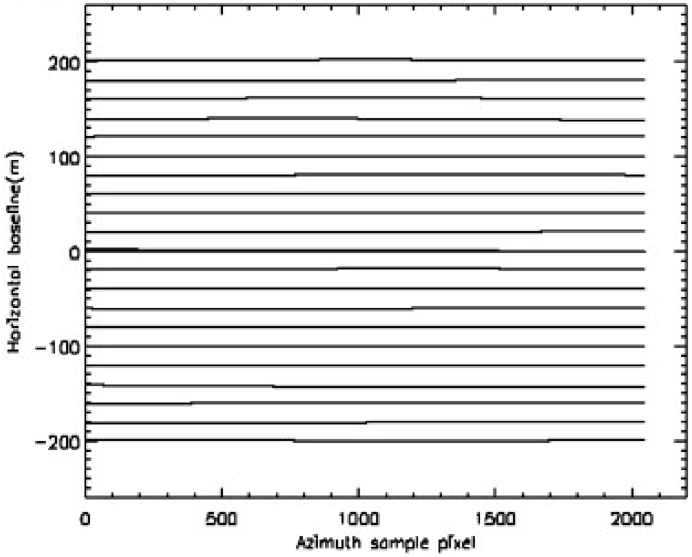

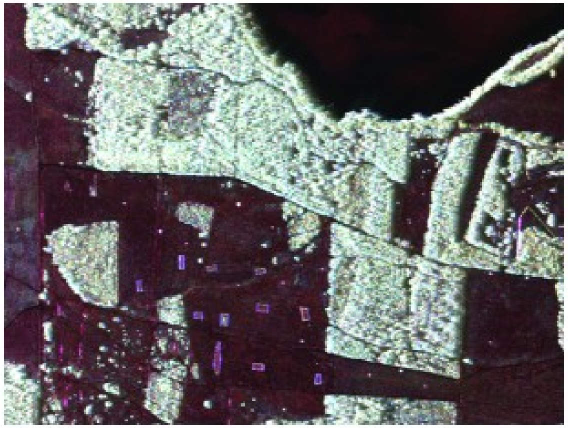

Huang, Y.; Ferro-Famil, L. & Reigber, A. "Under-Foliage Object Imaging Using SAR Tomography and Polarimetric Spectral Estimators", IEEE TGRS 2011

TomoSAR imaging of concealed objects

VV refectivity tomograms

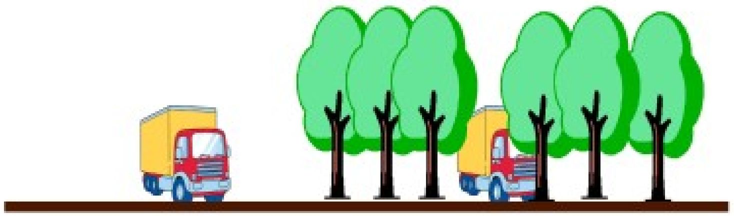

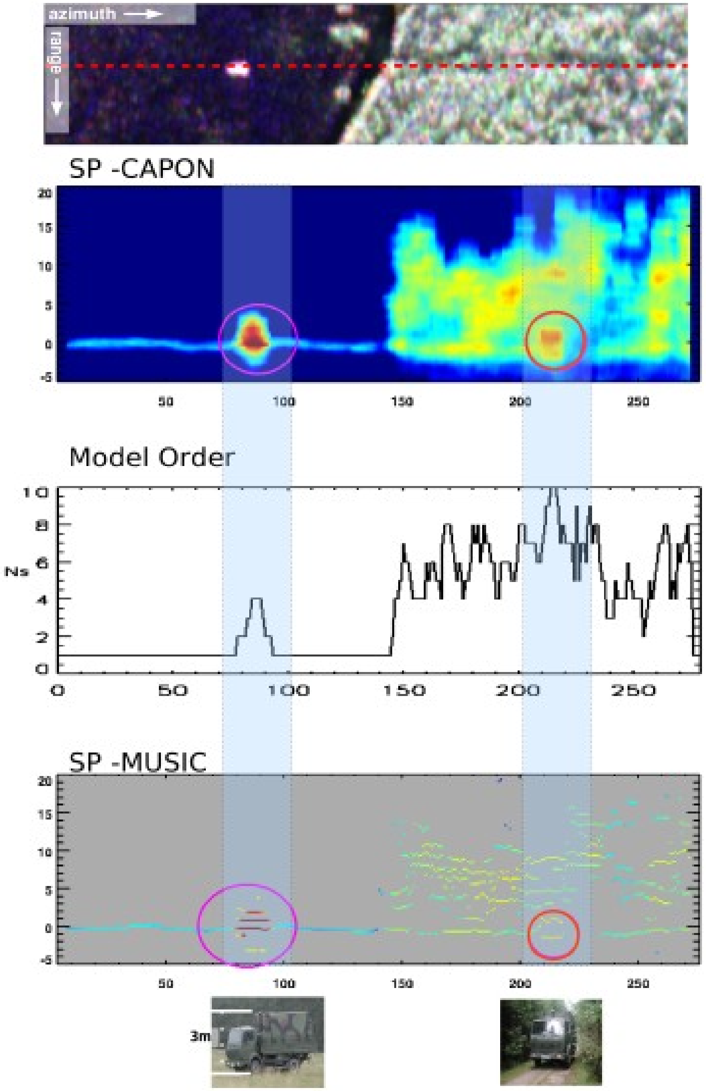

Capon :

limited resolution

$\Rightarrow$ overestimated H_{truck}

MUSIC :

- ☺ Sub-canopy truck
  $\Rightarrow$ hybrid scatterer
- ☹ Uncovered
  $\Rightarrow$ coherent scatterer
- ☹ Spurious sidelobes.

TomoSAR imaging of concealed objects

High Resolution tomograms of underfoliage objects

SSF : shape and reflectivity

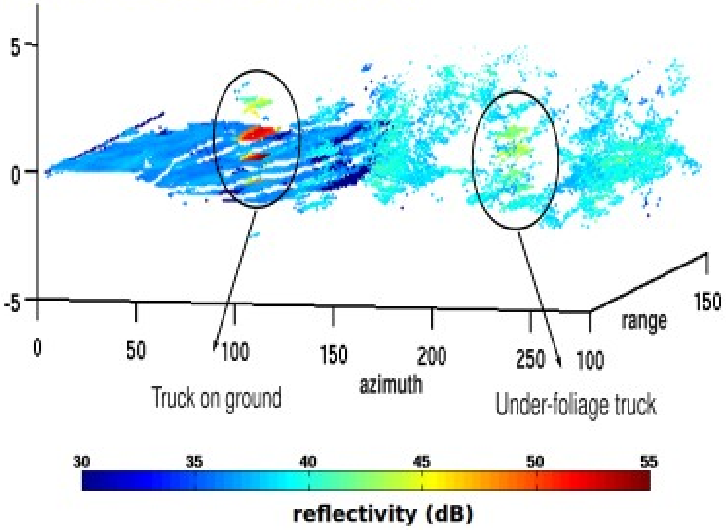

FP-NSF : scattering mechanisms

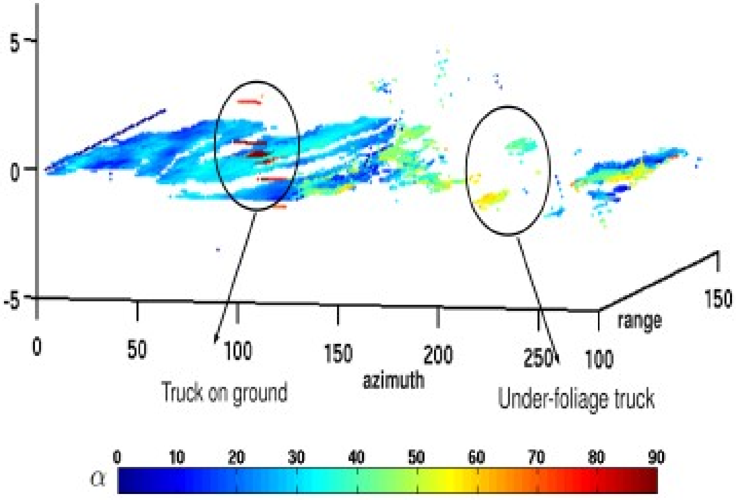

TomoSAR imaging of concealed objects

Sparse (compressive) sensing solution

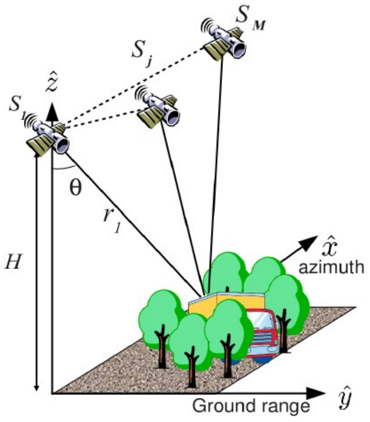

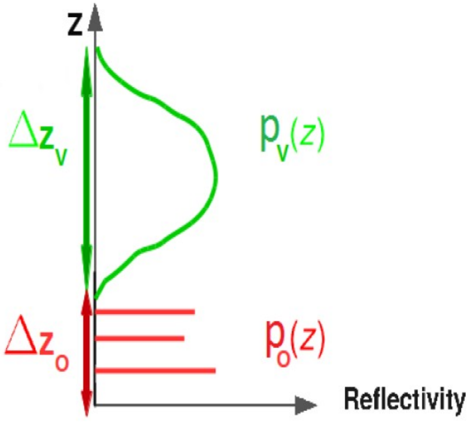

- a few wavelet components

- a few discrete contributions

$$\boxed{\min_{\mathbf{p}} ||\mathbf{B}\mathbf{p}||_1 \text{ subject to } \quad ||\mathbf{R} - \widehat{\mathbf{R}}||_F \leq \epsilon \qquad \widehat{\mathbf{R}} = \mathbf{A}(\mathbf{z})\,\mathrm{diag}(\mathbf{p})\mathbf{A}^H(\mathbf{z})}$$

$$\mathbf{B} = \begin{bmatrix} \mathbf{I}_{(N_o \times N_o)} & \mathbf{0} \\ \mathbf{0} & \mathbf{\Psi}_{(N_v \times N_v)} \end{bmatrix} \in \mathbb{R}^{(N_s \times N_s)} \qquad \mathbf{p} = [\mathbf{p}_o^T \quad \mathbf{p}_v^T]^T \in \mathbb{R}^{+N_s \times 1}$$

TomoSAR imaging of concealed objects

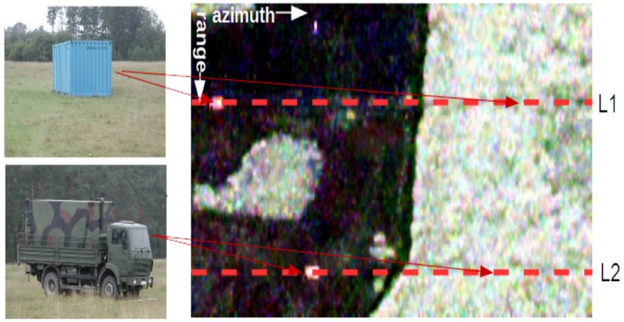

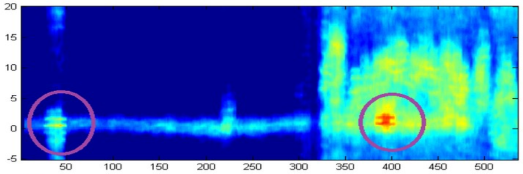

(a) Capon

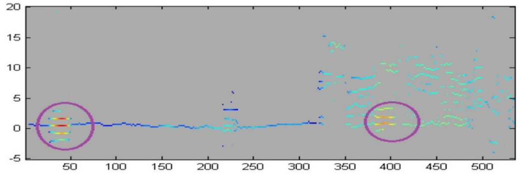

(b) MUSIC

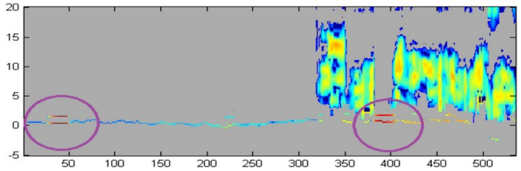

(c) Proposed method with merging

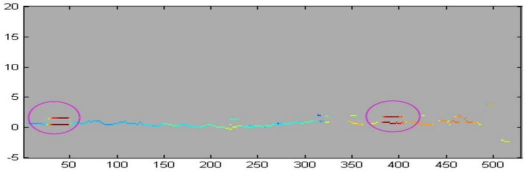

(d) Ground and underfoliage scattering ($\mathbf{p}_o$) estimated by proposed method with merging

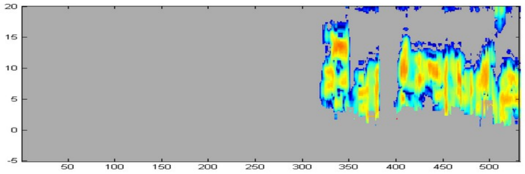

(e) Canopy power ($\mathbf{p}_v$) estimated by proposed method with merging

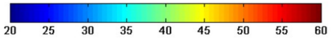

(f) dB

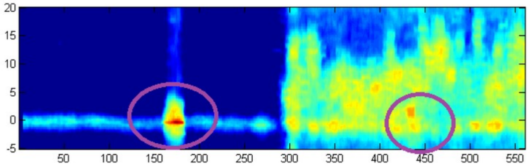

(a) Capon

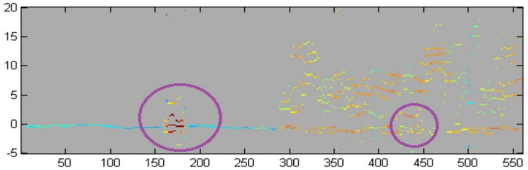

(b) MUSIC

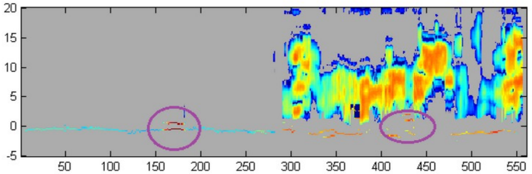

(c) Proposed method with merging

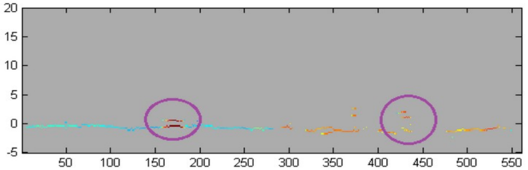

(d) Ground and underfoliage scattering ($\mathbf{p}_o$) estimated by proposed method with merging

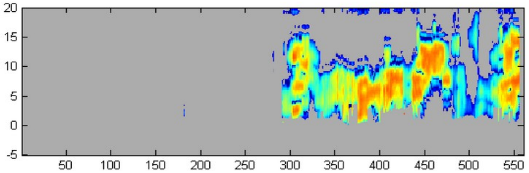

(e) Canopy power ($\mathbf{p}_v$) estimated by proposed method with merging

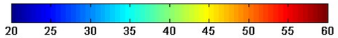

(f) dB

TomoSAR imaging

of a tropical forest at P band

Preparation of the BIOMASS mission

Context: ESA's BIOMASS mission

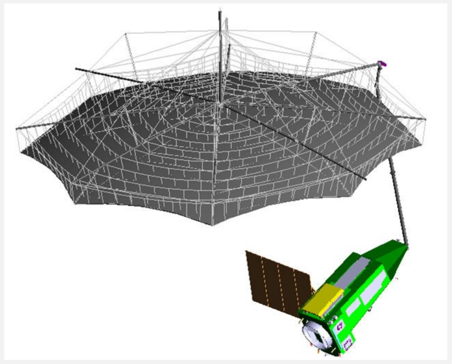

BIOMASS
P-band
polarimetric SAR

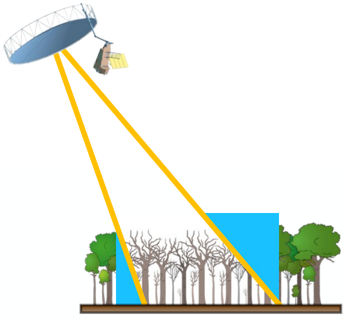

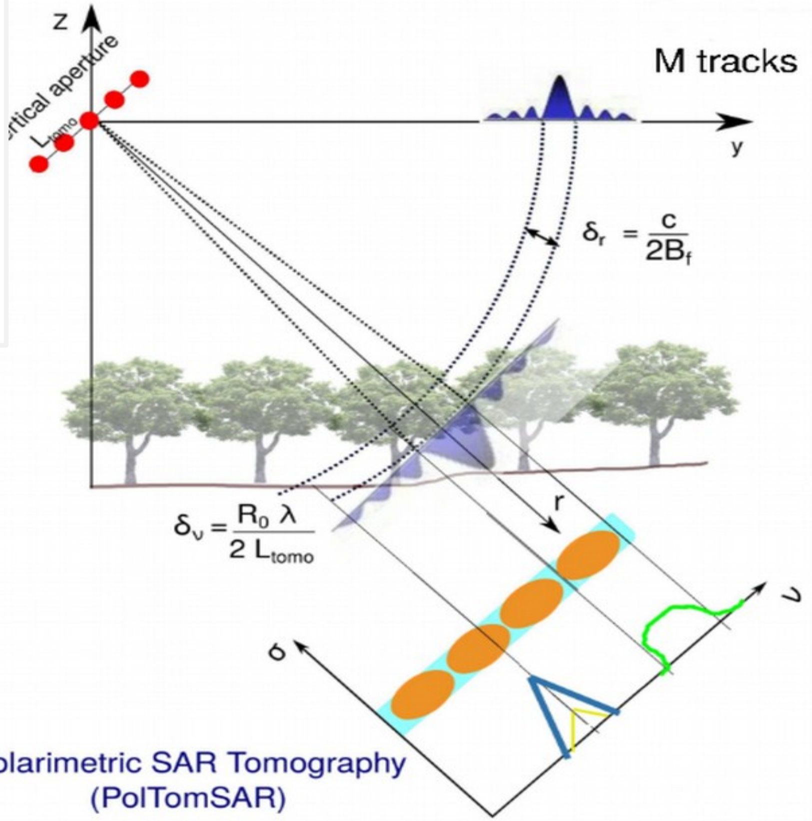

Polarimetric SAR Tomography
(PolTomSAR)

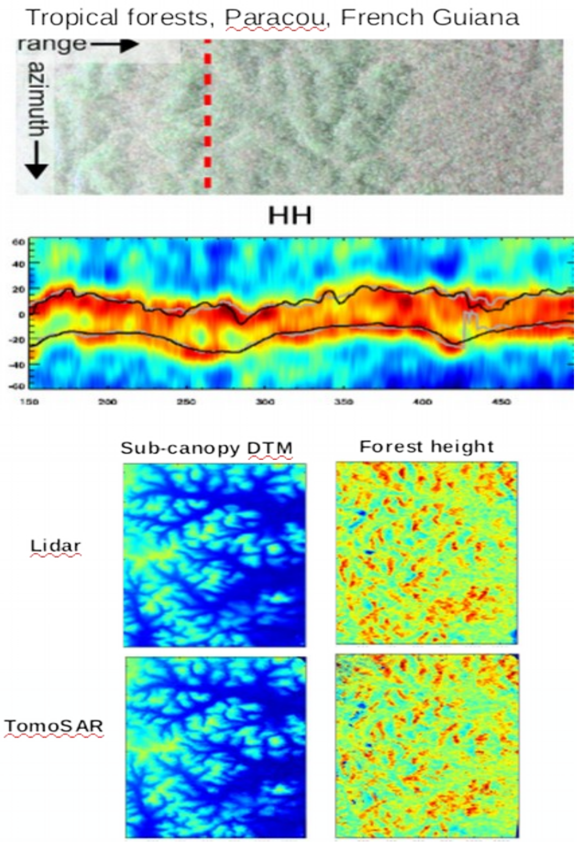

BIOMASS products supporting the scientific objectives

AGB density [t/ha]

Above Ground Biomass (tons/hectare)

- 200 m resolution
- 1 map every 6 months
- global covera0ge of forested areas
- accuracy of 20%, or 10 t ha^{-1} for biomass < 50 t ha^{-1}

Forest Height [m]

Upper canopy height (meter)

- 200 m resolution
- 1 map every 6 months
- global coverage of forested areas
- accuracy of 20-30%

Disturbances [ha]

Areas of forest clearing (hectare)

- 60×50 m resolution
- 1 map every 6 months
- global coverage of forested areas
- 90% classification accuracy

Issues

Global coverage restriction (SOTR)
→ Europe and North/Central-America are excluded

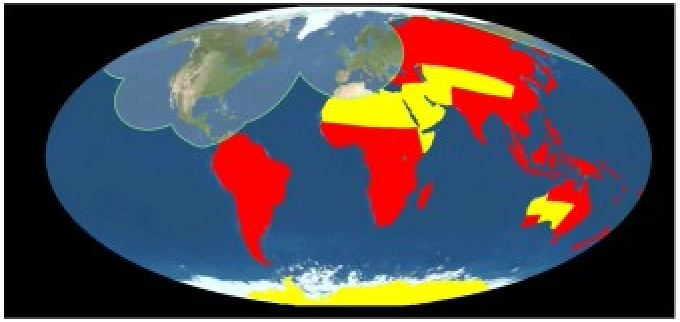

Temporal decorrelation
→ repeat-pass multi-baseline InSAR

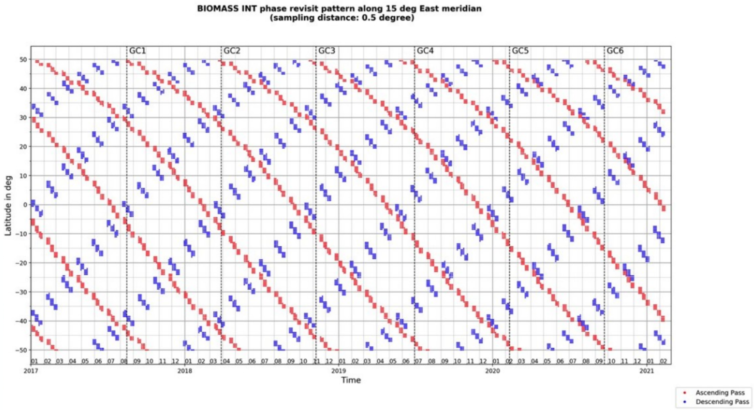
BIOMASS INT phase revisit pattern along 15 deg East meridian
(sampling distance: 0.5 degree)

Potentially delayed launch (Vega-C)
→ current launch date: May 2025

Context: ESA's BIOMASS mission

Tomographic Phase:
7 x 3-day repeat
15 months for global coverage

Interferometric Phase:
3 x 3-day repeat; 7 months for global coverage
≈ 4 years time series

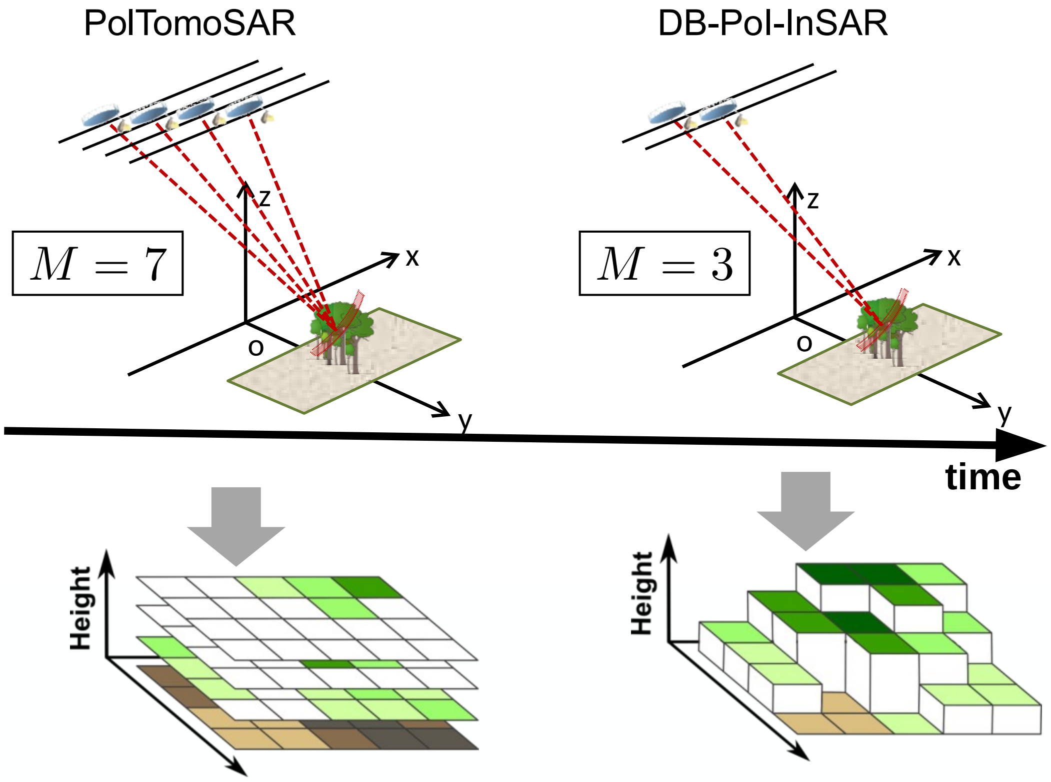

Objectives

- Performance quantification tool

→ Minimal achievable estimation uncertainty

- Key forest parameters

→ DTM, FH, (AGB proxy)

- Assess simulated BIOMASS configuration

→ Airborne vs BIOMASS resolutions

- Synergistic use of BIOMASS modes

→ Performance improvement using priors

Evaluation data set

- TropiSAR Campaign, 2009
- ONERA SETHI
- P-Band
- 6 tracks
- $\delta_{az} = 1.245m$
  $\delta_{rg} = 1m$
- $\delta_z = 12.5m$
- Ground truth
  - LiDAR data
  - Biomass measurements for 16 ROIs

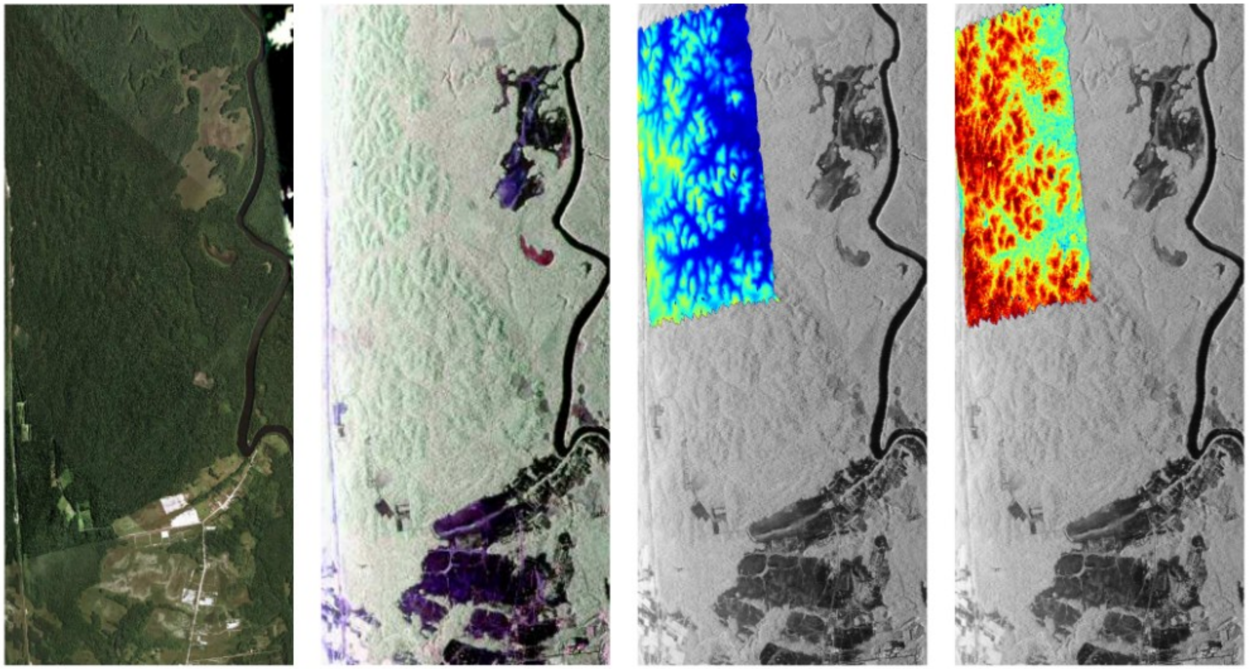

(a) Optical Image (b) SAR Image (c) Lidar DTM (d) Lidar DSM

Simulation of BIOMASS data

Performance evaluation principle

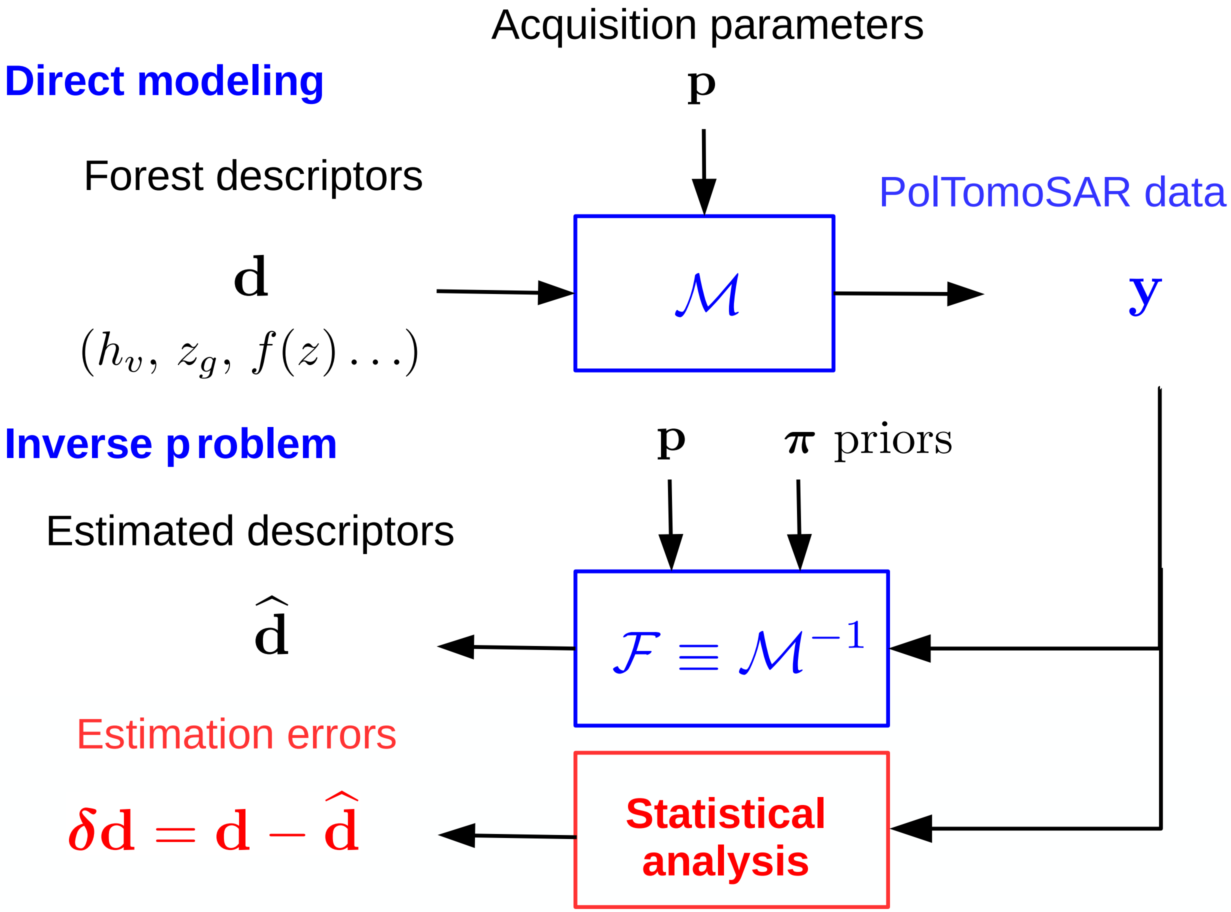

Acquisition parameters

Direct modeling

$\mathbf{p}$

Forest descriptors

PolTomoSAR data

$\mathbf{d}$

$(h_v, z_g, f(z)\dots)$

$\mathcal{M}$

$\mathbf{y}$

Inverse problem

$\mathbf{p}$ $\boldsymbol{\pi}$ priors

Estimated descriptors

$\widehat{\mathbf{d}}$

$\mathcal{F} \equiv \mathcal{M}^{-1}$

Estimation errors

$\delta\mathbf{d} = \mathbf{d} - \widehat{\mathbf{d}}$

Statistical analysis

<u>What is needed</u>

- Valid direct model

- Forest configuration

  & acquisition conditions

- Potential priors

- Theoretical statistical analysis

↓

minimal achievable uncertainty of parameter estimates

L. Ferro-Famil & S.Tebaldini

Airborne vs simulated BIOMASS coherence maps

Airborne data

$\delta_{az} \approx 1\,m \quad \delta_{rg} \approx 1\,m$

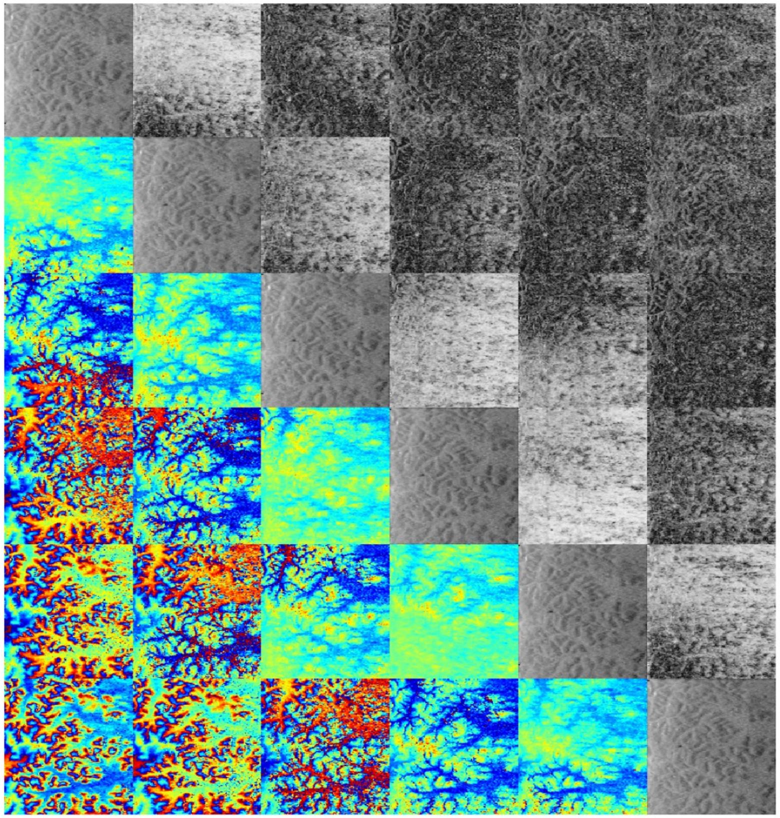

Simulated BIOMASS data

$\delta_{az} = 12.5\,m \quad \delta_{rg} = 25\,m$

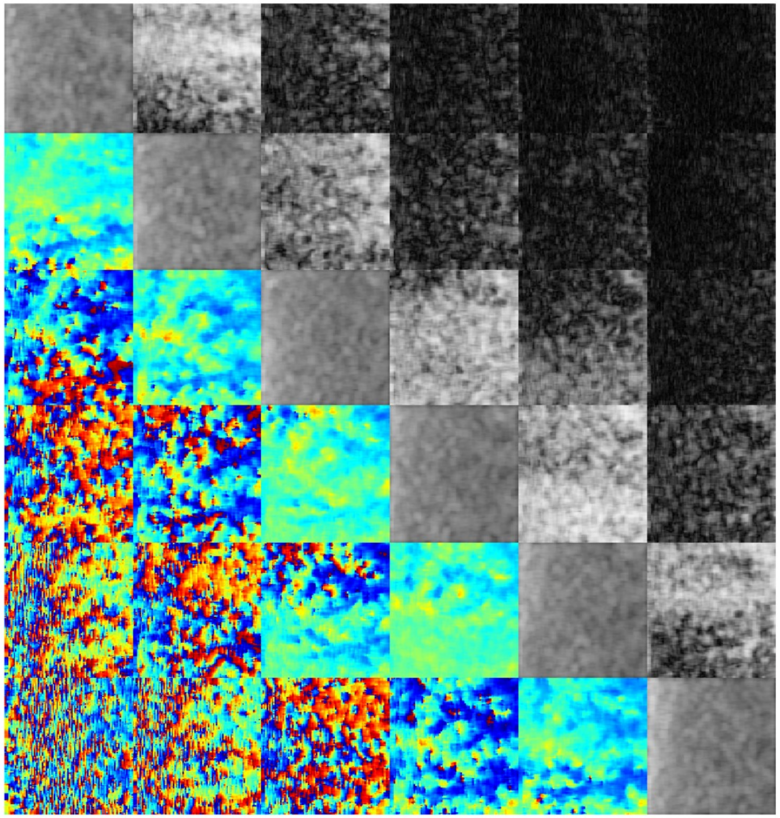

- Important loss of spatial resolution
- Range decorrelation

L. Ferro-Famil & S.Tebaldini

Model selection and validation

Model selection

Low rank reflectivity profile + decorrelation terms

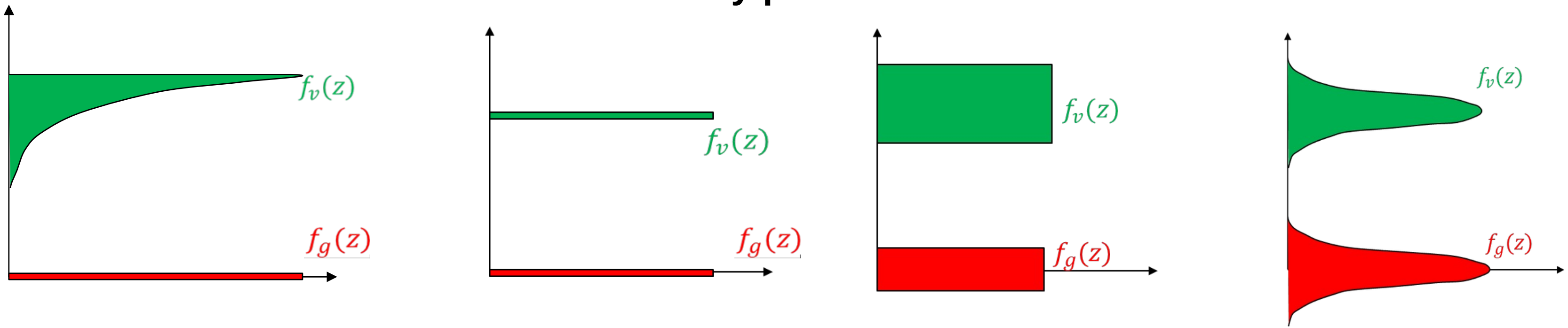

Validation of radiometric representativity

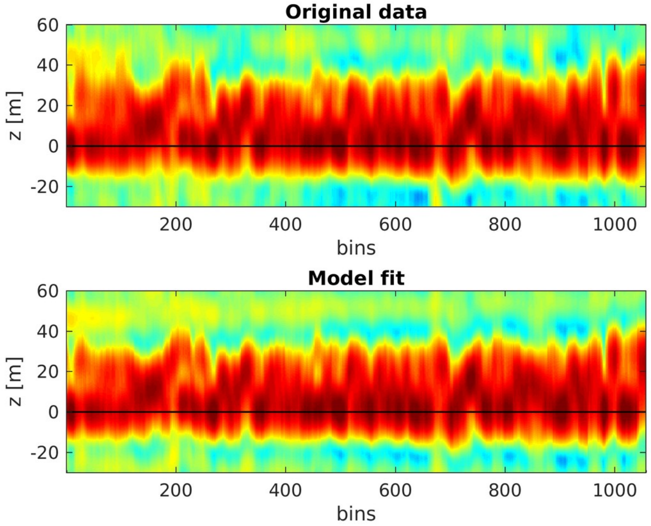

Airborne data

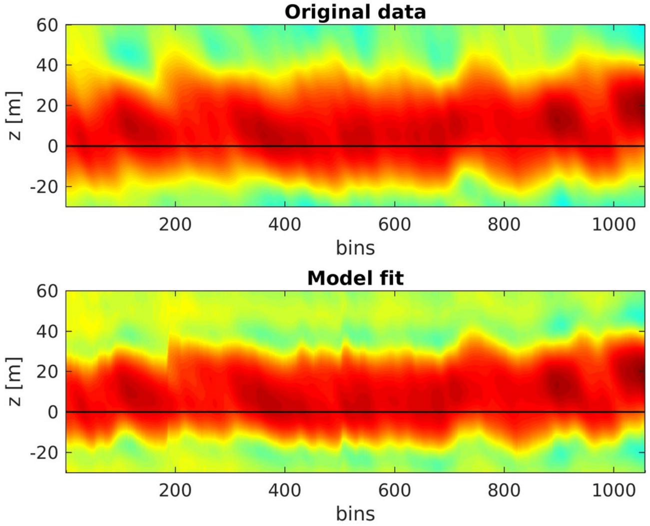

Simulated
BIOMASS data

Theoretical limits vs experimental performance

DTM estimation, airborne configuration

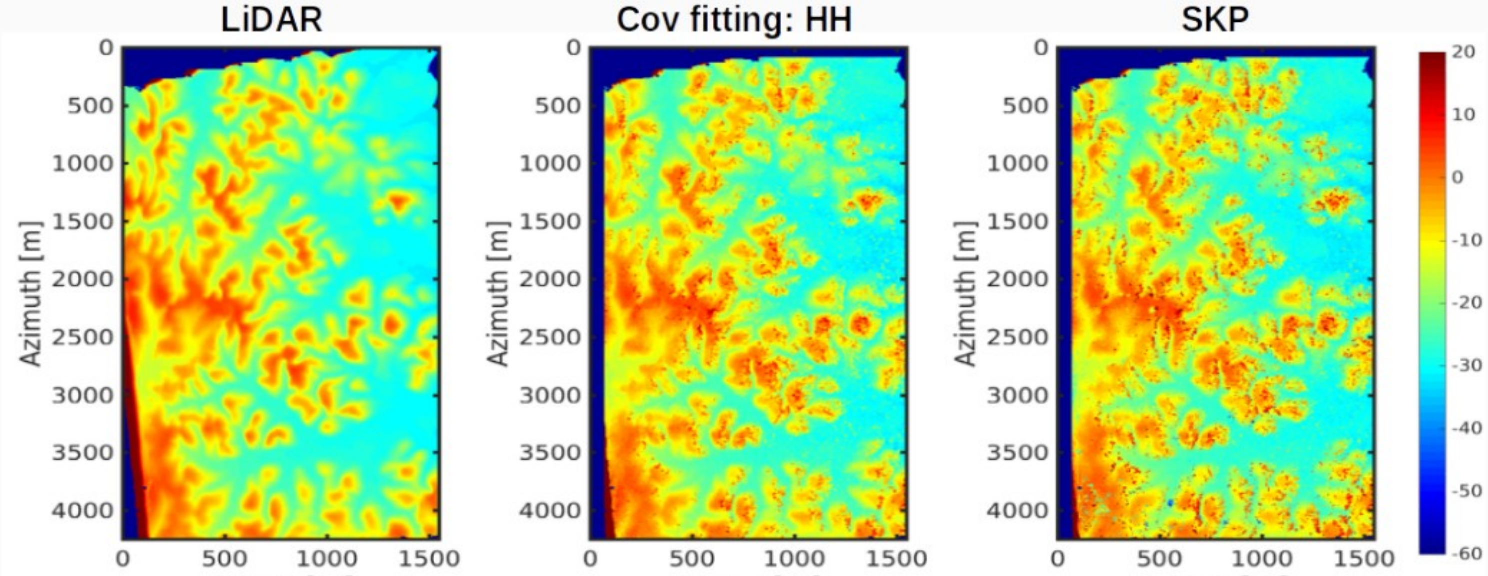

LiDAR

Cov fitting: HH

SKP

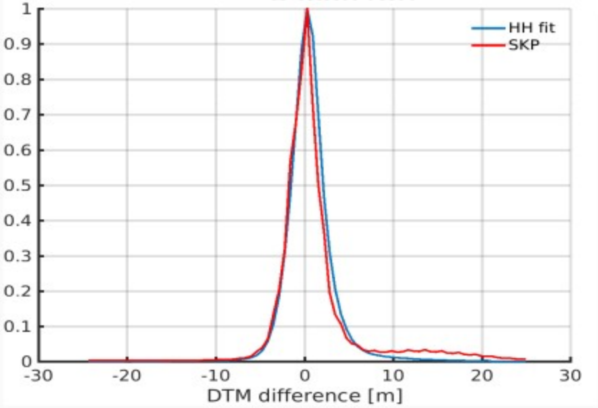

Tomo - Lidar	bias	sdev
Cov fit	0.10 m	1.26 m
SKP	0 m	1.67 m

- Similar good performance
- SKP: potential unstability, a few large errors

Theoretical limits vs experimental performance

CHM estimation, airborne configuration

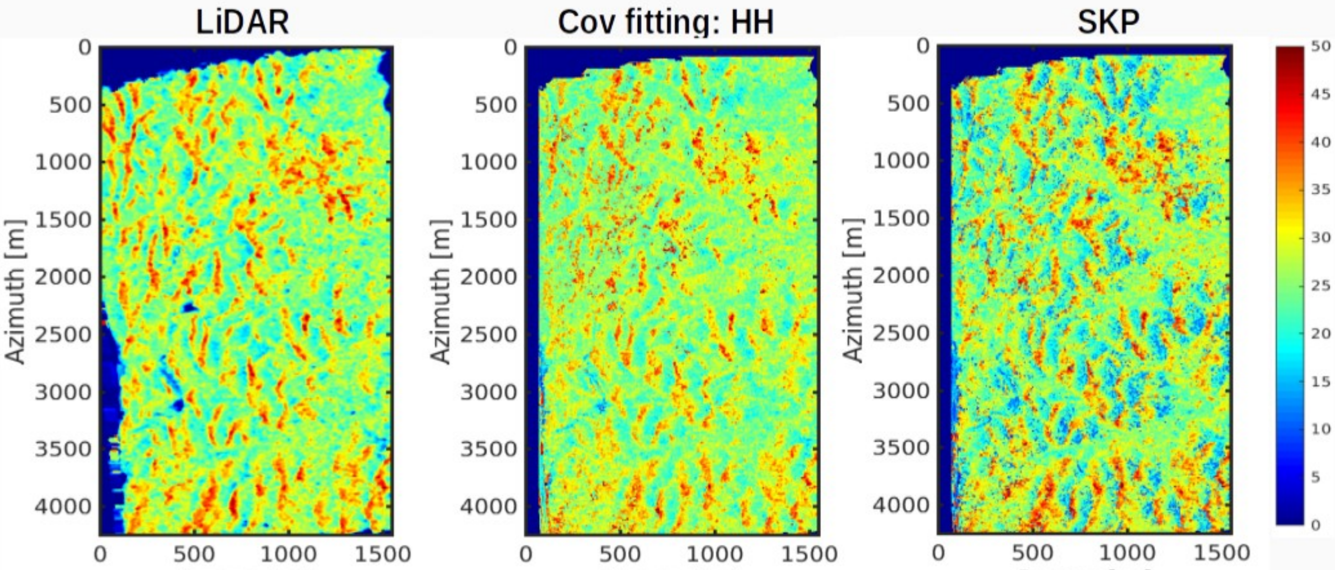

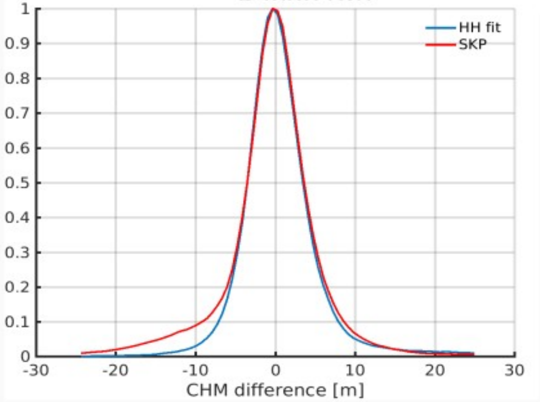

Tomo - Lidar	bias	sdev
Cov fit	$-0.18\,m$	$2.40\,m$
SKP	$-0.02\,m$	$2.83\,m$

- SKP: less stable

Theoretical limits vs experimental performance

DTM estimation, spaceborne configuration

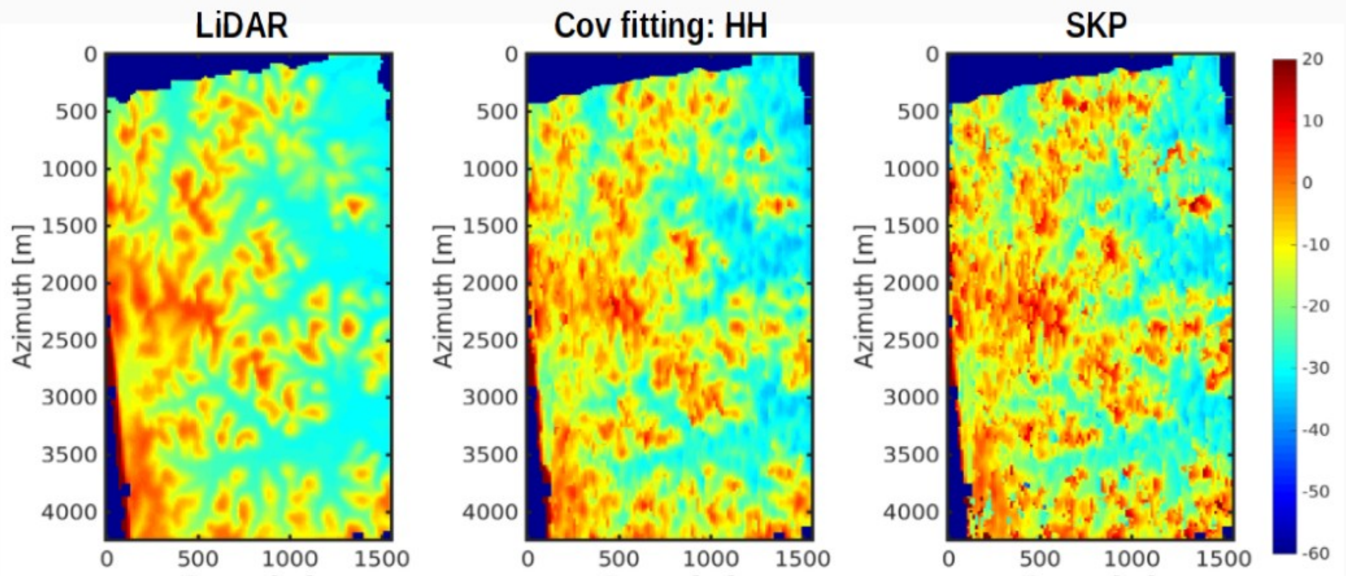

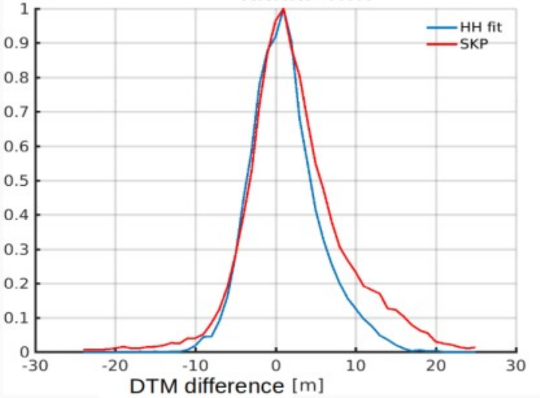

Tomo - Lidar	bias	sdev
Cov fit	0.33 m	2.67 m
SKP	1.10 m	3.63 m

- SKP: overestimate ground elevation, some systematic large errors

Theoretical limits vs experimental performance

CHM estimation, spaceborne configuration

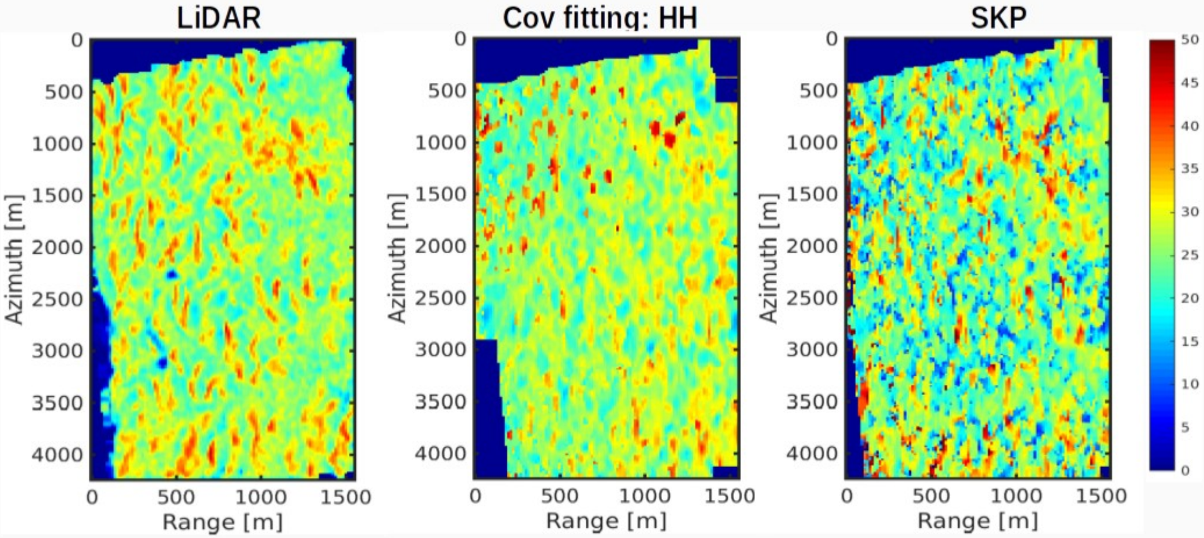

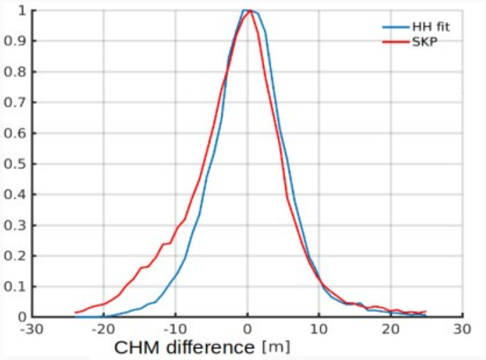

Tomo - Lidar	bias	sdev
Cov fit	$-0.20\ m$	$3.31\ m$
SKP	$-1.42\ m$	$4.21\ m$

- SKP: underestimate CHM with larger errors
- Cov-fitting:
  overall smaller errors & uncertainty

Minimal achievable uncertainty: application to real data

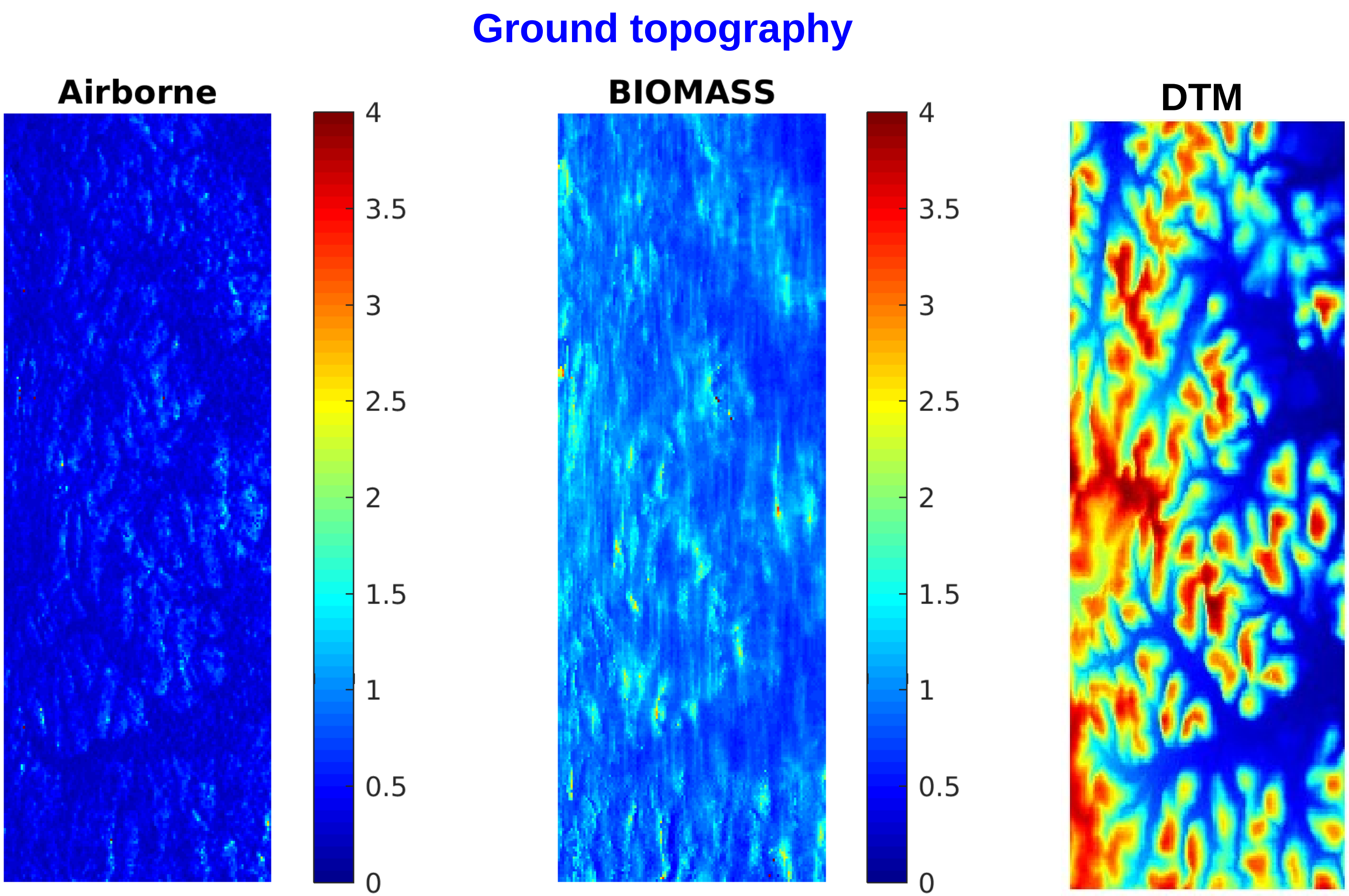

DTM uncertainty sensitivity to range slope well assessed by this method

Minimal achievable uncertainty: application to real data

Tree height

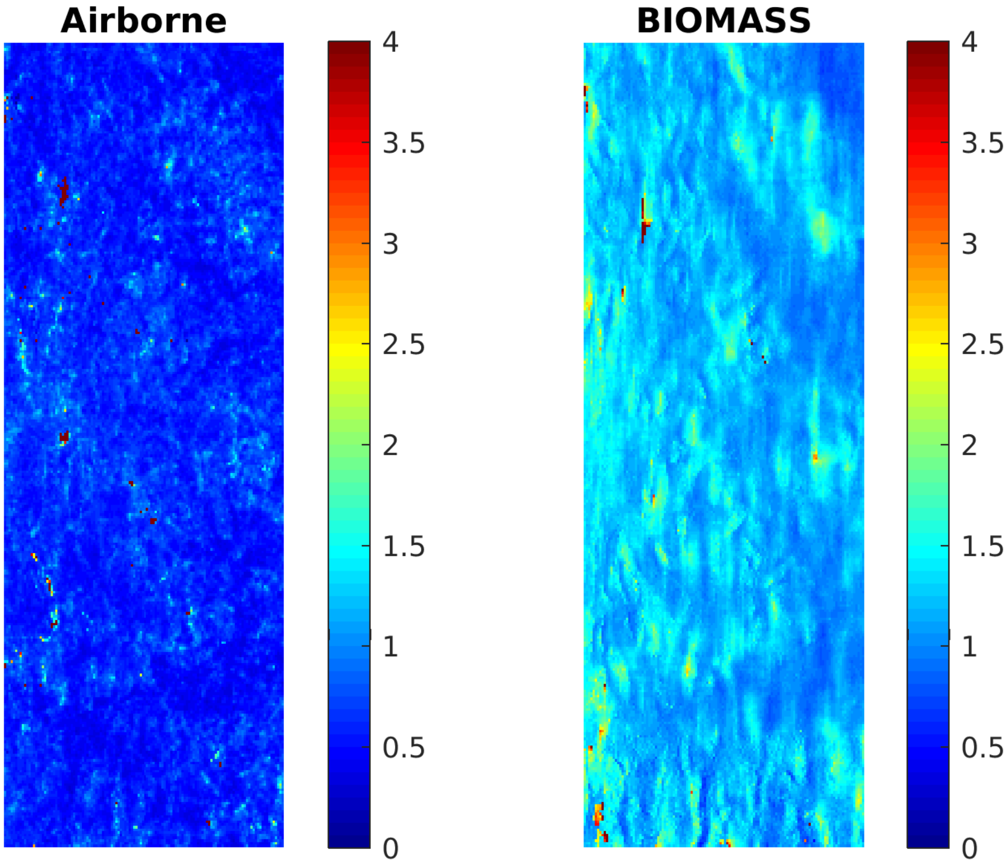

DTM

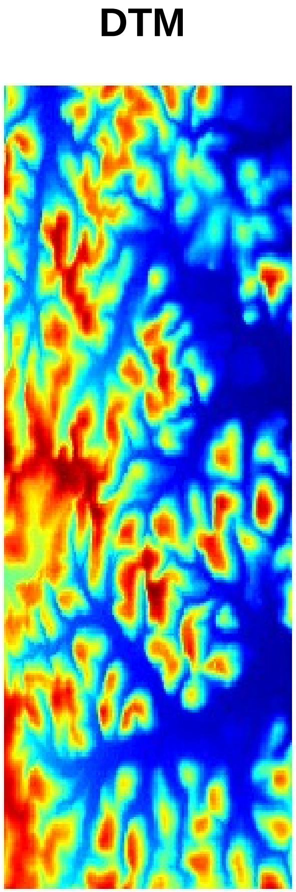

Minimal achievable uncertainty: application to real data

GVR

$$L = \frac{I_v}{I_g + I_v}$$

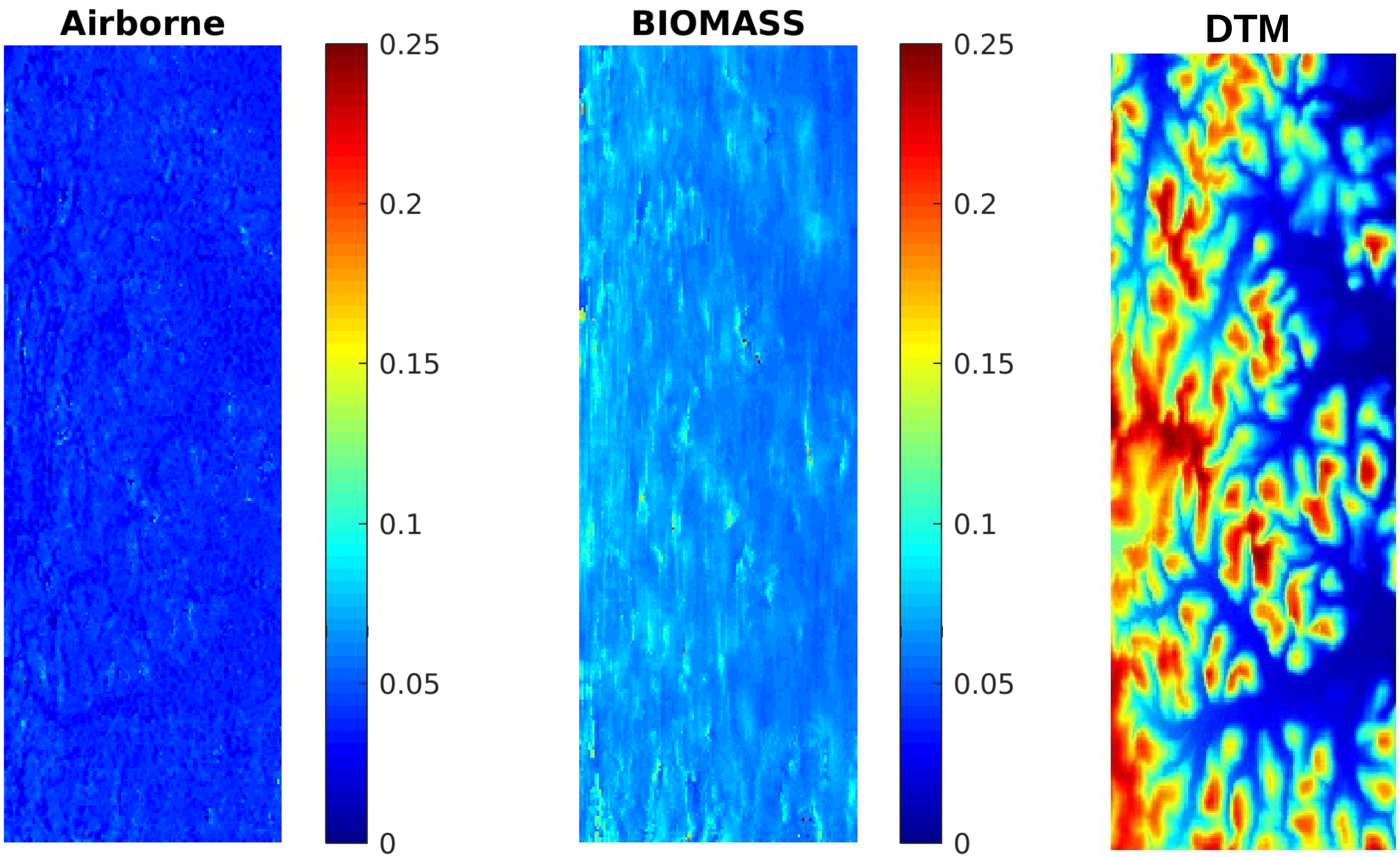

L. Ferro-Famil & S.Tebaldini

Synergistic use of priors

Tomographic Phase:
7 x 3-day repeat
15 months for global coverage

Interferometric Phase:
3 x 3-day repeat; 7 months for global coverage
≈ 4 years time series

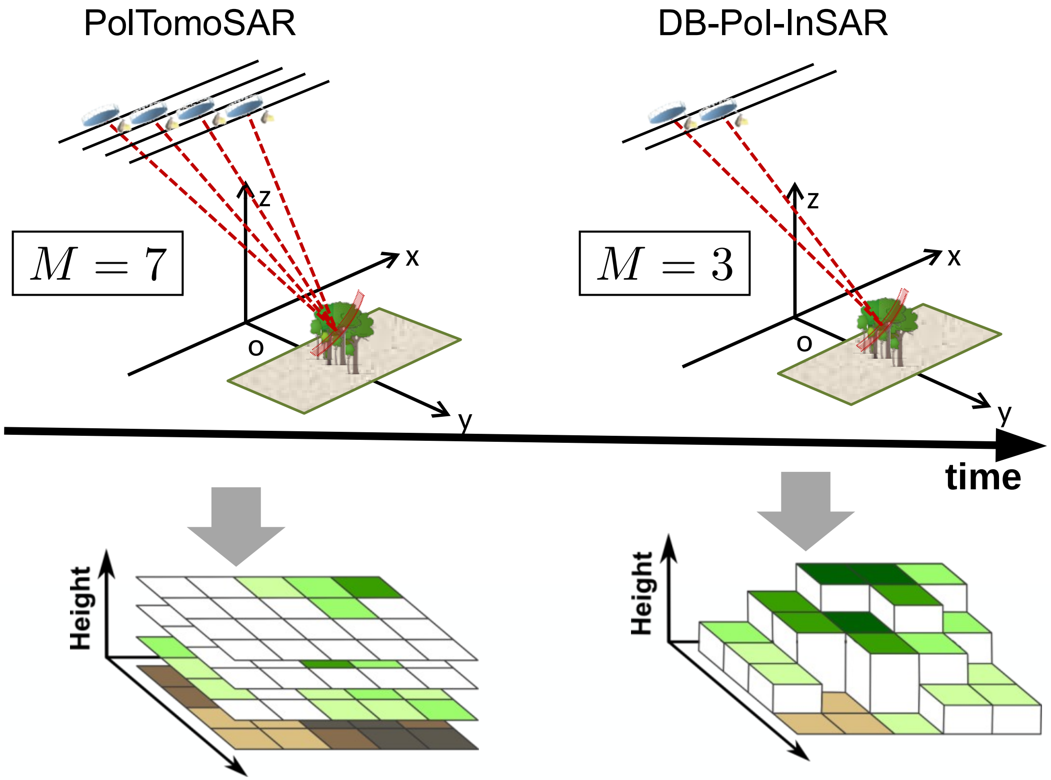

Synergistic use of priors

Inject Tomo DTM **estimate prior**

...to improve Dual Baseline Performance

Synergistic use of Tomo DTM prior in Dual Baseline process

Ground topography

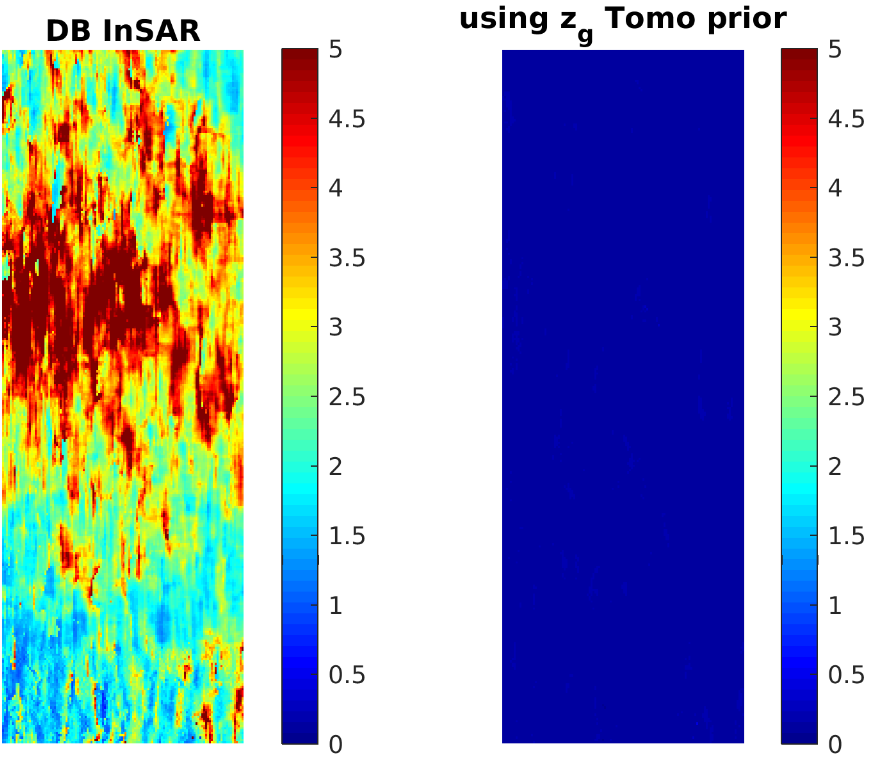

Local low vertical resolution region

Highly informative prior → drastic reduction of uncertainty of the concerned parameter

Direct Model: Random Volume over Ground

Tree height

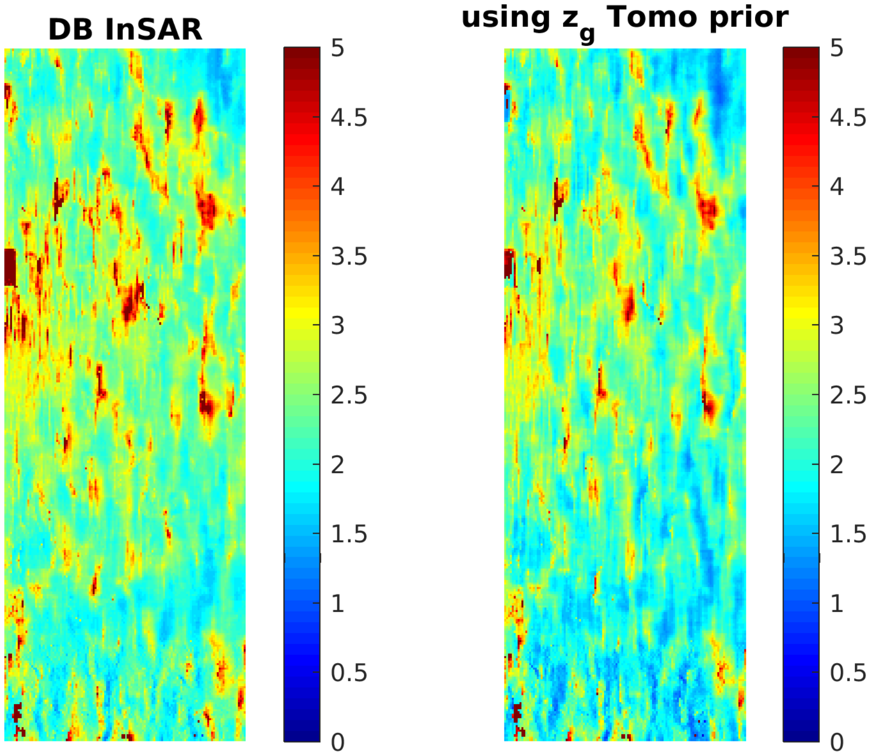

DTM prior → moderate improvement of tree height uncertainty

Direct Model: Random Volume over Ground

GVR $$L = \frac{I_v}{I_g + I_v}$$

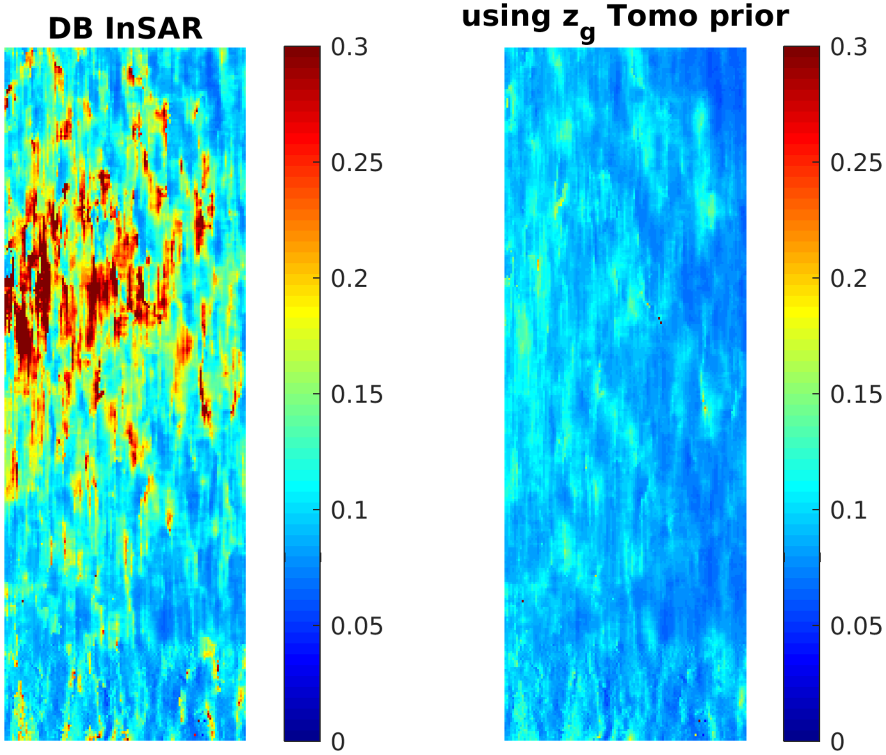

DTM prior → strong improvement of GVR uncertainty
Important for ground and forest volume characterization

Analysis of forest using Polarimetric SAR tomography

Full-Rank specan techniques
and
SKP algebraic decomposition

Need for full-rank Polarimetric SAR Tomography

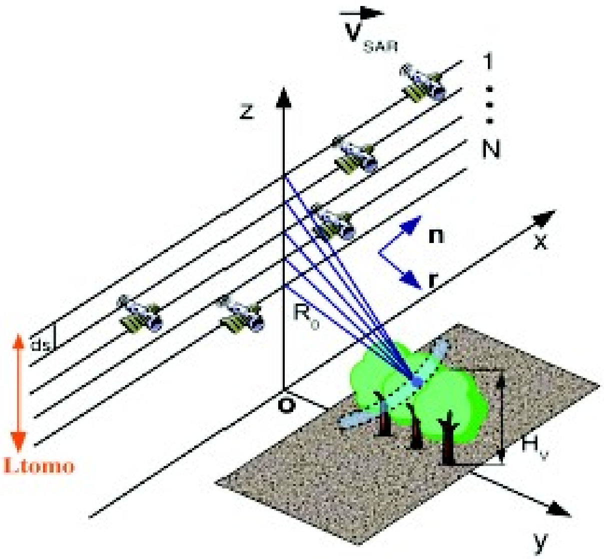

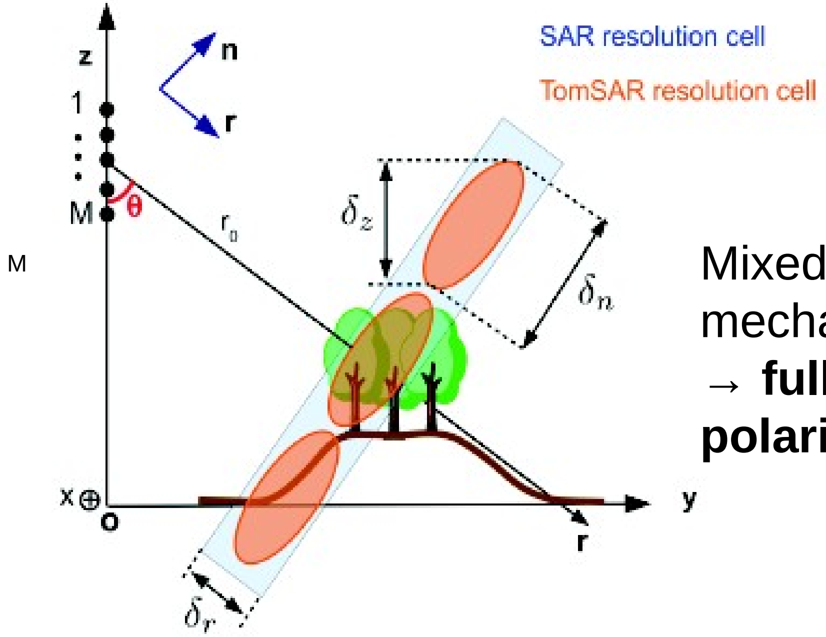

Mixed scattering mechanisms
→ **full rank polarimetry**

Intensity
$\sigma(x,r)$

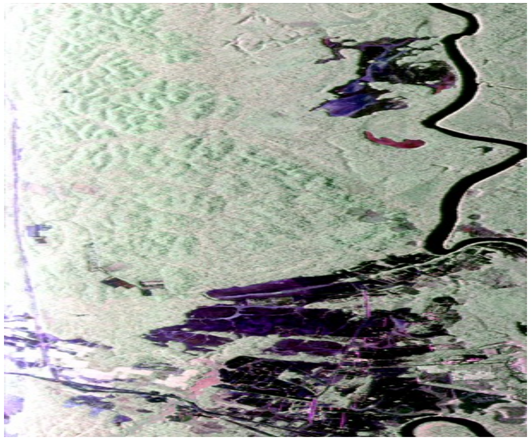

Rank 1 polarimetry (Pauli)
k(x,r)

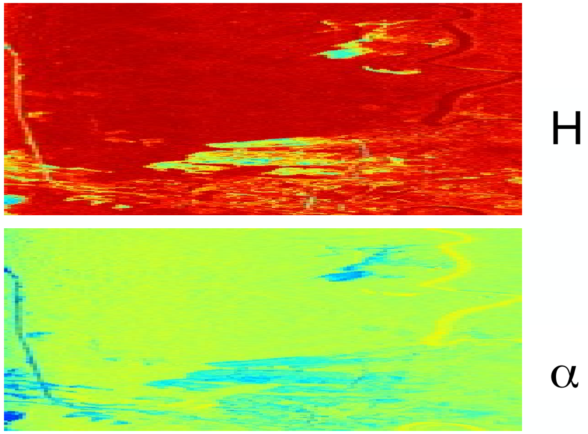

Full rank polarimetry
T(x,r)

Need for full-rank Polarimetric SAR Tomography

Multibaseline polarimetric SAR tomography

MB SAR Tomography

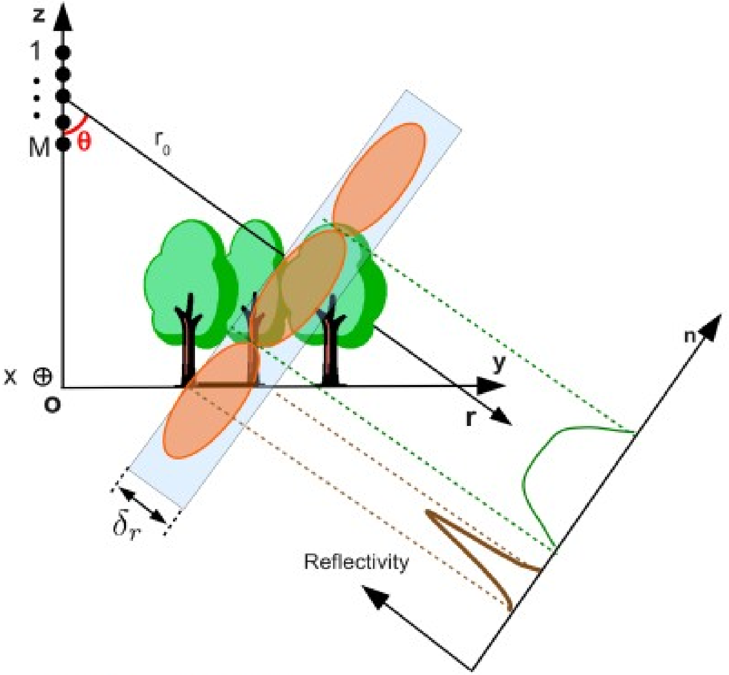

TomoSAR : reflectivity

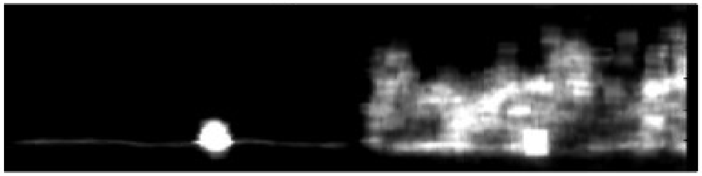

Polarimetric MB SAR Tomography

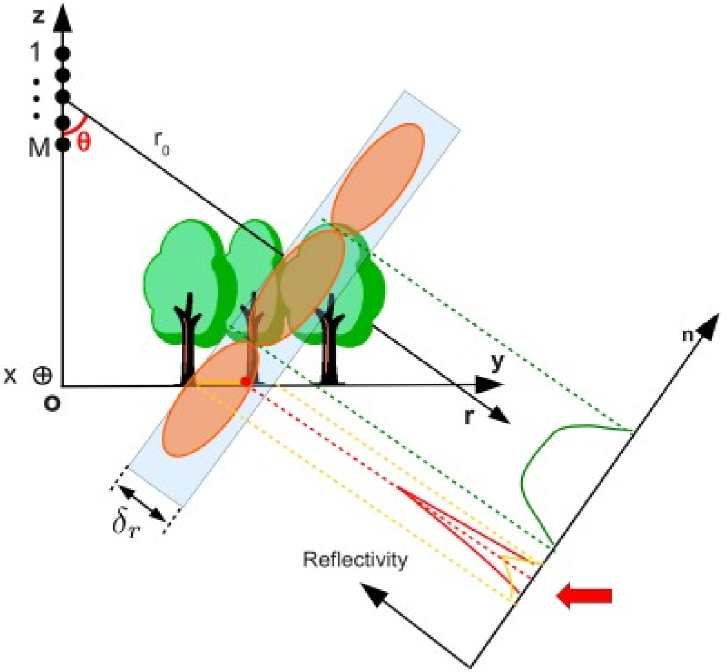

PolTomSAR: α

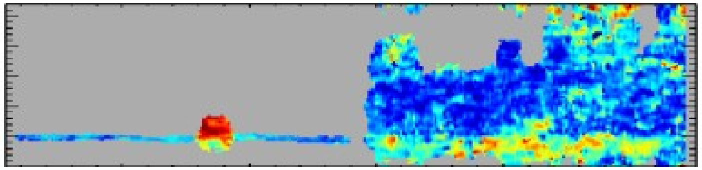

Full-rank Polarimetric SAR Tomography

M PolSAR images

$$\mathbf{y}_{PS} = \begin{bmatrix} \mathbf{y}_1 \\ \mathbf{y}_2 \\ \mathbf{y}_3 \end{bmatrix} \in \mathbb{C}^{3M}$$

$$\mathbf{R}_{PS} = \begin{bmatrix} \mathbf{R}_{11} & \mathbf{R}_{12} & \mathbf{R}_{13} \\ & \mathbf{R}_{22} & \mathbf{R}_{23} \\ & & \mathbf{R}_{33} \end{bmatrix}$$

$$\gamma_{ij}(w_1, w_k)$$

$$\gamma_{ij}(w_2, w_k)$$

$$\gamma_{ij}(w_3, w_k)$$

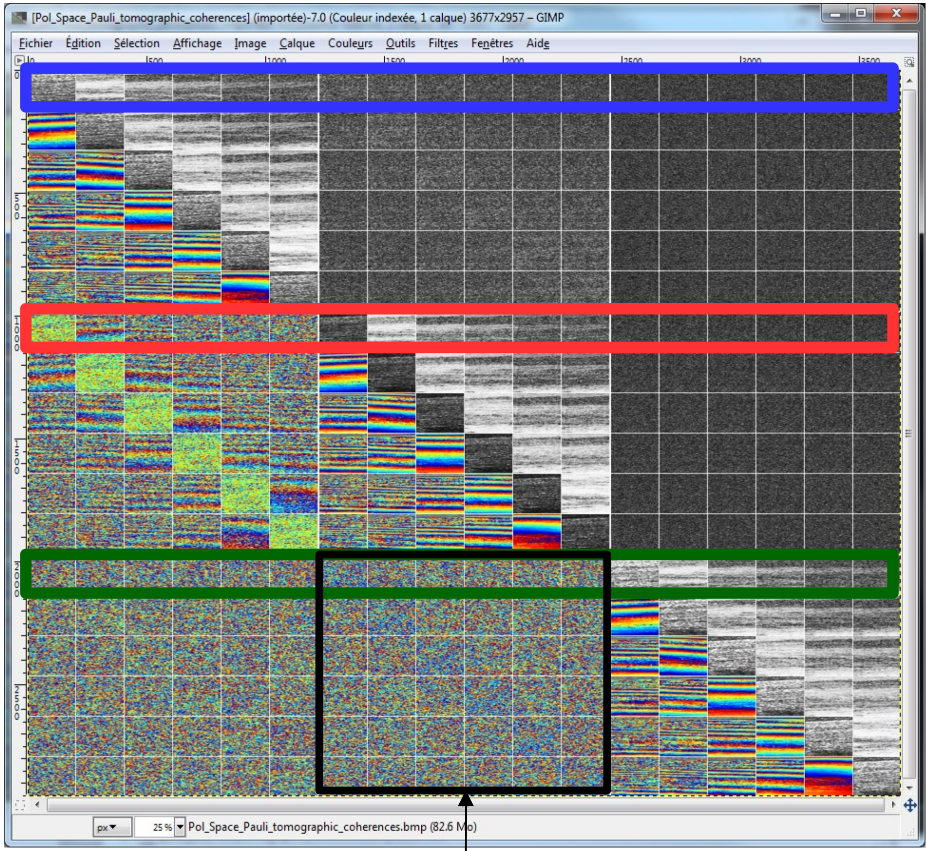

$$\mathbf{R}_{ij} \in \mathbb{C}^{M \times M}$$

Full rank analysis strategies

- ○ Full-rank P-Capon (LFF et al. 2012)

$$\mathbf{R}_{PS} \longrightarrow \sigma(z)\mathbf{T}(z)$$

- ○ SKP decomposition (Tebaldini 2009)

$$\mathbf{R}_{PS} = \sum_i \mathbf{T}_{P_i} \otimes \mathbf{R}_{S_i} \longrightarrow \sum_i \sigma_i(z)\mathbf{T}_{P_i}$$

Full-rank Polarimetric SAR Tomography

Pol ch. 1 $\gamma_{ij}(w_1, w_k)$

Pol ch. 2 $\gamma_{ij}(w_2, w_k)$

Pol ch. 3 $\gamma_{ij}(w_3, w_k)$

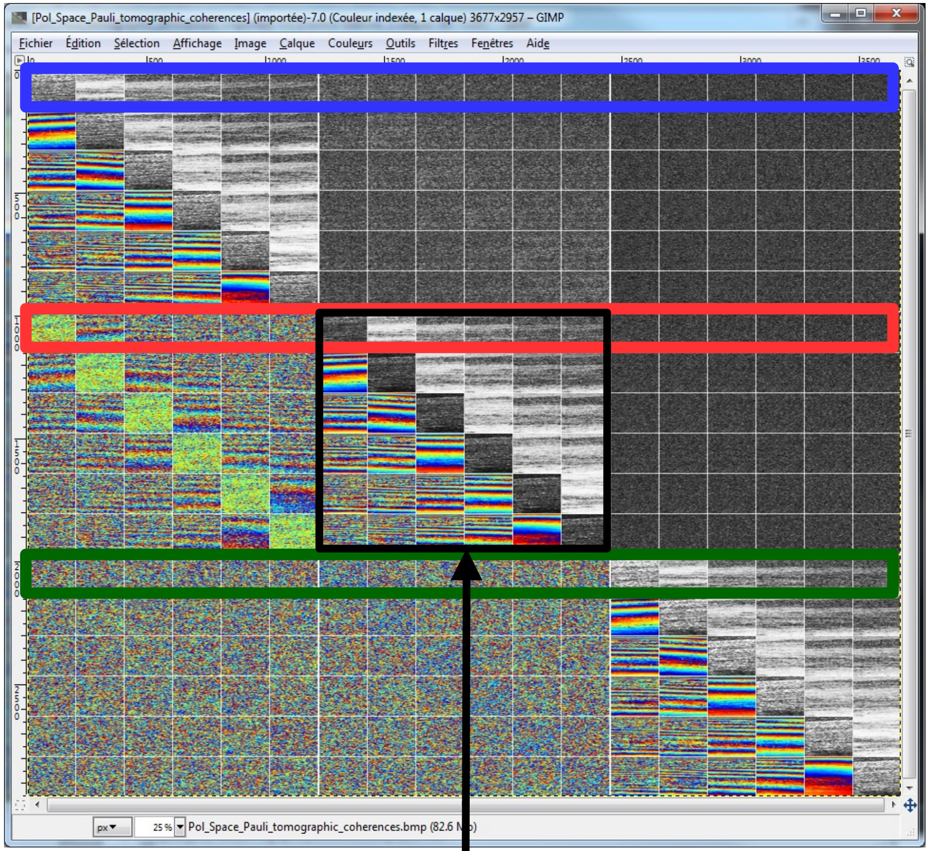

$\mathbf{R}_{ij} \in \mathbb{C}^{M \times M}$

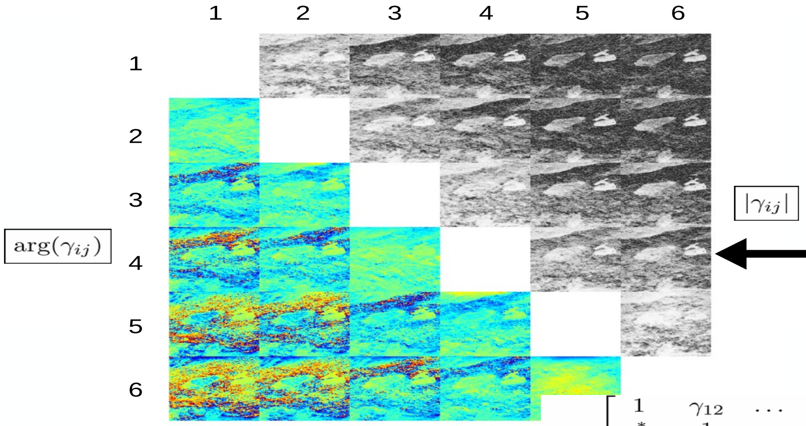

$$\widetilde{\mathbf{R}} = \begin{bmatrix} 1 & \gamma_{12} & \cdots & & \gamma_{1M} \\ \gamma_{12}^* & 1 & \gamma_{23} & \cdots & \gamma_{2M} \\ & & \ddots & & \\ \gamma_{1M}^* & & & & 1 \end{bmatrix}$$

Combined
spatial & polarimetric
correlations

Full-rank Polarimetric SAR Tomography

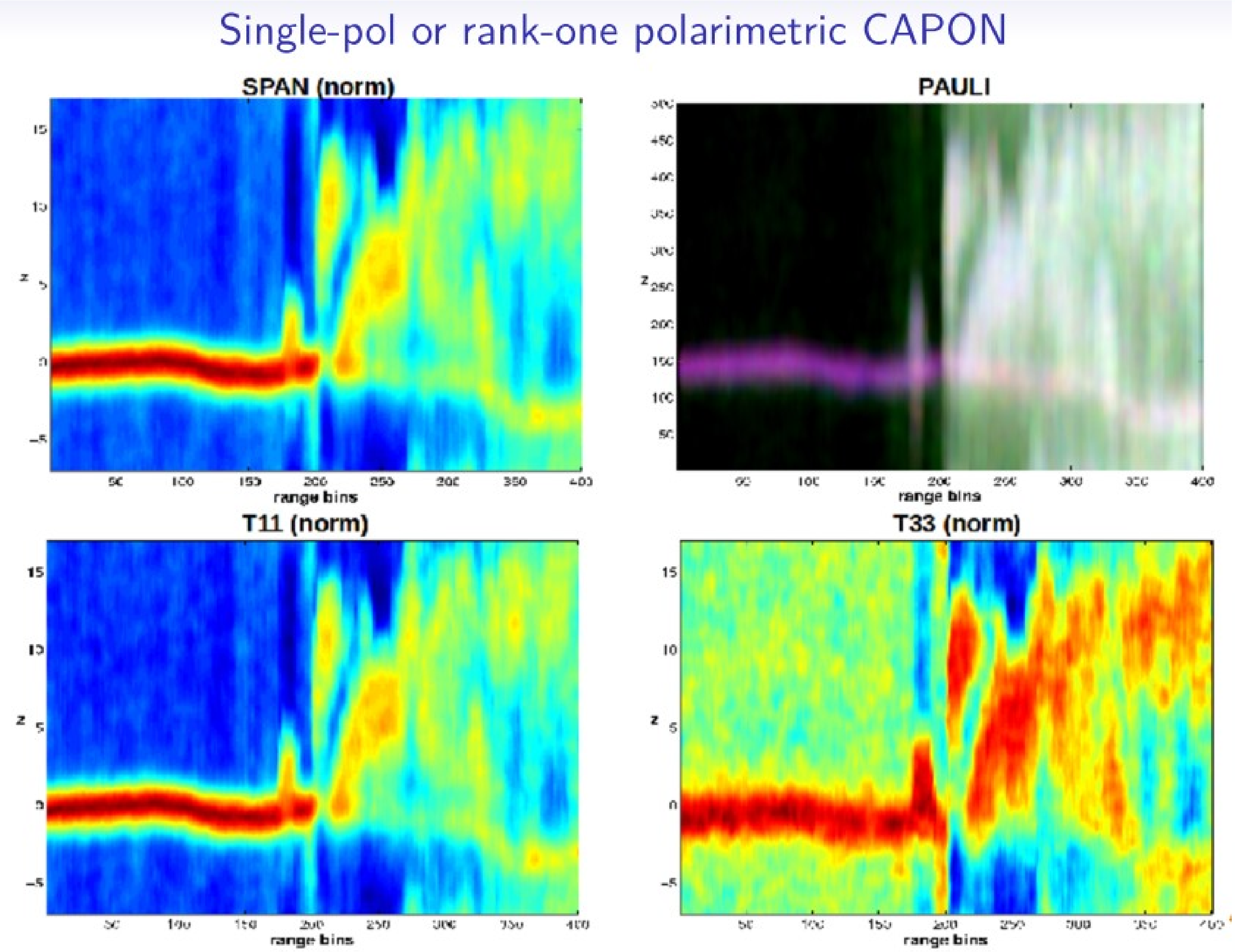

Single-pol or rank-one polarimetric CAPON

Full-rank Polarimetric SAR Tomography

Full-Rank Polarimetric CAPON

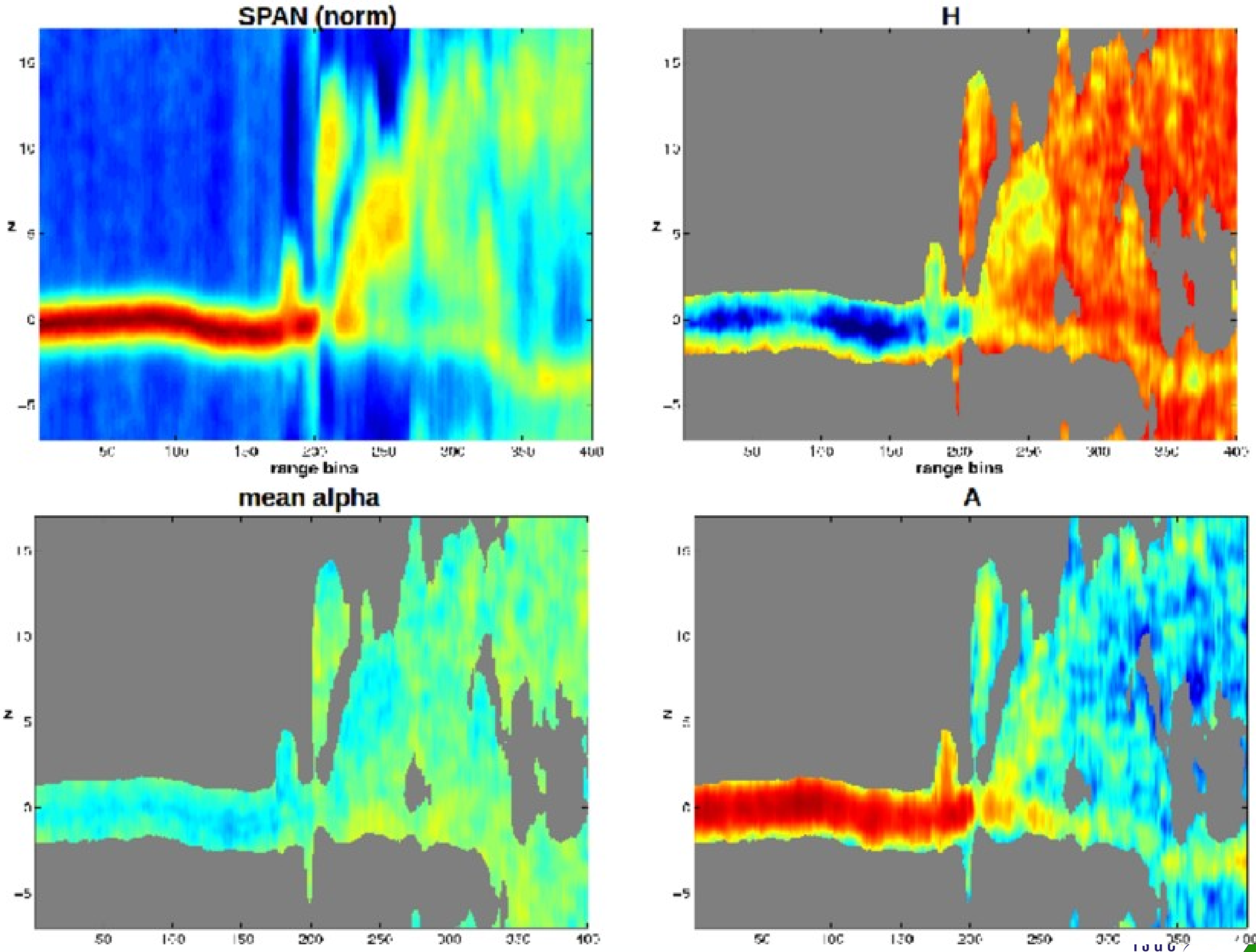

Full-rank Polarimetric SAR Tomography

FR-P-CAPON over the Dornstetten temperate forest at L band

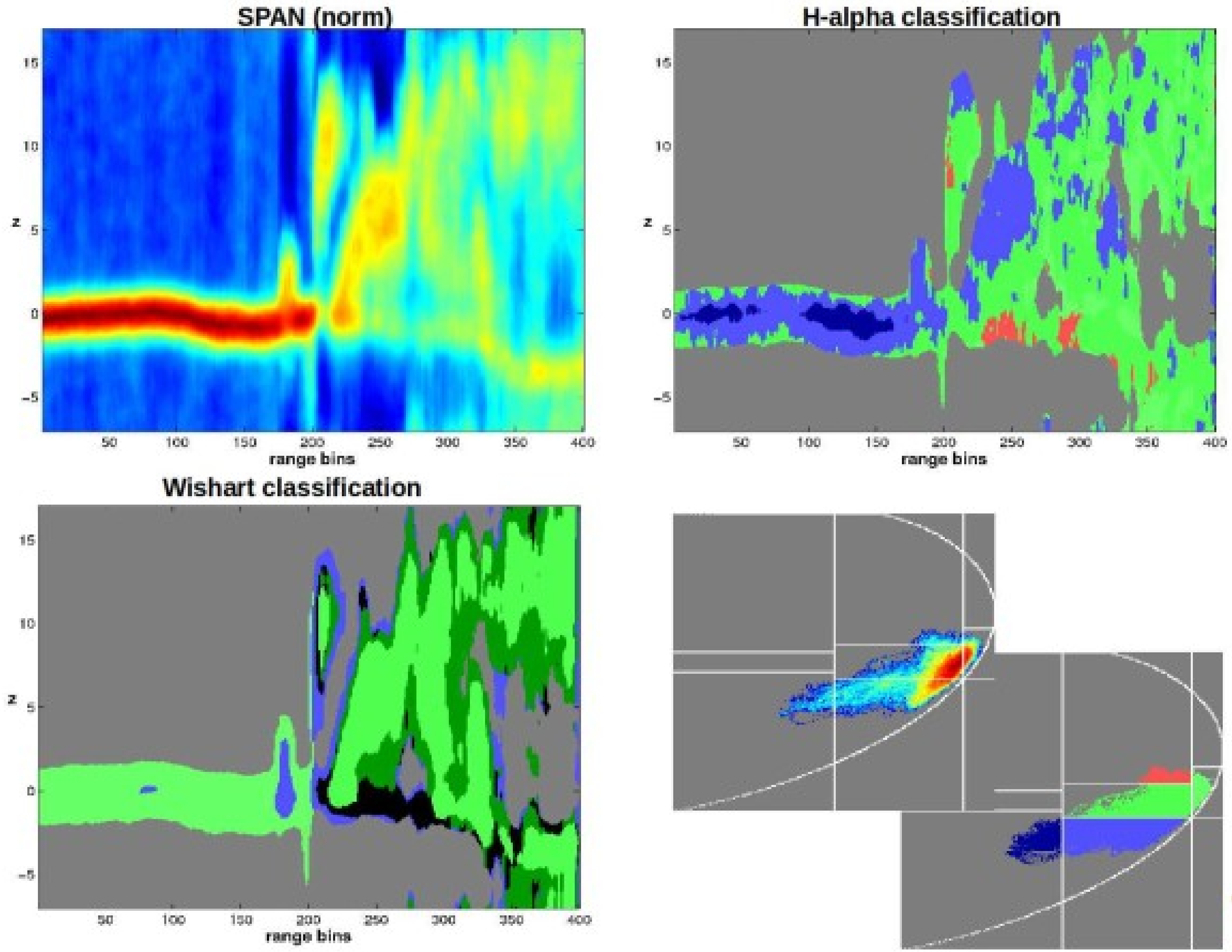

Full-rank Polarimetric SAR Tomography

FR-P-CAPON over the Dornstetten temperate forest at L band

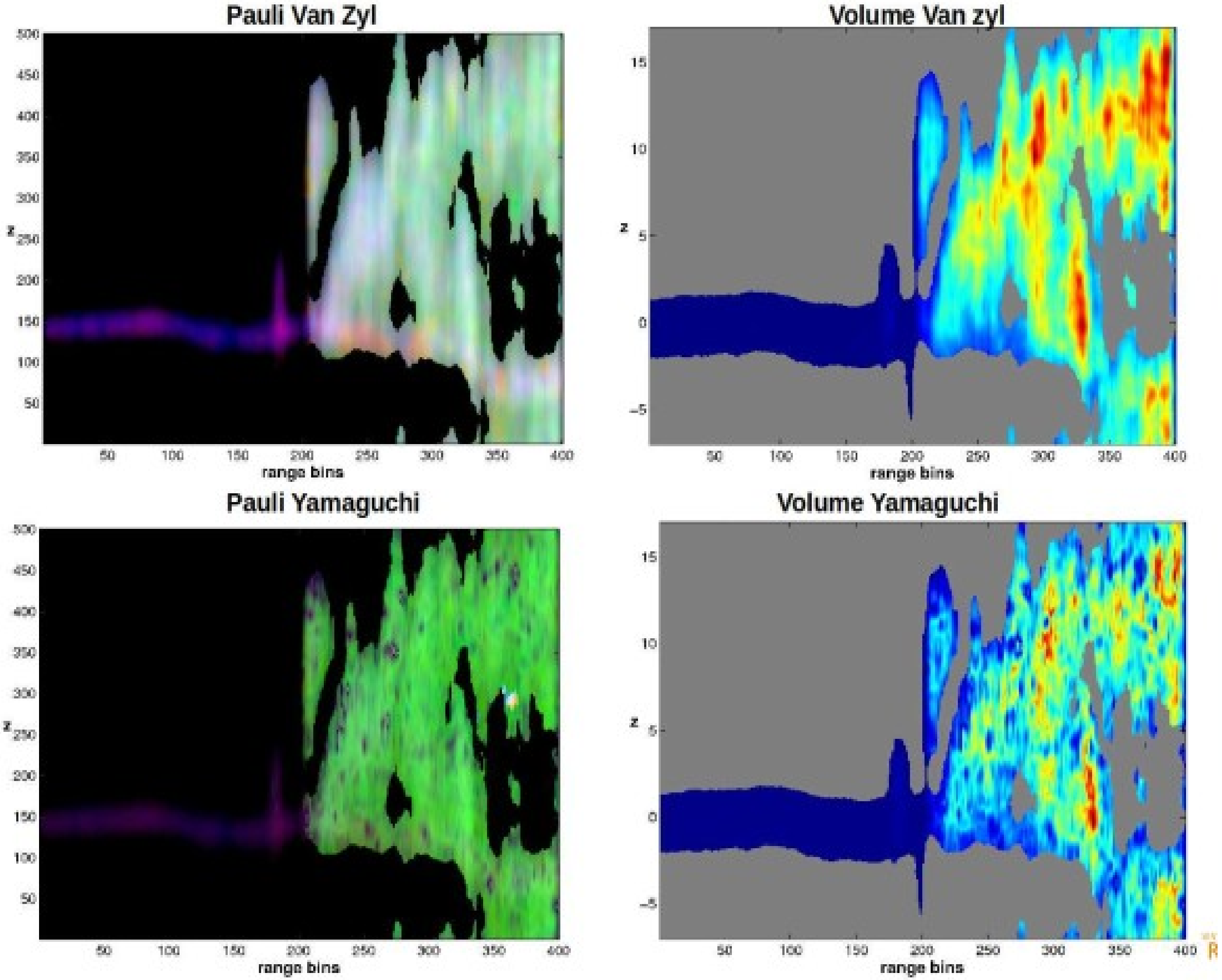

L. Ferro-Famil & S.Tebaldini

Full-rank Polarimetric SAR Tomography

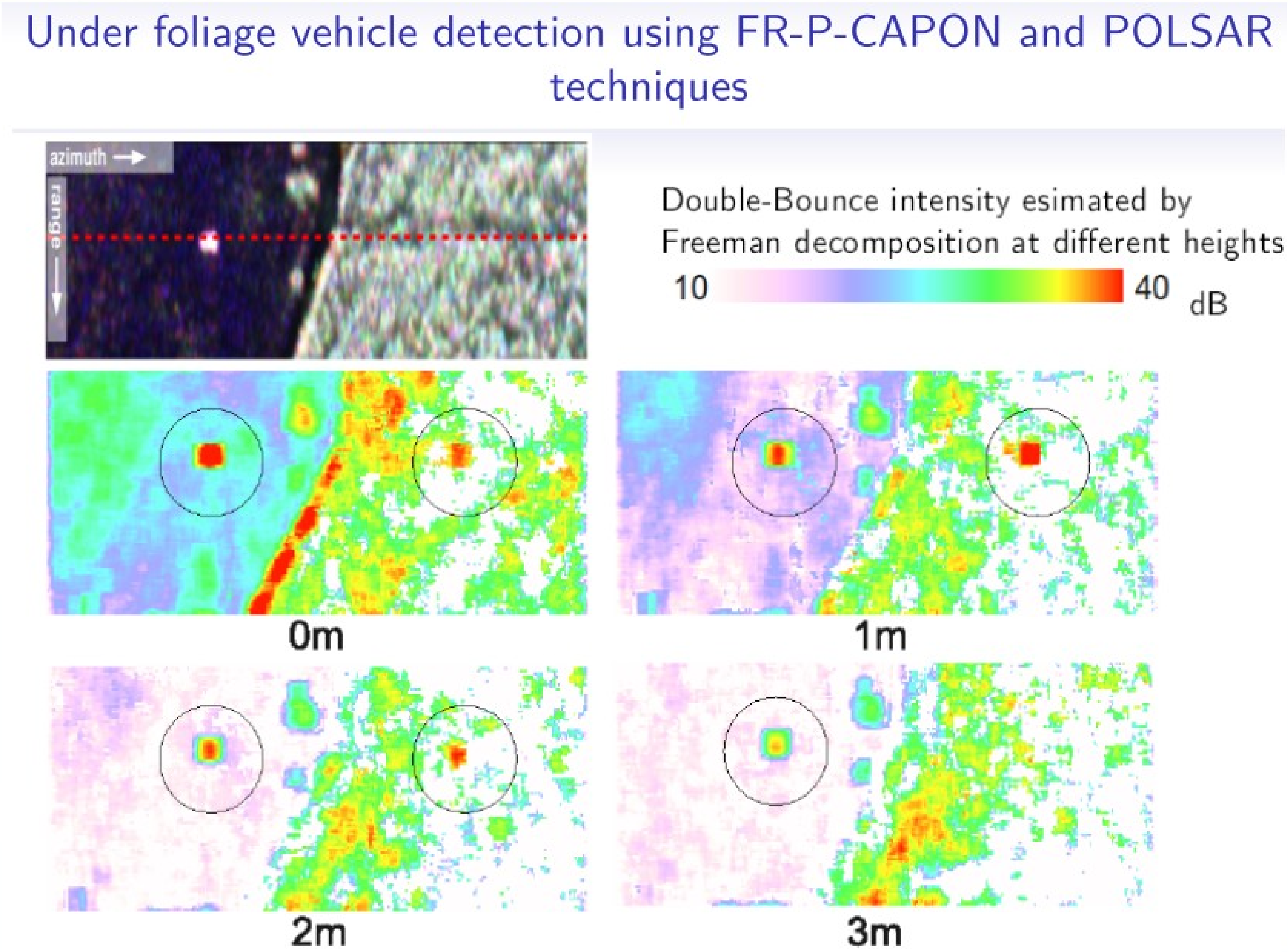

Under foliage vehicle detection using FR-P-CAPON and POLSAR techniques

Double-Bounce intensity esimated by Freeman decomposition at different heights

Full-rank Polarimetric SAR Tomography

3-D SAR imaging using PolTomSAR

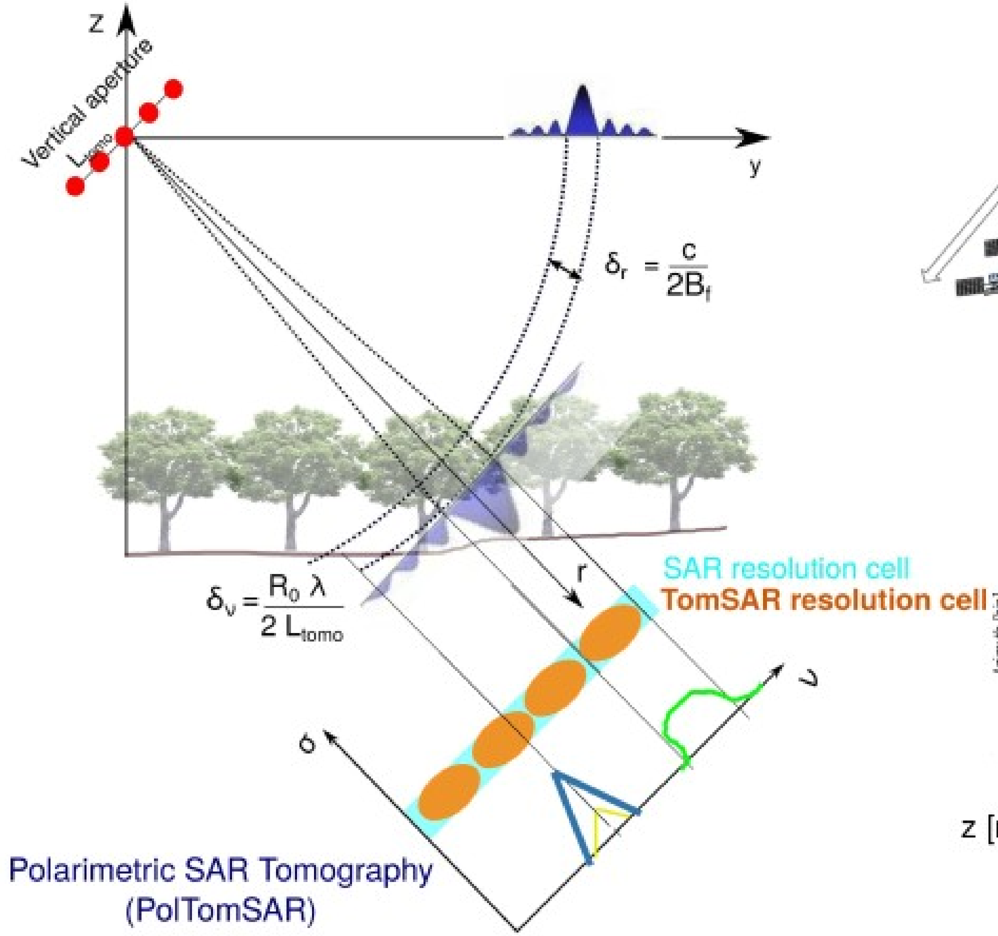

Polarimetric SAR Tomography (PolTomSAR)

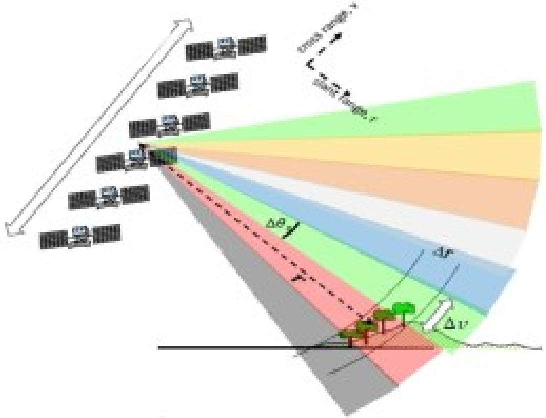

Antenna array formation at each (x,r) position

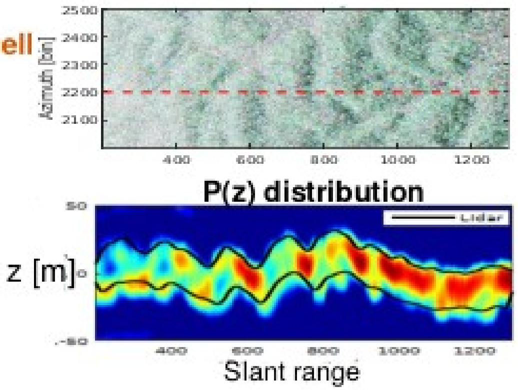

Full-rank Polarimetric SAR Tomography

RVoG characterization using PolinSAR

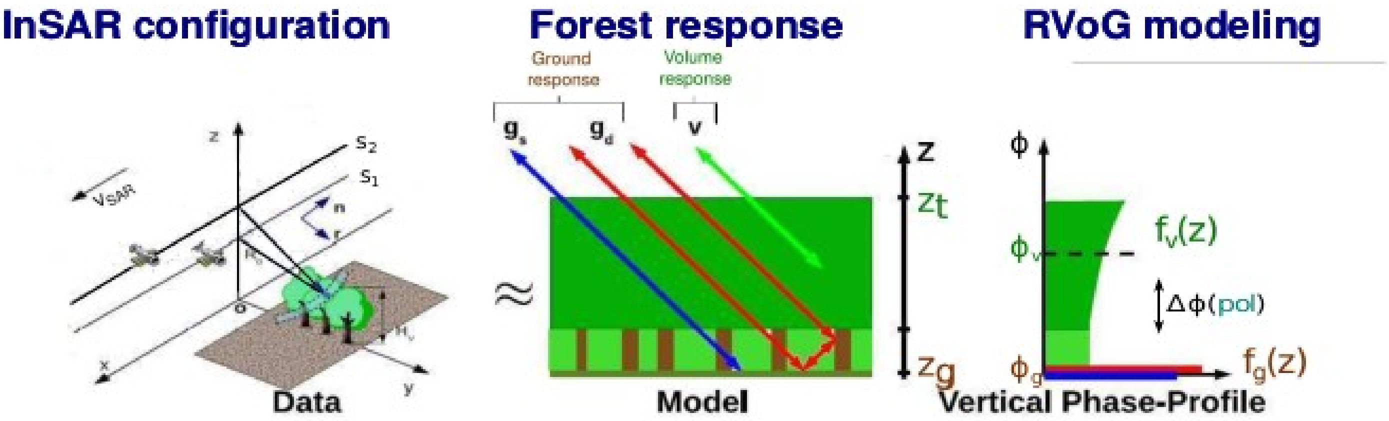

- Vertical structure: $f(z) = f_g(z) + f_v(z)$
- Coherence: $\gamma = \frac{\int f(z) e^{jk_{z\mathbf{12}} z} dz}{\int f(z) dz} = L\gamma_v + (1-L)\gamma_g$

  Volume-Contribution-Ratio (VCR): $L = \frac{I_v}{I_v + I_g}$

γ_v, γ_g, L estimation $\rightarrow$ PolInSAR: $\gamma(\mathrm{pol}) = L(\mathrm{pol})\gamma_v + (1 - L(\mathrm{pol}))\gamma_g$

Full-rank Polarimetric SAR Tomography

Using Multi-Baseline inSAR: TomSAR

TomSAR configuration **Forest response** **RVoG modeling**

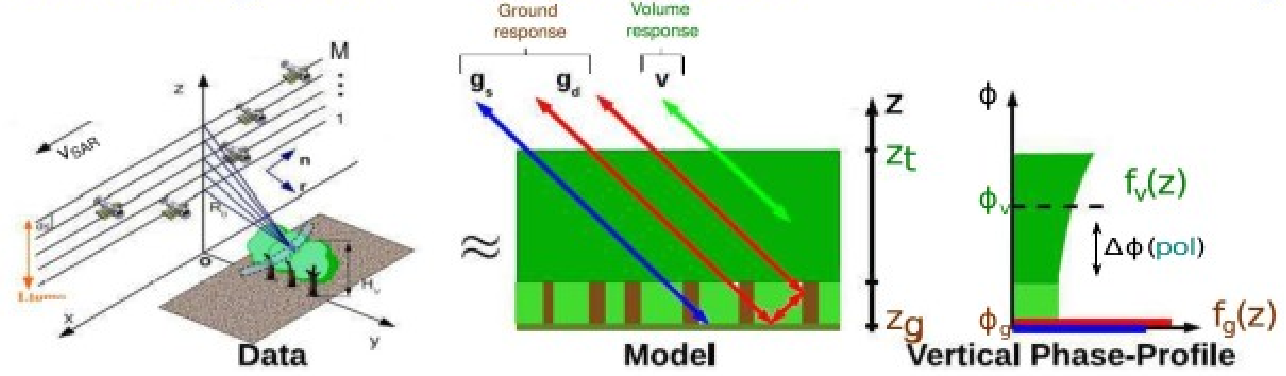

Spatial baseline diversity: $M(M-1)/2$ coherences

$$\gamma_{12} = \frac{\int f(z) e^{jk_{z12} z} dz}{I}$$

$$\vdots$$

$$\gamma_{1M} = \frac{\int f(z) e^{jk_{z1M} z} dz}{I} \longrightarrow \hat{f}(z)$$

$$\vdots$$

$$\gamma_{(M-1)M} = \frac{\int f(z) e^{jk_{z(M-1)M} z} dz}{I}$$

Polarimetric diversity
required for separating
$f_g(z) / f_v(z)$

Full-rank Polarimetric SAR Tomography

Using PolTomSAR

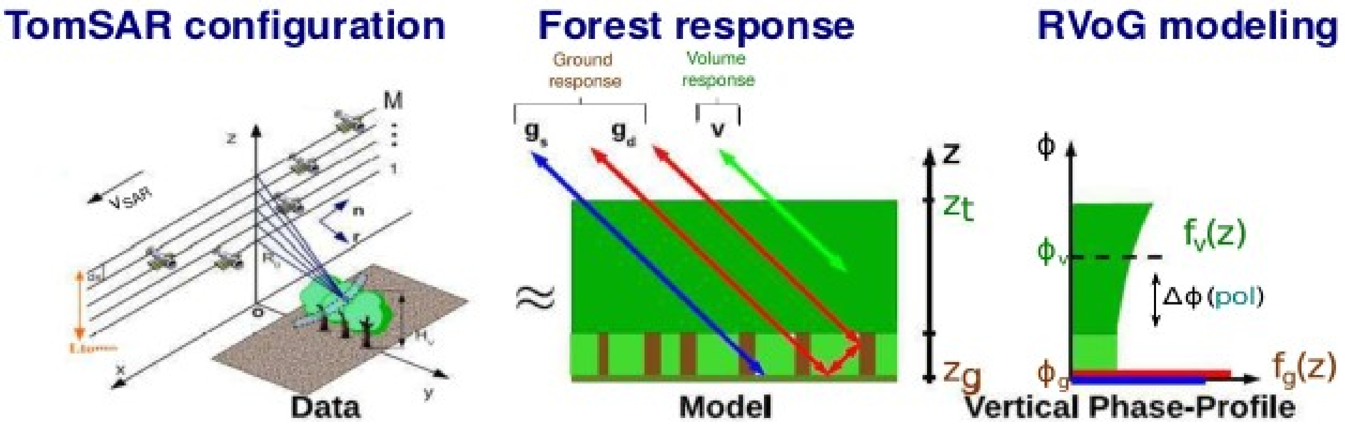

$$\begin{bmatrix}\gamma_{12}(\text{pol})\\ \vdots \\ \gamma_{1M}(\text{pol})\\ \vdots \\ \gamma_{(M-1)M}(\text{pol})\end{bmatrix} = L(\text{pol})\begin{bmatrix}\gamma_{v\mathbf{12}}\\ \vdots \\ \gamma_{v\mathbf{1}M}\\ \vdots \\ \gamma_{v(M-\mathbf{1})M}\end{bmatrix} + (1-L(\text{pol}))\begin{bmatrix}\gamma_{g\mathbf{12}}\\ \vdots \\ \gamma_{g\mathbf{1}M}\\ \vdots \\ \gamma_{g(M-\mathbf{1})M}\end{bmatrix}$$

PolTomSAR covariance matrix

$$\gamma_{ij}(\text{pol}_{1,2,3}) \longrightarrow \underset{\text{SKP2-decomposition}}{\boxed{\mathbf{R}_{P-S} = \mathbf{C}_\mathrm{g} \otimes \mathbf{R}_\mathrm{g} + \mathbf{C}_\mathrm{v} \otimes \mathbf{R}_\mathrm{v}}} \in \mathbb{C}^{3M\times 3M}$$

Full-rank Polarimetric SAR Tomography

Ground-volume decomposition implies:

- Separation of Structural Properties

  => Separated Tomographic Imaging of Ground-only and Volume-only Contributions

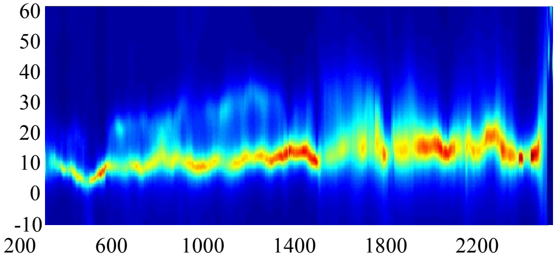
HV

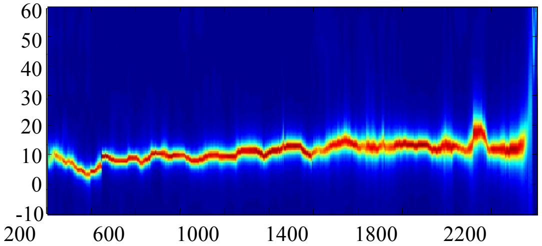
Ground

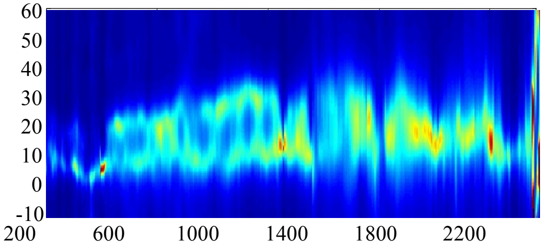
Volume

- Separation of Polarimetric Properties

  => Evaluation of the Ground to Volume Backscattered Power Ratio for each polarization

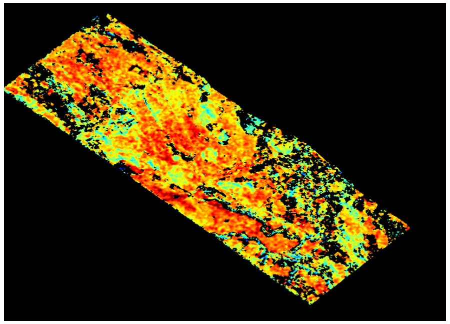
P-Band HH

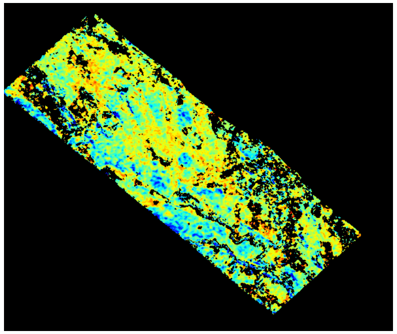
P-Band HV

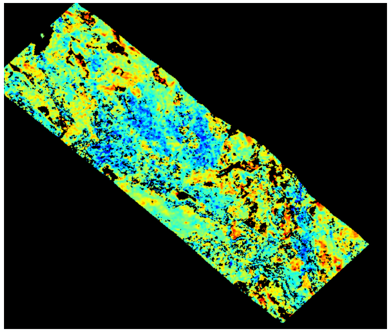
L-Band HH

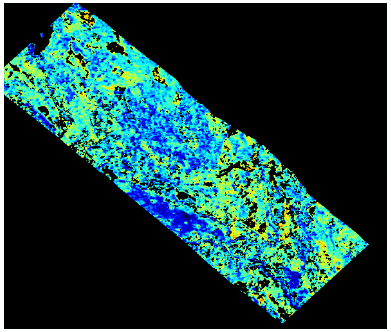
L-Band HV

SKP Decomposition

General procedure for ground and volume decomposition

Approximate W by retaining the first two KPs of the SKP Decomposition

Choose the proper values of *a*, *b* :

1. **Select values of *a*, *b* that give rise to (semi) positive definite R_g, R_v, C_g, C_v**

   → physical validity of the solution

2. **Optimize some criterion in order to pick a unique solution**

Region of physical validity for the ground and volume coherences in the interferometric pair formed between tracks 1 and 2 (Numerical simulation)

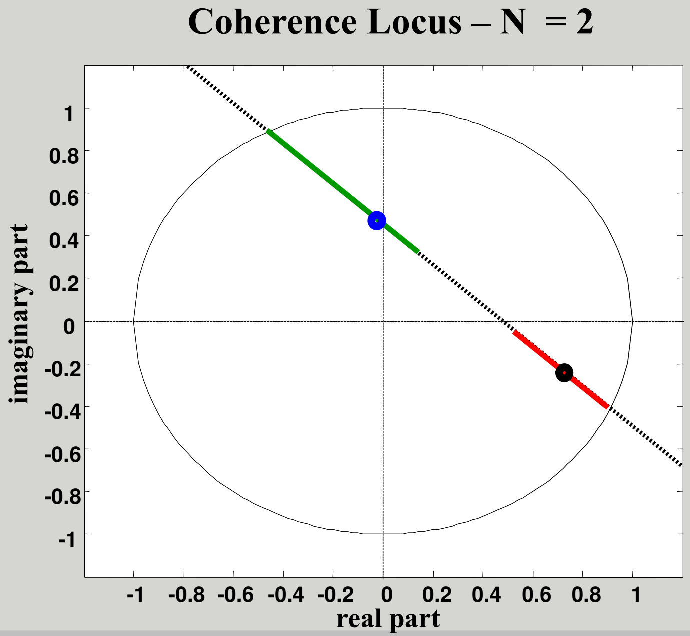

Single Baseline case :

The region of physical validity is formed by two branches, spanned by the parameters *a, b*

The union of branches *a, b* results in the same region of physical validity as in PolInSAR

Physically valid solutions

🟥 ***Branch a***

🟩 ***Branch b***

● **True Volume Coherence**

● **True Ground Coherence**

SKP Decomposition

General procedure for ground and volume decomposition

Approximate W by retaining the first two KPs of the SKP Decomposition

Choose the proper values of *a*, *b* :

1. Select values of *a*, *b* that give rise to (semi) positive definite R_g, R_v, C_g, C_v
   🔔 physical validity of the solution
2. Optimize some criterion in order to pick a unique solution

Region of physical validity for the ground and volume coherences in the interferometric pair formed between tracks 1 and 2 (Numerical simulation)

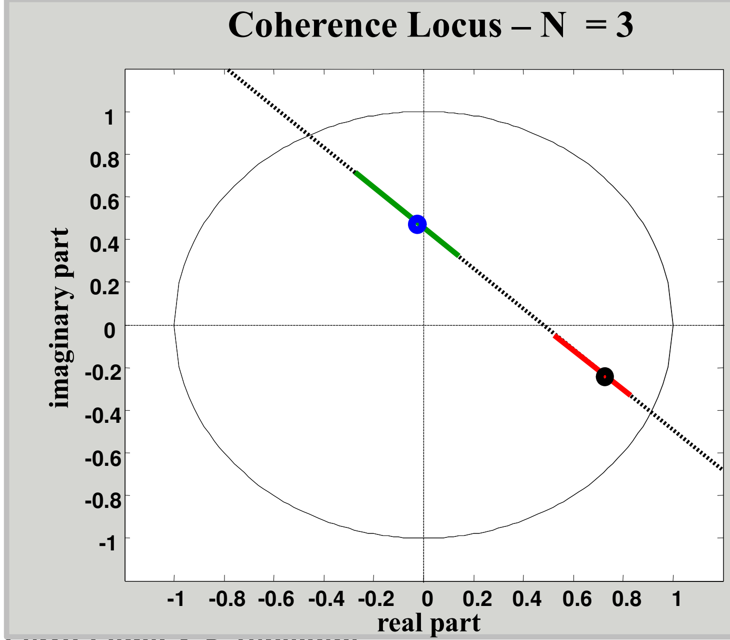

Multi-Baseline case : the region of physical validity tends to ***shrink***, depending on the number of available tracks

Physically valid solutions

🟥 *Branch a*

🟩 *Branch b*

● True Volume Coherence

● True Ground Coherence

SKP Decomposition

General procedure for ground and volume decomposition

Approximate W by retaining the first two KPs of the SKP Decomposition

Choose the proper values of *a*, *b* :

1. **Select values of *a*, *b* that give rise to (semi) positive definite R_g, R_v, C_g, C_v**

   → physical validity of the solution

2. **Optimize some criterion in order to pick a unique solution**

Region of physical validity for the ground and volume coherences in the interferometric pair formed between tracks 1 and 2 (Numerical simulation)

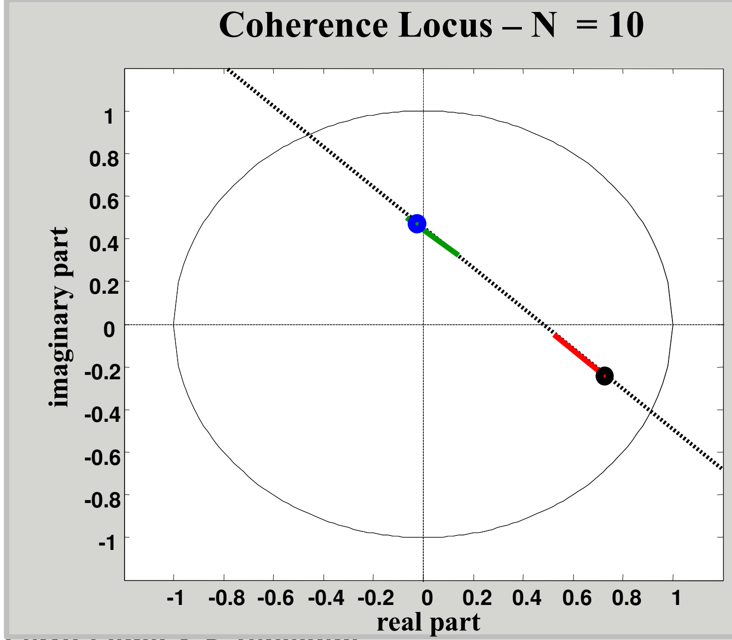

Coherence Locus – N = 10

Multi-Baseline case : the region of physical validity tends to *shrink*, depending on the number of available tracks

- **The higher the number of tracks, the easier it is to pick the correct solution**

Physically valid solutions

🟥 ***Branch a***

🟩 ***Branch b***

● **True Volume Coherence**

● **True Ground Coherence**

Case Study

Campaign	**BioSAR 2007 - ESA**
System	E-SAR - DLR
Period	Spring 2007
Site	Remningstorp, South Sweden
Scene	Semi-boreal forest
Topography	Flat
Tomographic tracks	9 – Fully Polarimetric
Carrier frequency	350 MHz
Slant range resolution	2 m
Azimuth resolution	1.6 m
Vertical resolution	10 m (near range) to 40 m (far range)

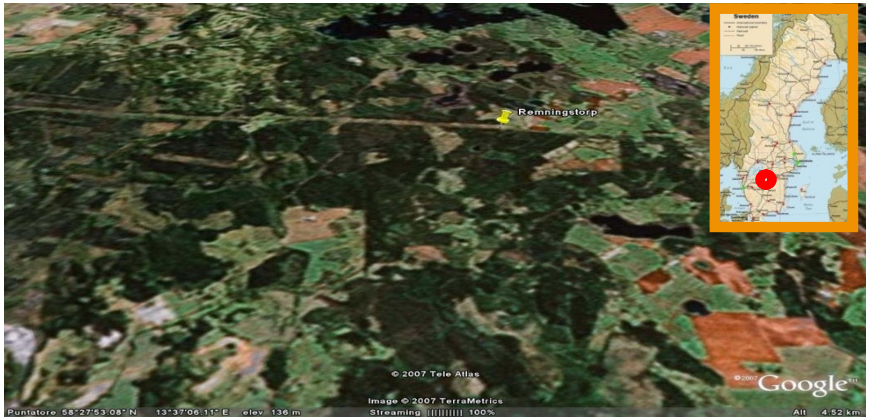

Case Study

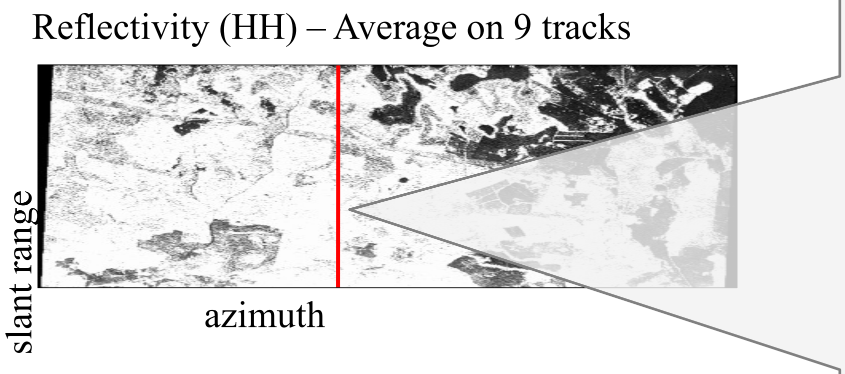

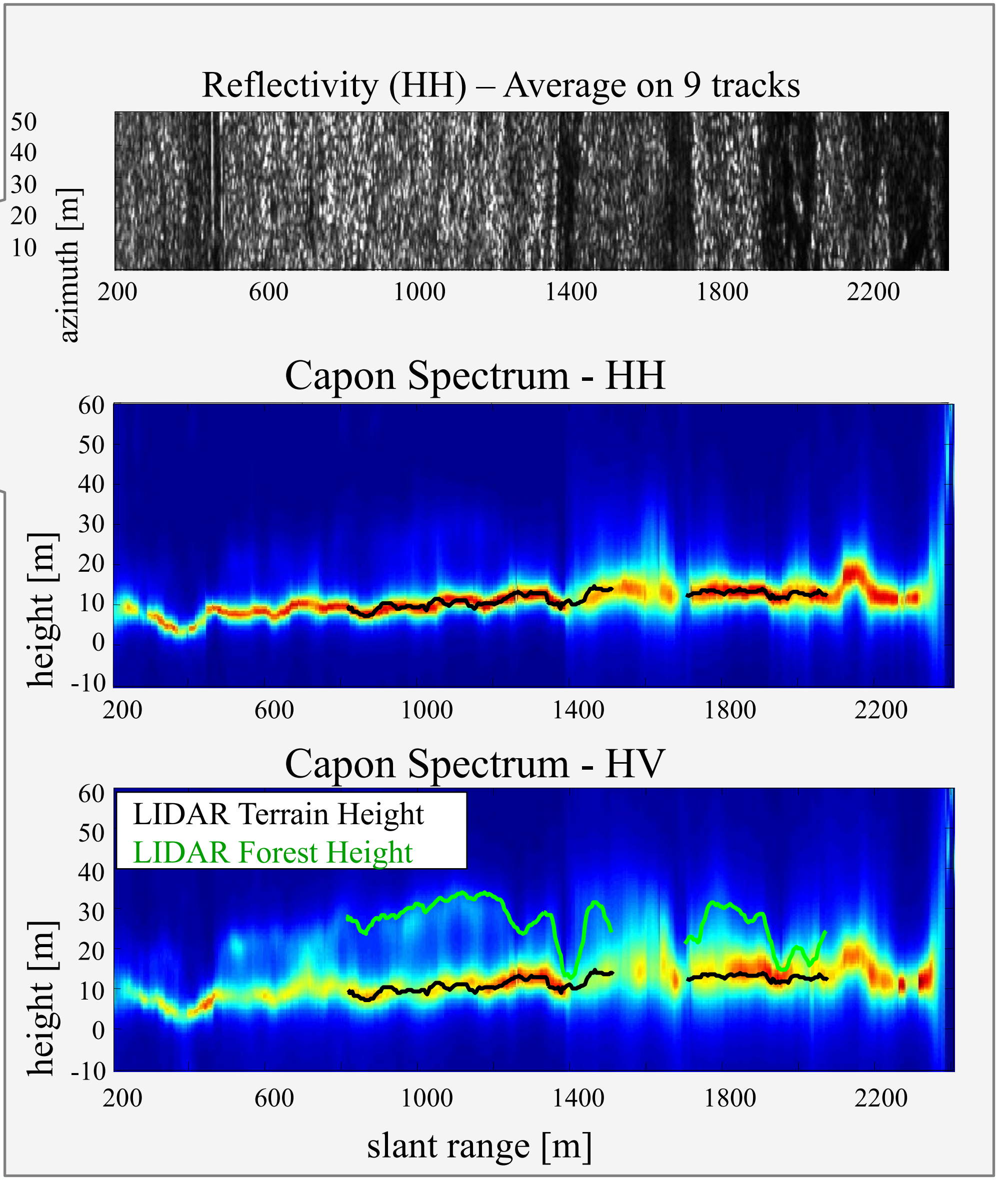

The analyzed profile is almost totally forested, except for the dark areas

HH:
- Dominant phase center is ground locked
- Vegetation is barely visible

Similar conclusions for VV

HV:
- Dominant phase center is ground locked
- Vegetation is much more visible

Case Study

Model validation: $\mathbf{W} \overset{?}{=} \mathbf{C}_g \otimes \mathbf{R}_g + \mathbf{C}_v \otimes \mathbf{R}_v$

Methodology:

evaluation of the error between the sample covariance matrix and its best L2 approximation with $K = \{1,2,3,4\}$ KPs

$$\hat{\mathbf{W}}_K = \arg\min_{\mathbf{W}_k} \left\{ \left\| \hat{\mathbf{W}} - \mathbf{W}_K \right\|_F \right\}$$

$$error = \frac{\left\| \hat{\mathbf{W}} - \mathbf{W}_K \right\|_F}{\left\| \hat{\mathbf{W}} \right\|_F}$$

Remark: the best L2 approximation is obtained simply by taking the dominant K terms of the SKP decomposition

$$\left\| \hat{\mathbf{W}} - \hat{\mathbf{W}}_2 \right\|_F < 0.1 \cdot \left\| \hat{\mathbf{W}} \right\|_F$$

> 90 % of the information can be represented by the sum of just two KPs

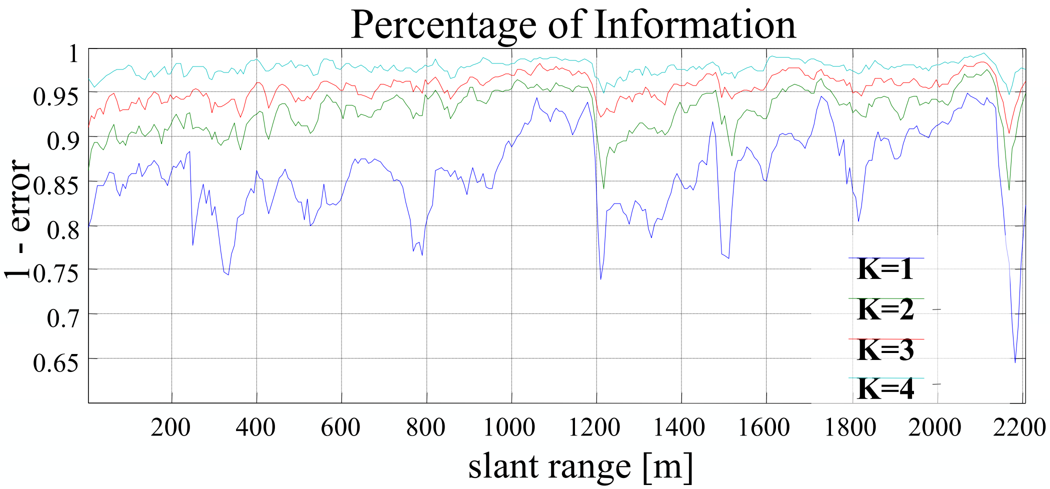

Case Study

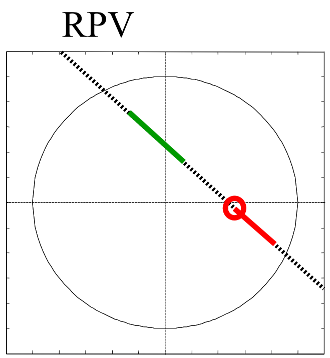

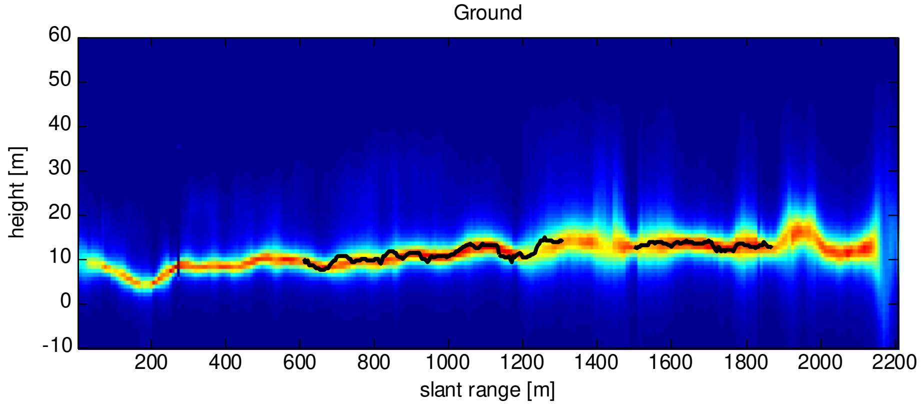

Residual volume contributions visible above the ground

Significant contributions from the ground level.
Volumetric scattering at the ground level
Consistent with:

- Backscattering from understorey or lower tree branches
- Multiple interactions of volumetric scatterers with the ground

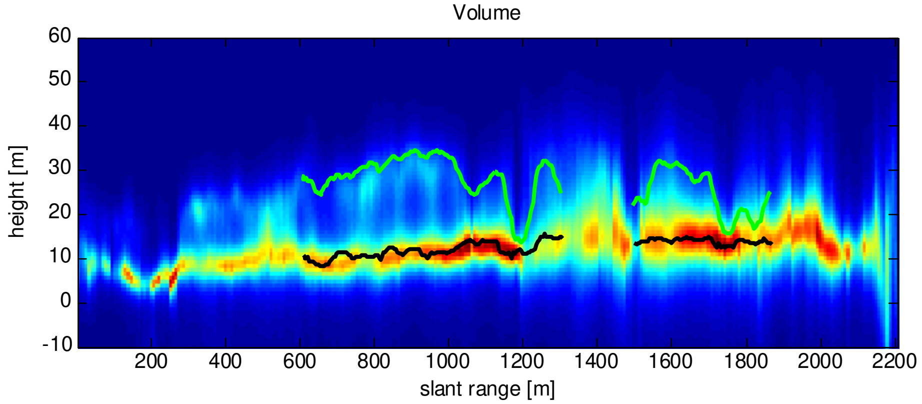

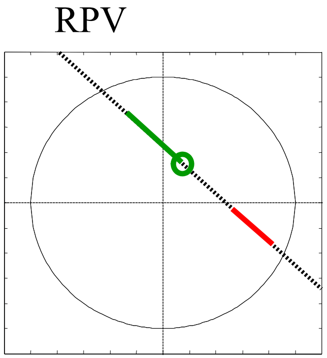

LIDAR Terrain Height
LIDAR Forest Height

Case Study

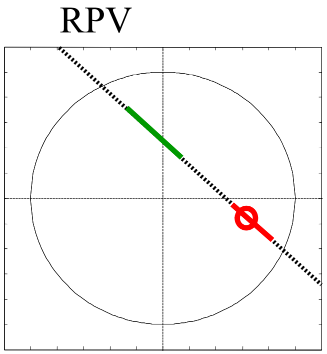

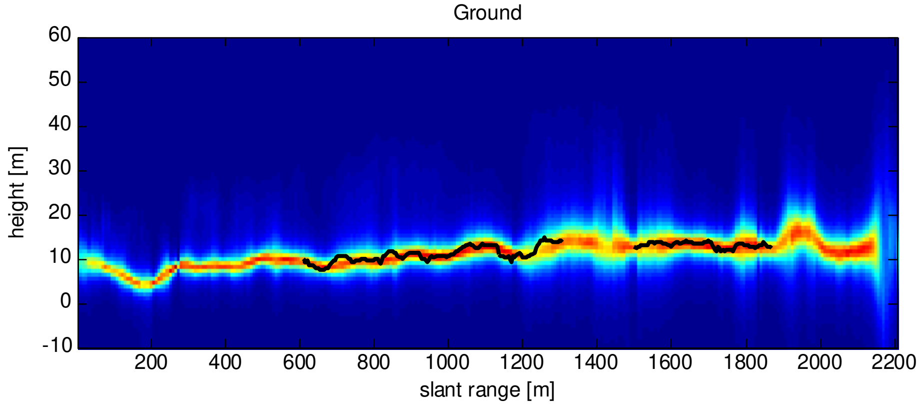

Improved volume rejection

Volumetric contributions from the ground level are partly rejected

Backscattering contributions from the whole volume structure are emphasized

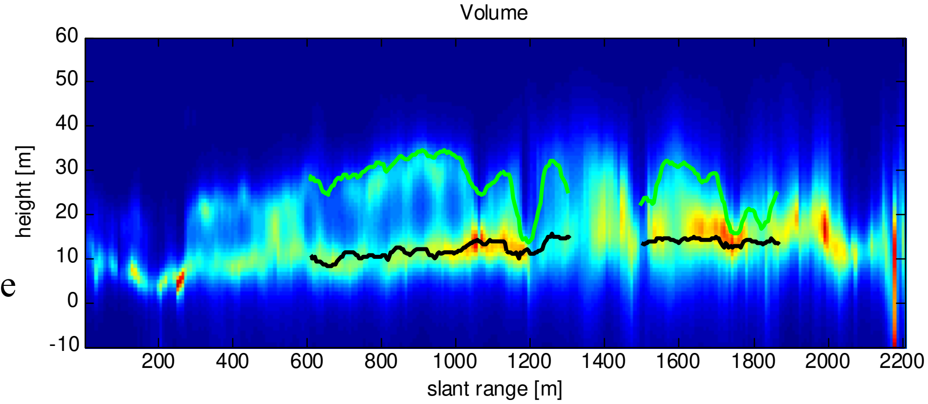

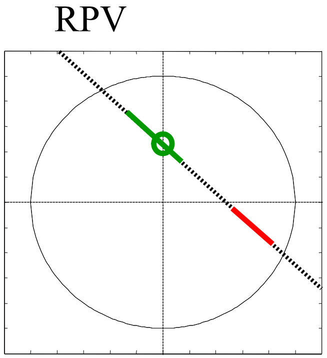

LIDAR Terrain Height
LIDAR Forest Height

Case Study

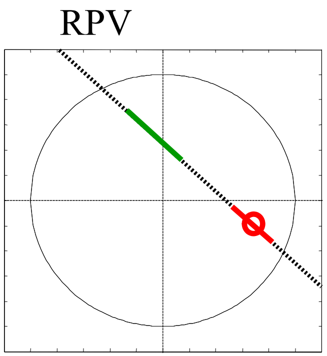

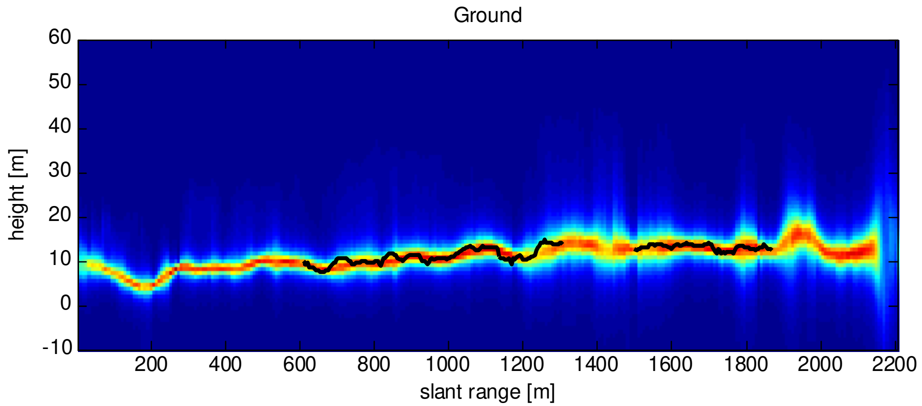

Improved volume rejection

Improved ground rejection

Backscattering contributions from the whole volume structure are emphasized

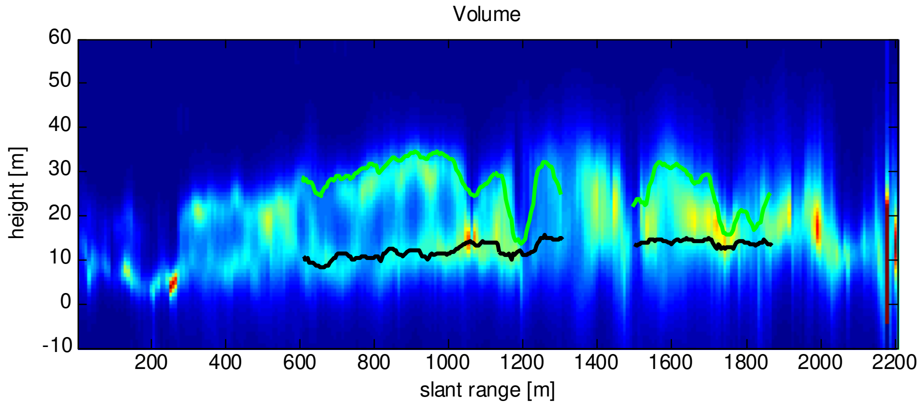

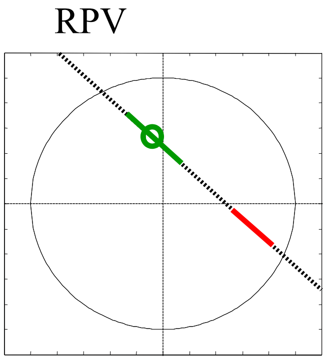

LIDAR Terrain Height
LIDAR Forest Height

Case Study

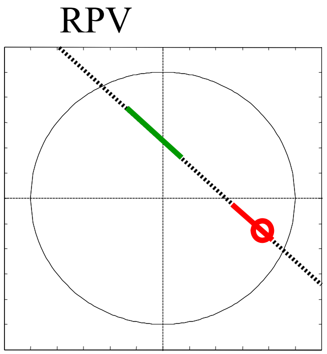

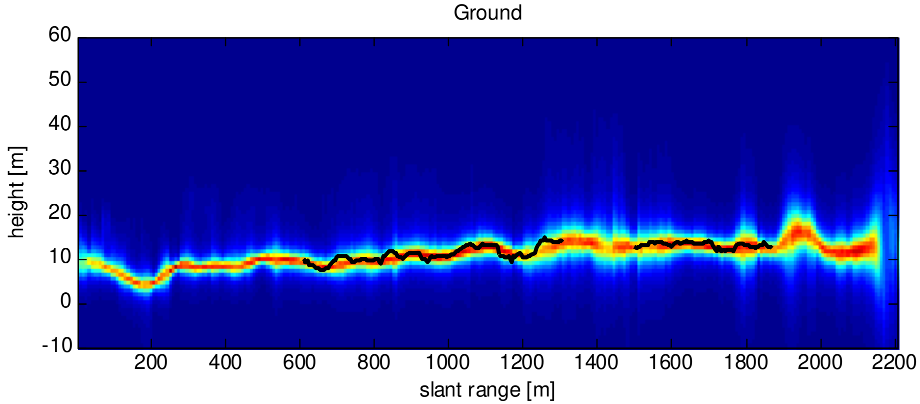

Improved volume rejection

Ground contributions rejected

Contributions from the lower canopy are partly rejected

Backscattering contributions from the upper volume structure are emphasized

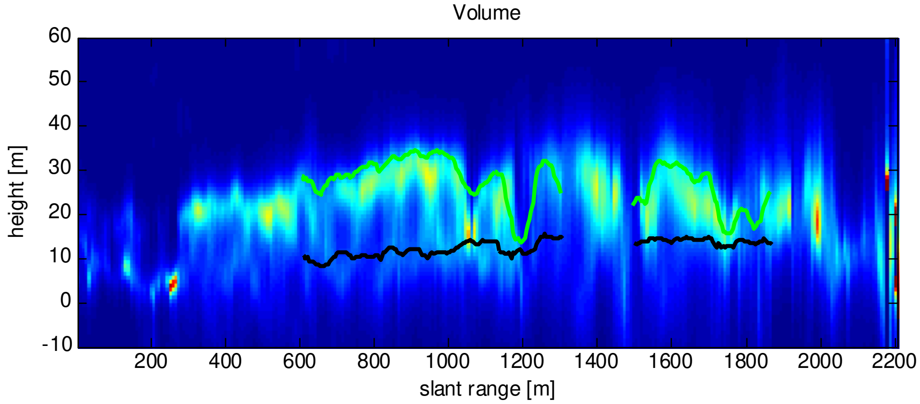

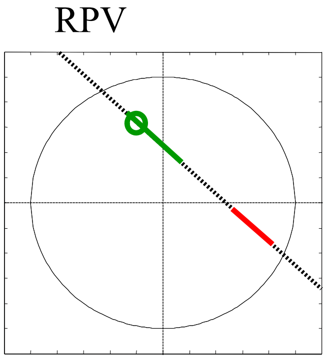

LIDAR Terrain Height
LIDAR Forest Height

Case Study

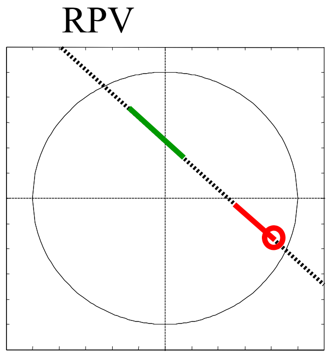

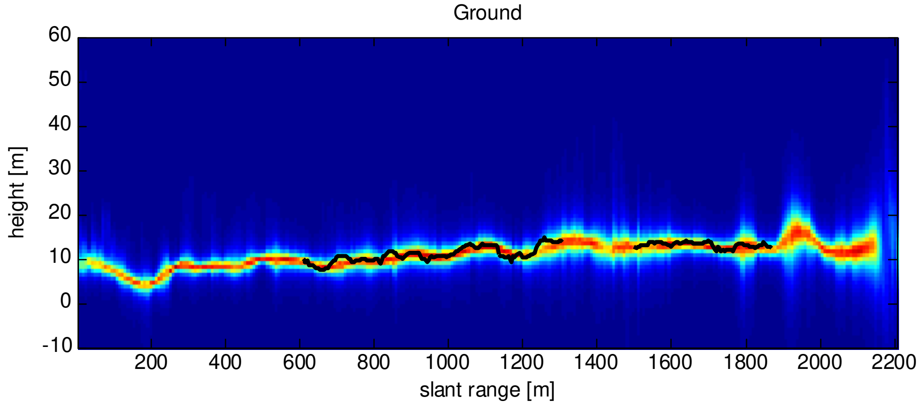

Maximum volume rejection

Ground structure is maximally coherent

Ground and lower canopy contributions are rejected

Only upper canopy contributions are visible

Volume structure is maximally coherent

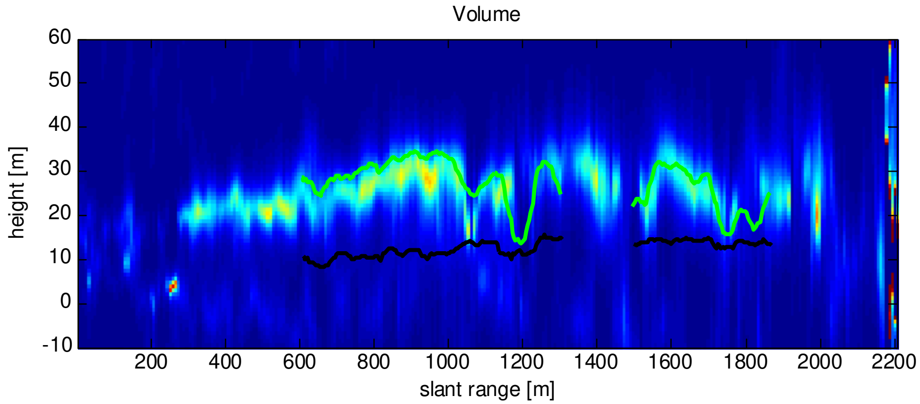

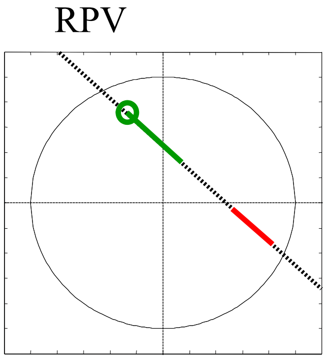

Volume top height is nearly invariant to the choice of the solution, therefore constituting a robust indicator of the volume structure

LIDAR Terrain Height
LIDAR Forest Height